Analysis of a Hybrid Energy Storage System and Electrified Turbocharger in a Performance Vehicle

ANALYSIS OF A HYBRID ENERGY STORAGE SYSTEM AND ELECTRIFIED TURBOCHARGER IN A PERFORMANCE VEHICLE

BY

TYLER STIENE, B.Eng.

A THESIS

SUBMITTED TO THE DEPARTMENT OF ELECTRICAL & COMPUTER ENGINEERING

AND THE SCHOOL OF GRADUATE STUDIES

OF MCMASTER UNIVERSITY

IN PARTIAL FULFILLMENT OF THE REQUIREMENTS

FOR THE DEGREE OF

MASTER OF APPLIED SCIENCE

Master of Applied Science (2016) McMaster University

(Electrical & Computer Engineering) Hamilton, Ontario, Canada

TITLE: Analysis of a Hybrid Energy Storage System and Electrified Turbocharger in a Performance Vehicle

AUTHOR: Tyler Stiene

B.Eng., Mechatronics Engineering and Management

McMaster University, Hamilton, Canada

SUPERVISOR: Dr. Ali Emadi

NUMBER OF PAGES: xxi, 211

Lay Abstract

Electrified vehicles have not typically been viewed as performance vehicles. A recent trend has seen a growing number of manufacturers turn to hybrid and electric powertrains to produce high performing vehicles. However, a performance vehicle's electrical power is conventionally limited by the size and power of its battery, adding weight and cost. Two technologies offer the ability to increase the power of these electrified components without the need for a large battery. First, Hybrid Energy Storage System combines ultra-capacitors and batteries to increase the power density of the system. Second, an Electrified Turbocharger improves the turbo lag of a turbocharged engine and also recovers waste heat energy from the exhaust gases which is then used to propel the vehicle. This research identifies and demonstrates the potential impact these two technologies have when included in an American Muscle Car.

Abstract

This research investigates the effects of both a Hybrid Energy Storage System and an Electrified Turbocharger in a consumer performance vehicle. This research also attempts to support the development of a prototype vehicle containing a Hybrid Energy Storage System currently being developed at McMaster University. Using a custom simulation tool developed in Matlab Simulink, Simulink models of each of the technologies were developed to predict the behavior of these subsystems across multiple physical domains. Control modeling, optimization and testing was completed for both systems. In addition, controls modeling for the Hybrid Energy Storage System was integrated with the development effort for a prototype vehicle considering the specifics of real world components.

To assess the impact of these technologies on a performance vehicle platform, the simulation tool tested each technology using multiple vehicle variations. Three vehicle variants were developed, representing: a conventional performance hybrid design, a hybrid vehicle containing an electrified turbocharger, and a vehicle containing a Hybrid Energy Storage System. Electrical system peak output power was the vehicle

specification held constant between each vehicle variant. Each vehicle variant was simulated against a number of traditional drive cycles representing everyday driving scenarios in an attempt to compare fuel economy while identifying each technologies individual impact on the vehicles performance. Finally, each vehicle variant was simulated using a custom performance drive cycle in a virtual race.

Both technologies as assessed and in comparison to a larger battery variant, did not result in improved fuel economies during conventional vehicle driving. Both the Hybrid Energy Storage System and electrified turbocharger demonstrated improved vehicle performance in particular scenarios.

Acknowledgements

This research was undertaken, in part, thanks to funding from the Natural Sciences and Engineering Research Council (NSERC), the Canada Excellence Research Chairs (CERC) Program and General Motors.

Thank you to my supervisor Dr. Ali Emadi for supporting and guiding not only my graduate work but the projects and experiences that have made my education a much more enriching experience.

I would like to also thank the many members of the McMaster Formula Hybrid and McMaster Engineering EcoCAR 3 Teams for their commitment to more than just a traditional approach to education as well as their willingness to push the boundaries of technology.

Finally, I would like to thank my girlfriend Aubrey Gribbon, my friends, and family who have supported me constantly and always understood that my time at McMaster was more than just an education. It was a passion.

Notation and Abbreviations

AFR Air Fuel Ratio

AVTC Advanced Vehicle Technology Competitions

BEV Battery Electric Vehicle

CAFE Corporate Average Fuel Economy

CD Charge Depleting

CS Charge Sustaining

ECU Engine Control Unit

EDLC Electric Double-layer Capacitor

EPA Environmental Protection Agency

ESS Energy Storage System

EV Electric Vehicle

F1 Formula 1

GRA Graduate Research Assistants

HESS Hybrid Energy Storage System

HEV Hybrid Electric Vehicle

HWFET Highway Fuel Efficiency Test

LEV Light Electric Vehicle

LQR Linear Quadratic Regulator

EcoCAR Team McMaster Engineering EcoCAR 3 Team

MLR Minimized Loss Request

OCV Open Circuit Voltage

PCM Phase Change Material

PID Proportional Integral Derivative

RPM Rotations Per Minute

SOC State of Charge

UDDS Urban Dynamometer Driving Schedule

US06C US06 City Sections

US06H US06 Highway Secitons

Contents

List of Tables

List of Figures

Chapter 1

Introduction

The automotive industry is on the brink of perhaps the most aggressive period of change it has ever seen. This period of change is being catalyzed by advancements in technology and evolving government regulations. Vehicle propulsion, connectivity, ownership and the responsibility of the driver are likely to change. These changes will profoundly impact many problems with today's vehicles including fossil fuel consumption, efficiency, safety, traffic congestion and cost. It is difficult to imagine the car of the future, but with so many innovative technologies emerging in both the automotive and technological industries, radical changes are inevitable.

1.1 Vehicle Electrification

Vehicle Electrification is used as a blanket term to describe reliance on electric propulsion rather than internal combustion. Due to several differentiating characteristics of an electric propulsion system, an electrified vehicle tends to be more efficient than the conventional fossil fuel equivalent. Improvements in all major fields contributing to electric vehicles have resulted in substantial cost reductions and improvements in reliability and performance over the last two decades. Improvements in batteries, electric motors, power electronics, material light-weighting, and SoC's (System on Chip) have all contributed to the growth of vehicle electrification.

There are two major types of electrified powertrains. The first, a Battery Electric Vehicle (BEV) sometimes referred to as simply an Electric Vehicle (EV), or on smaller platforms a Light Electric Vehicle (LEV), converts electrochemical energy stored in batteries to kinetic energy via electric motors. The second, a Hybrid Electric Vehicle (HEV) combines electric motors and an internal combustion engine in wide array of different architectures. In comparison, a conventional vehicle uses an internal combustion engine to convert fossil fuel (chemical energy) into kinetic energy. All vehicles can be designed to achieve specific combinations of vehicle range, cost, efficiency, and performance within the limits of the vehicle's underlying technology. Electrified vehicles in general provide a means of creating a more efficient vehicle. However electrified powertrains may restrict other specification as result of the limits of the underlying technologies. The figure below summarizes the conventional, EV and HEV vehicles.

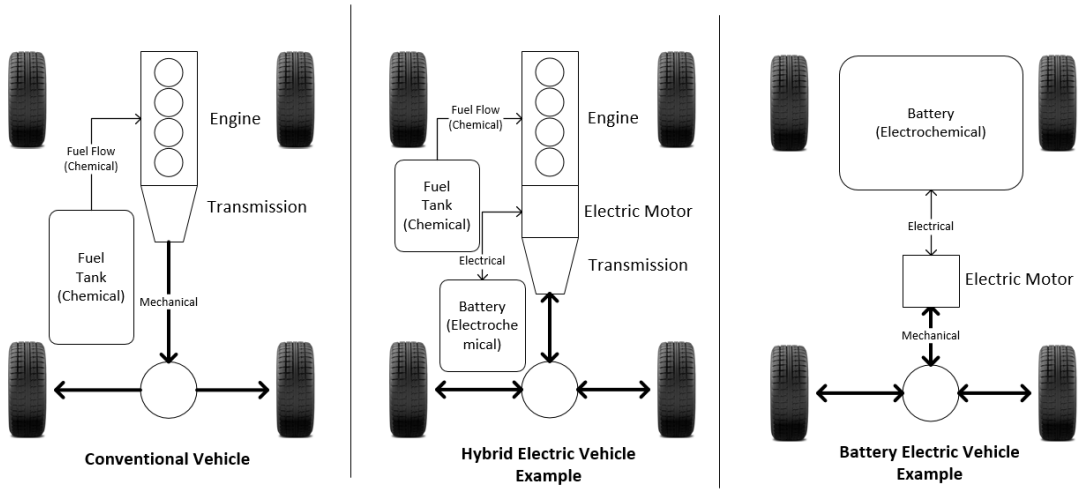

Figure 1.1: Examples Vehicle Architectures

1.1.1 Global Emission Standards

One of the driving forces of vehicle electrification is the desire to create more efficient vehicles. With global warming, air quality, and oil dependency concerns of both government and individuals, pressure has been placed on the automotive industry to produce cleaner more efficient vehicles. While EV's only account for a small market share of the overall vehicle market, some government policies have not had time to realize their full level of impact. An example of such a policy is the Corporate Average Fuel Economy (CAFE) standards which the US government has placed on vehicle manufacturers. The CAFE standards specify a target fuel economy that

manufacturers must achieve every year to avoid financial penalty. The policy considers the type of vehicle and is calculated by examining the mixture of vehicles sold by a manufacturer in certain markets.[2] The figure below shows the current requirements for a passenger vehicle with the 2012 Toyota Prius which is used by many as a reference point when comparing hybrid vehicle performance.

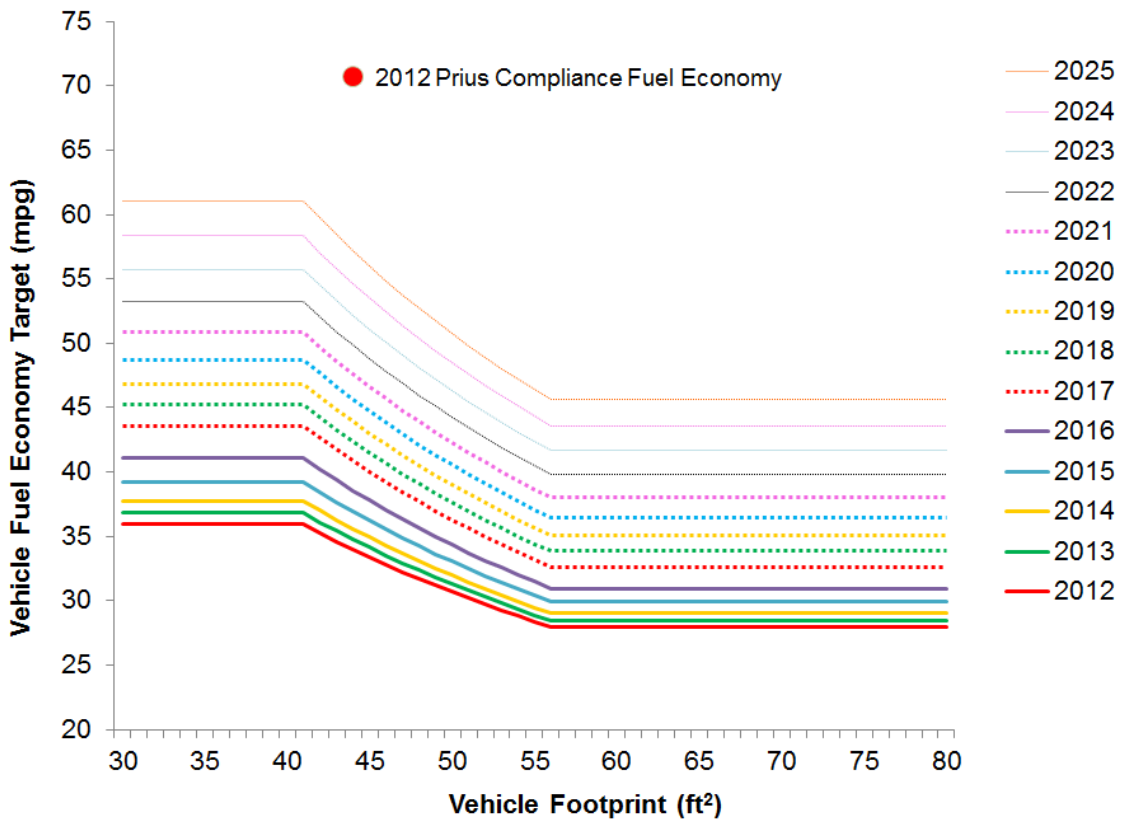

Figure 1.2: US CAFE Standard for Passenger Vehicles 2012 to 2025[57]

Governments around the world are creating policies to increase electric vehicle market

share by placing positive and negative pressure on the consumer. Policies including cash incentives, tax incentives, emissions taxes, and preferred parking can be found all over the world in an effort to promote greener vehicle choices. The table below briefly outlines some examples of these policies . While the table is not exhaustive and many incentives contain details and requirements that are to difficult to summarize in a table, it provides insight into the size and effect of the various policies. It is also important to note that many policies have short life spans and as a result many have already expired.

Table 1.1: Examples of Incentive Programs Focused on Promoting the Sale of Electrified Vehicles[59]

Location	**Incentive**	**Cut off**	**Announcement**
India	20% ex-factory price max ₹100,000	130,000 Vehicles	2014
France	€10,000 but capped at 30% of vehicle price varies with fuel economy		Updated 2015
Germany	Up to 4,000	440,000 Vehicles	2016
Denmark	Tax and Parking Incentives		2009
Sweden	Up to 40,000 kr subsidy	5,000 Vehicles	2012
United Kingdom	Up to GB£4,500		Updated 2015
Canada - Ontario	Up to CA$8,500	10,000 Applicants	2010
Canada - Quebec	Up to CA$8,500	CA$50 Million	2012
Canada - British Columbia	Up to CA$5,000	1,370 Vehicles	2011
United States	Up to US$7,500	200,000 Vehicles per Manufacture	2008

1.1.2 Levels of Vehicle Electrification

Unlike conventional vehicles, which consist of an engine and transmission driving the wheels, electrified vehicles allow for a variety of possible configurations. Within these configurations exist a range of complexities, power flows, and efficiencies. To help individuals understand various architectures, standard levels of electrification

have been defined to help categorize these vehicles into similar types and electrical performance levels. Figure 1.3 outlines the different levels of electrification with the conventional vehicle being represented at the origin of this chart.

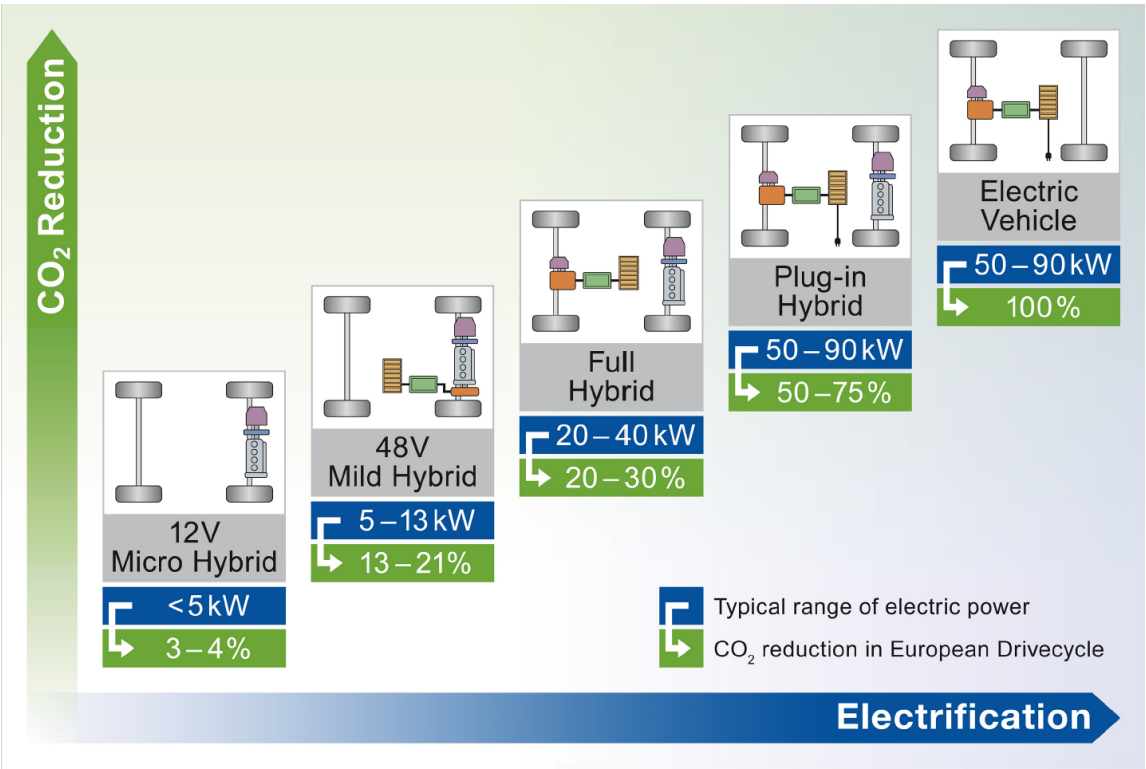

Figure 1.3: Vehicle Electrician vs CO2 Reduction[25]

1.2 Hybrid Electric Vehicles

As previously stated, HEVs combine internal combustion engines with electric motors to provide the vehicle's propulsion. HEVs represent electrified vehicle spectrum ranging from light hybrids to extend range electric vehicles. HEVs can further be categorized by the electrical power flow between components in the vehicle.

1.2.1 Series Hybrid

A series hybrid vehicle is identified by the mechanical disconnect of the internal combustion engine from the drivetrain of the vehicle. In a series hybrid vehicle, energy converted from fuel in the internal combustion engine is not directly sent to the drivetrain. It is first converted to electrical energy which is then stored in the battery or converted back to mechanical energy by an electric motor. This allows the internal combustion engine to be operated continuously at its most efficient operating point. However energy cannot be converted without additional losses which potentially limits the efficiency of the system. Series architectures tend to be best suited for higher levels of vehicle electrification in which large and efficient electrical systems are present in the vehicle. Figure 1.4 demonstrates a possible series hybrid architecture in which an electric motor operates as the primary drive and a second electric motor operates as a generator with the internal combustion engine.

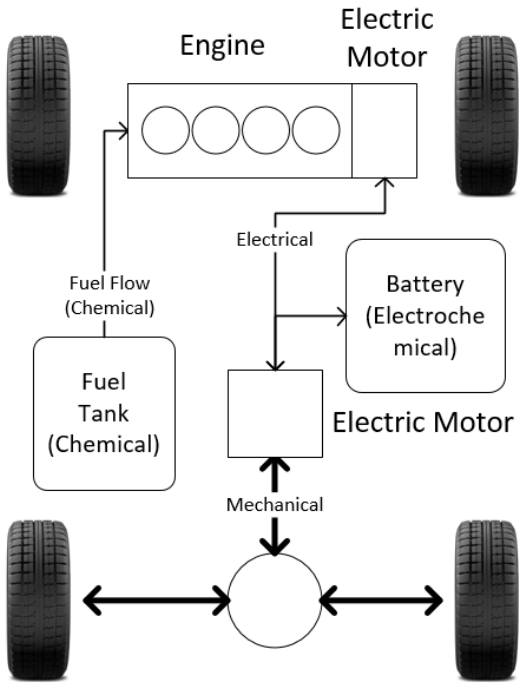

Figure 1.4: Series Hybrid Example

1.2.2 Parallel Hybrid

A parallel hybrid vehicle is identified by its ability to have both the internal combustion engine and electric motor propel the vehicle. These configurations usually include a disconnecting mechanism either on one or both of the power plants to achieve the ability to operate separately. Some parallel architecture configurations allow a complex blending of the two systems. In some configurations, the individual power plants may be responsible for producing torque on separate axles of the vehicle.

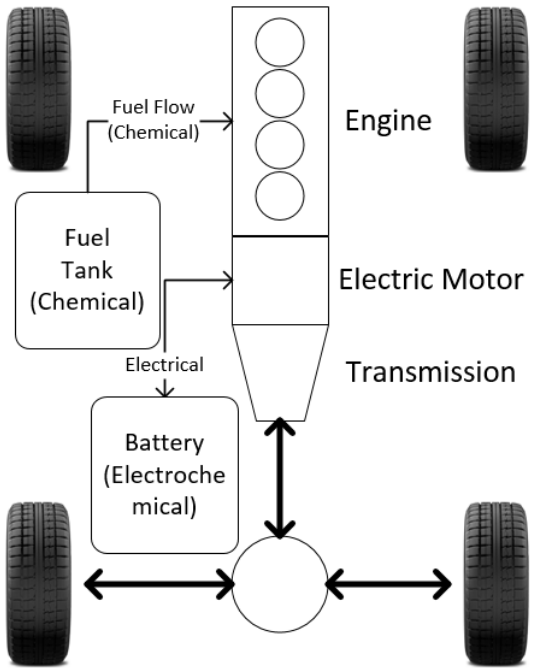

Figure 1.5: Parallel Hybrid Example

1.2.3 Series-Parallel Hybrid

A Series-Parallel hybrid is a vehicle that has the ability to operate in both series and parallel modes. This is usually achieved by disconnecting the internal combustion and an electric motor from drive-line while a secondary motor remains connected to propel the vehicle. These systems are complex but provide flexibility. It is common that series mode operation be performance-limited and that the vehicle will switch to parallel mode when the driver requests more torque than is available during series

mode operation.

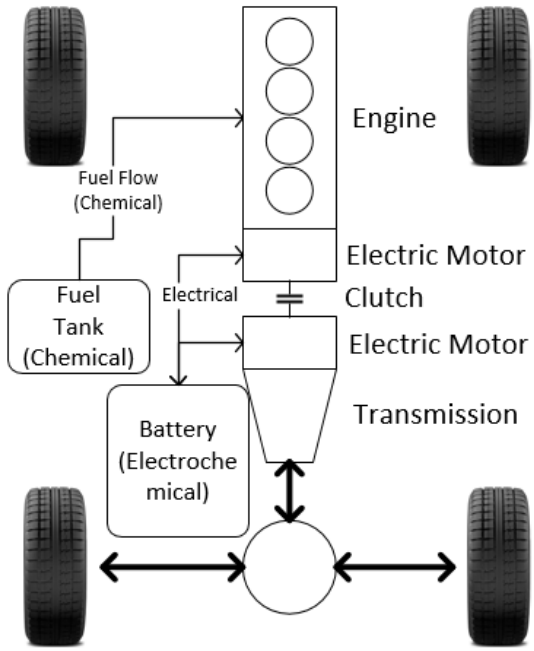

Figure 1.6: Series-Parallel Hybrid Example

1.3 Hybrid Energy Storage System

A Hybrid Energy Storage System (HESS) is an Energy Storage System (ESS) that is composed of two different types of energy storage components. This is analogous to a hybrid vehicle in which two different types of torque-producing systems are used to achieve propulsion. In both systems, component roles are duplicated in an attempt to capitalize on the positive aspects of each of the technologies.

A HESS could be composed of a number of different technologies that can store and retrieve energy. Some of these possibilities include batteries, capacitors, kinetic, hydraulic, and pneumatic energy storage systems. In some scenarios a HESS can be hard to identify. For example, a battery-battery HESS contains two different types of batteries to store and deliver required amounts of energy and power. For the purposes of this research, the HESS was defined to be a combination of batteries and ultra-capacitors to be used in an electrified vehicle.

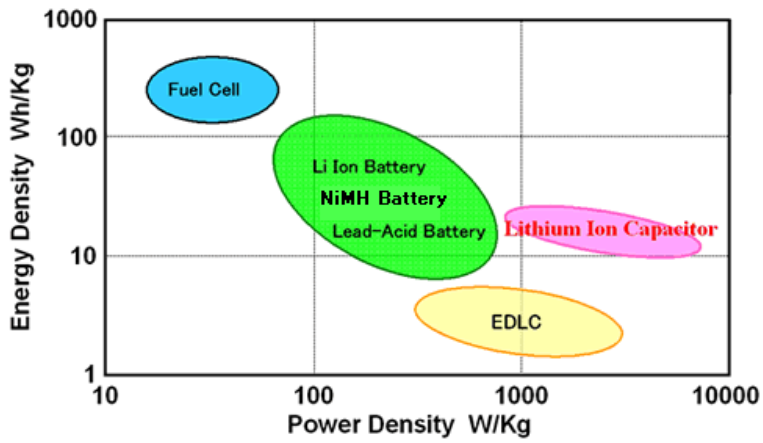

Figure 1.7: Ragone Chart Using Common Energy and Power Densities[58]

One of the primary objects of a HESS is to achieve power and energy density requirements not possible by any one technology. Figure 1.7 is a Ragone chart showing the energy density and power density ranges of several different energy storage technologies. Looking specifically at batteries and ultra-capacitors it can be seen that batteries are much more energy dense than ultra-capacitors while the

reverse is true for power density.

1.3.1 Typical Battery Configurations

In generating an understanding of an HESS, it is important to first understand what a typical battery configuration is for BEVs and HEVs. Batteries commonly use amp-hour (Ah) as a metric to describe both power and energy. While this works well in other applications that use lower fixed voltages (like electric drills) this is not common in the automotive industry. Standard units including Kilowatt-Hour (kWh) and Kilowatt (kW) are used to describe energy and power respectively in vehicle batteries.

Unlike many battery powered products available (cell phones, laptops), achieving higher voltages is important. Automotive battery packs are designed to meet a vehicles required operating voltage range, energy and power by connecting many smaller cells together in series and parallel to meet the requirements of the vehicle. A common notation is used to describe how cells are arranged in a battery pack. For example, a battery consisting of 20 cells in which sets of 4 are connected in parallel and these 5 sets are connected in series would be described as a 5s4p configuration. This simple notation uses numbers and letters to describe the arrangement of the cells. Figure 1.8 provides a visual representation of this battery pack.

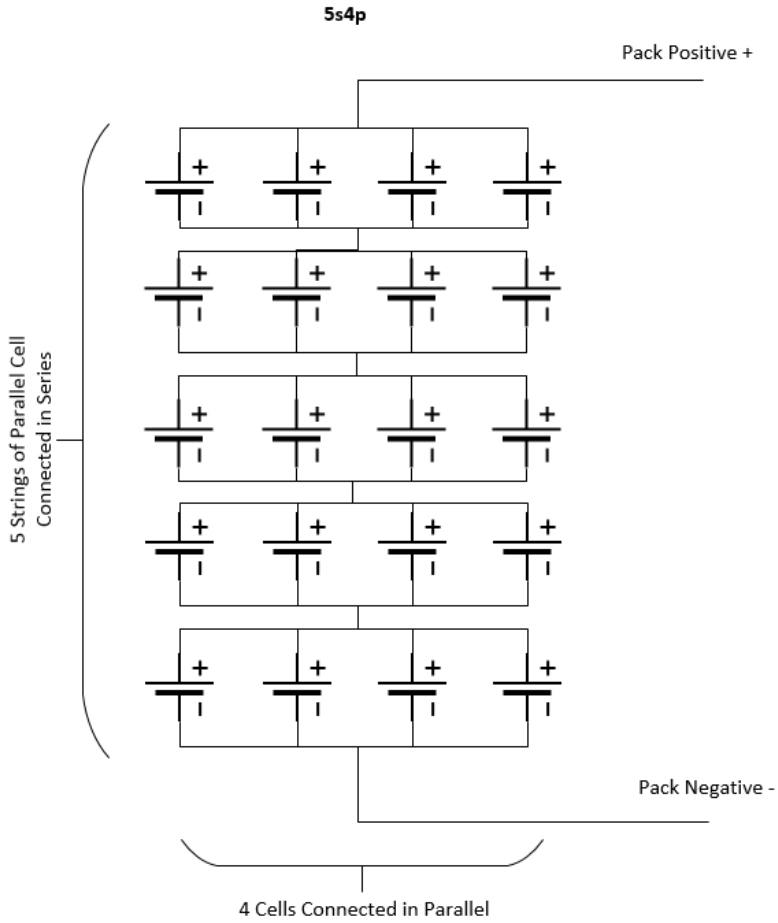

Figure 1.8: Example Battery Configuration

Developing an understanding of how connecting battery cells in series and parallel is important to understanding how a battery pack can be designed for a specific vehicle. Continuing with the 5s4p pack, using the specifications of the cell that will be used later in thesis the specifications of the example pack can be easily calculated. Table 1.2 contains the result of these simple calculations and present the energy, charge

power and discharge power of the 5s4p pack.

Table 1.2: Pack Configuration Example Using LG Chem HG2 Specifications[10]

Specification	**Cell**	**5s4p Pack**
Voltage Min/Max/Nominal	2.5/4.2/3.6 V	12.5/21/18
Capacity	3 Ah	12 Ah
Max Discharge Current	20 A	80 A
Max Charge Current	4 A	16 A
Energy	10.8 Wh	0.216 kWh
Discharge Power	72 W	1.440 kW
Charge Power	14.4 W	288 W

1.3.2 Hybrid Energy Storage Architectures

Figure 1.9 demonstrates a number of possible HESS architectures. While the figure does contain a number of architectures this figure is not exhaustive. HESS architecture affects the characteristics of the system as well as the number of controllable variables in the system. HESS architectures can be loosely divided into two major categories, active and passive.

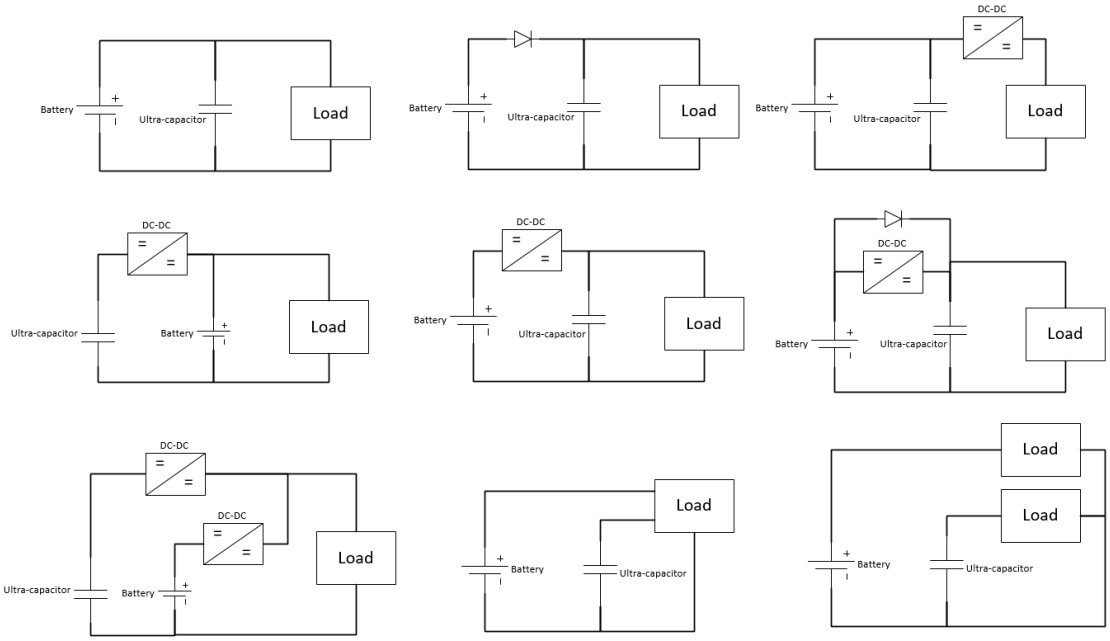

Figure 1.9: Examples of HESS Configurations

Passive HESS

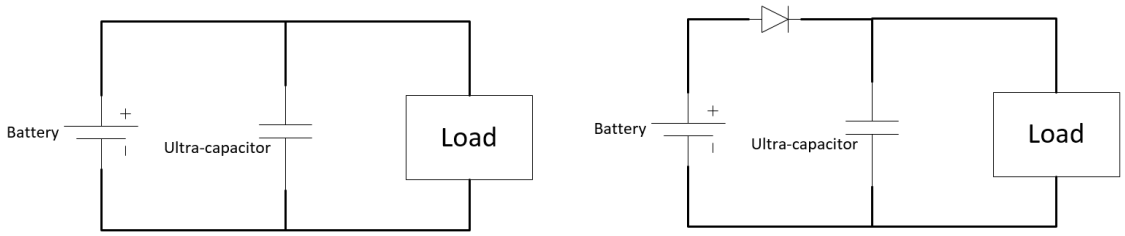

Figure 1.10: Passive HESS Configurations

A passive HESS architecture requires no additional power electronics to control the flow of energy in a HESS. Figure 1.10 outlines two different passive HESS architectures. The architecture on the left is the simplest architecture in terms of number of components required as no additional components are required for this system. As this HESS charges and discharges the voltage levels of these two storage components are fixed together. Due to the differences in internal resistances and transient response, current flow in, out, or between the ultra-capacitors and batteries can vary. This topology is difficult to design as in-depth model of each component is required to understand the behavior of the pack and to ensure safe operation of the components. In Chapter 2 the difficulties of creating accurate battery models will be discussed.

Another passive topology is presented in the right of Figure 1.10. Adding a diode

between the two energy storage systems changes the behavior of the system. While an in-depth model of the systems is still required, the discharge behavior and the interplay during charging has been simplified. This topology prevents the battery from charging when the HESS is charged through regenerative braking or series generation. While this may prolong the life of the battery, the loss of ability to recover the energy to the battery may limit the effectiveness of the entire vehicle.

Active HESS

An active HESS uses additional power electronics to control the flow of energy in a portion or all of the energy storage system. Figure 1.11 outlines two different active architectures. In general, active architectures are more controllable and require less initial design work at the cost of increased complexity and financial cost. It is also important to note that the efficiency of the power electronics may limit the overall efficiency of the HESS.

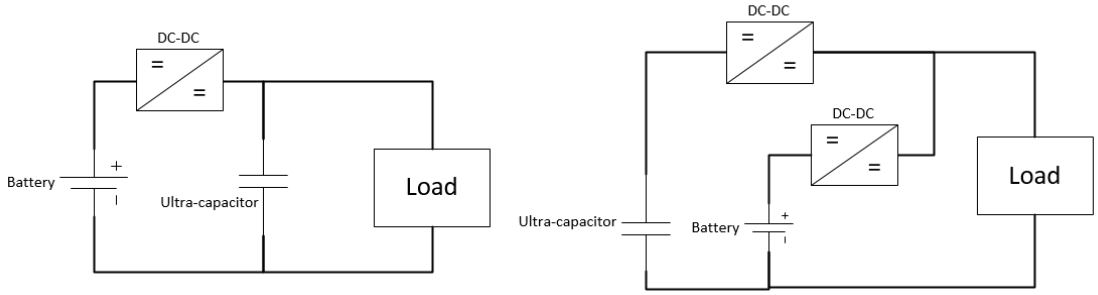

Figure 1.11: Active HESS Configurations

1.3.3 Novel Ultra-capacitor Designs

Although not a focus of this thesis, advancements in ESS technology have combined different types of technology at a more granular level. An example of this is the JSR Li-ion ultra-capacitor that is effectively both an ultra-capacitor and battery as it operates using principals from both technologies.

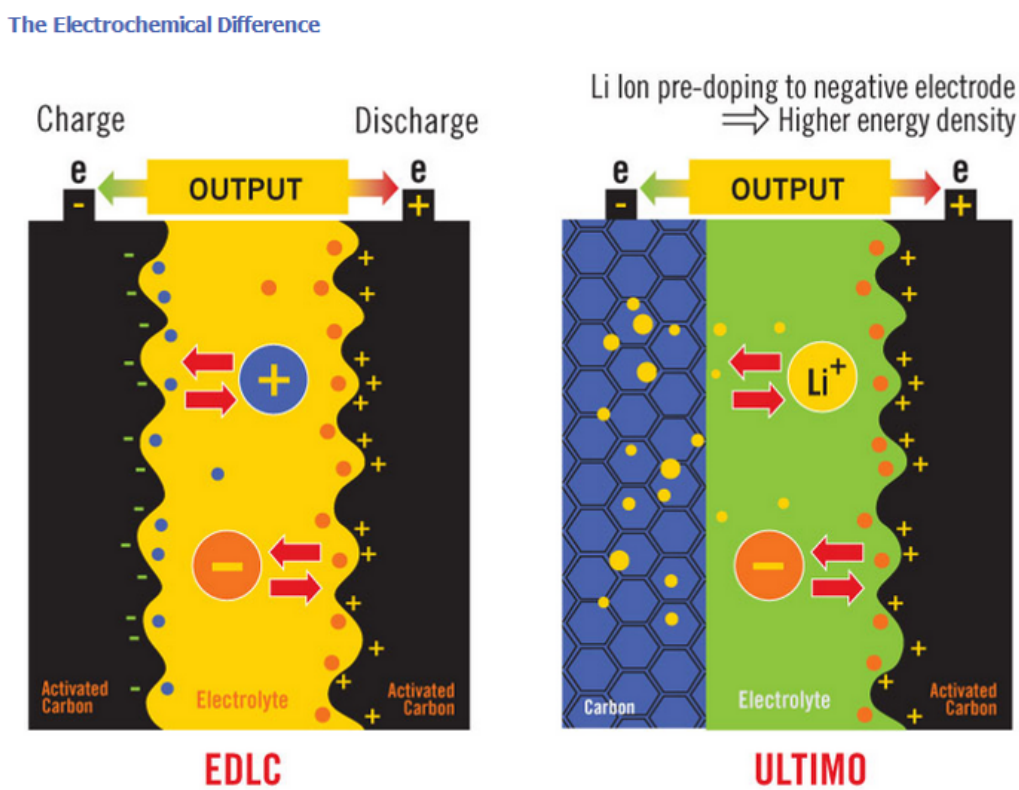

Figure 1.12: Comparison Between a Traditional EDLC and a JSR Micro Ultimo Cell[41]

JSR Ultimo is defined as a lithium doped ultra-capacitor as more of its electrical behaviour resembles an ultra-capacitor. What is unique about these cells is the pre-doping of the negative electrode, allowing for higher energy densities using a reaction that resembles a battery. Figure 1.12 provides a visual representation of the cell's design while Table 1.3 compares the cell's specification with a conventional ultra-capacitor and battery cell.

Table 1.3: Comparisons of a Battery, Ultra-capacitor and Li-ion Ultra-capacitor[10, 39, 40]

Specification	**LG Chem HG2 (Battery)**	**Maxwell K2 (Ultra-capacitor)**	**JSR Micro Ultio 3300**
Voltage Min/Max/Nominal	2.5/4.2/3.6 V	0/3/1.5 V	2.2/3.8/3 V
Capacity	3 Ah	3000 F	3300 F
Energy	10.8 Wh	7.7 Wh	4 Wh (Useable)
DC Resistance	25 mOhm	0.27 mOhm	1 mOhm
Max Discharge Current	20 A	2200 A	360 A
Max Charge Current	4 A	2200 A	360 A
Mass	48 g	520 g	308 g
Volume	65x18.5 mm (Cylinder)	138x60.7 mm (Cylinder)	150x93x15.8 mm
Energy Density (Mass)	225 Wh/kg	7.2 Wh/kg	13 Wh/kg
Power Density (Mass)	1.5 kW/kg	7.7 kW/kg	3.5 kW/kg

1.4 Turbochargers and Electric Turbochargers

Adding a turbocharger or supercharger attempts to increase both engine efficiency and power. The act of turbocharging or supercharging an engine involves pressurizing the intake plenum, which allows the engine to consume more air and burn more fuel for every engine cycle. Turbochargers recover additional power from the exhaust heat and

pressure energy while a supercharger uses a direct connection to the crankshaft. In both systems the power is then used to drive a compressor. Figure 1.13 demonstrates typical turbocharger and supercharger configurations. Turbochargers can be more beneficial as they use recovered waste energy from the exhaust gases instead of using mechanical power from the engine. This allows a turbocharged system to achieve higher efficiencies. However, taking energy from the exhaust can be delayed as the engine must generate substantial exhaust flow before the turbocharger can effectively pressurize the intake.

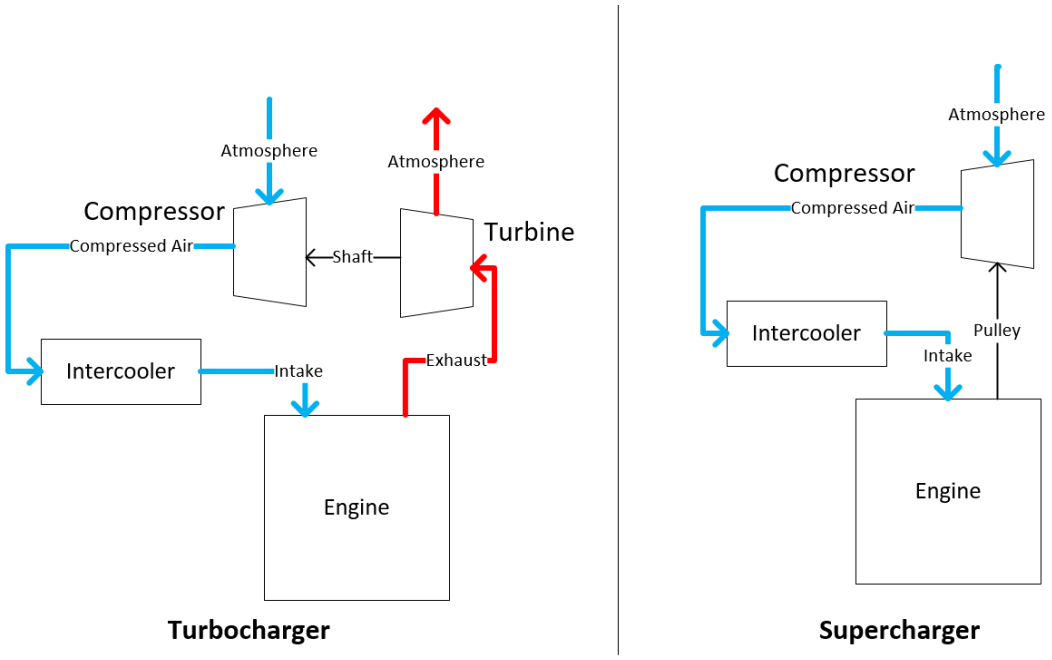

Figure 1.13: Comparison Between Turbocharger and Supercharger

1.4.1 Engine Downsizing

In an attempt to create more fuel-efficient vehicles, manufacturers regularly turn to turbochargers to make the engines more efficient. This is done through the practice of engine downsizing in which a smaller, more efficient turbocharged engine can be used to achieve the necessary peak power demands of the vehicle. The general principal behind this approach is understood when a typical efficiency map of an engine is examined. Internal combustion engines tend to be more efficient under load and not at their peak operating speed. Placing a large powerful engine in a vehicle results in the engine not being heavily loaded during typical driving. Figure 1.14 is an engine efficiency map. This demonstrates the typical efficiency behavior of an engine with the most efficient areas being in the lower RPM range and higher load (higher torque) regions of the map. When the engine is downsized, the continuous power demand of a vehicle is moved closer to this more efficient region allowing the vehicle to achieve greater continuous efficiencies while driving. Almost every manufacturer has an example of using engine downsizing and turbo-charging to achieve greater fuel efficiency. The process can also be seen in almost all vehicle categories from small economy vehicles to luxury or performance sedans and even SUVs and trucks.

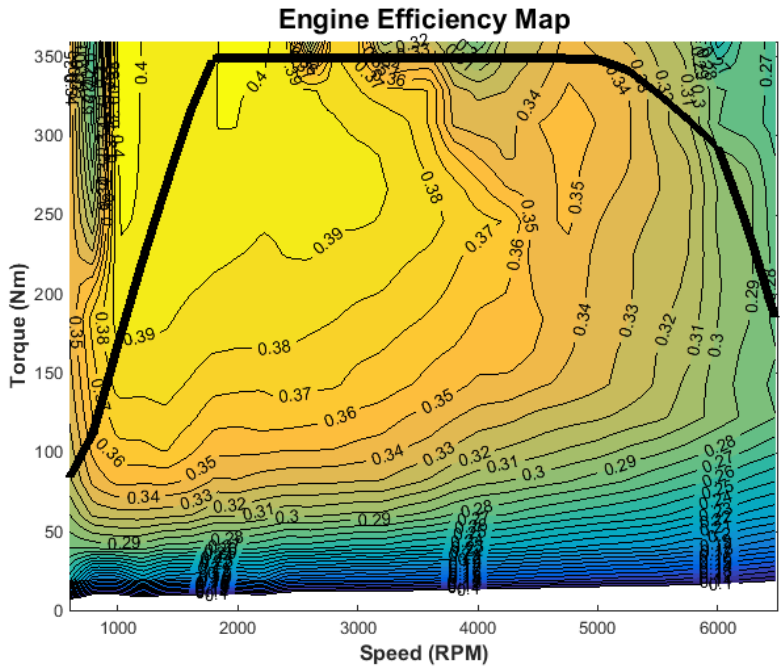

Figure 1.14: Example Engine Efficiency Contour Plot

1.4.2 Turbo Lag

Turbo lag is a major characteristic of a turbocharged engine. It is described as a delayed response of the engine to meet peak power demands from the driver. A turbocharger requires a significant amount of exhaust energy to reach efficient operation before it becomes effective at adding pressure to the intake plenum. During the time of low intake plenum pressure the engine is unable to burn enough fuel to meet the power demands resulting in a lag of performance. Manufacturers use many different techniques to reduce turbo lag and increase the engine's overall

responsiveness. These techniques include: twin-turbocharged configurations, internal design changes of the turbocharger, and creating shorter exhaust and intake plenum. Advancements in simulation and materials have also contributed to reducing turbo lag.

More recently, automotive manufacturers have explored using electrified systems to reduce turbo lag. Adding an electric motor to the shaft connecting the compressor and turbine or supplying an additional electric motor to operate a separate compressor allows an electrical system to aid in pressurizing the intake plenum. With turbo lag typically lasting through a small part of the operating range of a vehicle (a few tenths of second after the throttle has been opened) the additional electrical system only needs to apply a short burst of power to help the system reach its sustainable operating region. 1.15 is a simple diagram demonstrating the layout of components in one possible electrified turbocharger design and is the design that will be used later in this thesis.

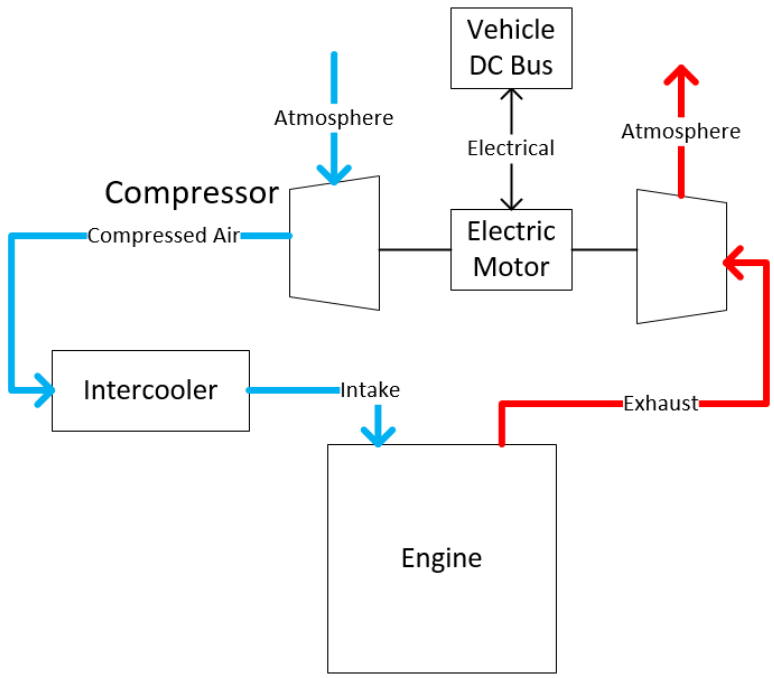

Figure 1.15: Electrified Turbo Configuration

1.4.3 Exhaust Gas Energy Recovery

Exhaust Gas Energy Recovery is the process of recovering energy from the heat and pressure of the exhaust. While a conventional turbocharger is an exhaust gas recovery system the energy recovered is only used to pressurize the intake plenum. Using a similar configuration discussed to reduce turbo lag, exhaust gas energy can be recovered and used by the electrical system. In a hybrid vehicle the recovered electrical energy can be used to either power the propulsion system or auxiliary

components within the vehicle. As the technology is relatively new, not all possible applications have been explored. Exhaust Gas Energy Recovery system tend to focus on vehicle applications that experience periods of high continuous engine load. While the average small sized passenger vehicle might not see large enough demands the trucking industry is an example that provides sufficient peak power demands. When a fully loaded large truck attempts to climb an incline or accelerate to high speeds, the demand on the engine can be large enough for an extended period of time. An exhaust gas energy recovery system may allow the engine to supplement a hybrid system without the need for a large battery. One notable example of exhaust gas energy recovery systems currently is its application in Formula 1. This will be discussed in greater detail in Formula 1 Electrification.

1.5 Current Automotive Trends

Government policies and the advancement in electrified technologies are currently contributing to a recent steady increases in electrified vehicle market share. The first electric vehicles were produced in the late 1800s however gasoline vehicle remained the dominant vehicle due to the relative ease of moving and storing energy as fossil fuels. In the late 1990's, the Honda Inight and the Toyota Prius were the first mass-produced electrified vehicles available for purchase. While BEVs have been available cost, range anxiety, and social perception of these vehicles have limited the adoption of HEVs and BEVs. Tesla's introduction of the Model S has change the perception of BEVs and has played a major role in many manufacturers placing focus on future electric

vehicles. Manufacturers including General Motors, Nissan, Volkswagen, BMW and Mercedes have announced that they will be selling competitive electric vehicles to Tesla's current offering within the next 5 years. Tesla's announcement of the Model 3 and its reception by the general public has demonstrates the willingness of the public to purchase electric vehicles if the vehicle meets certain requirements.

1.5.1 Electrification Market Share

While a large amount of focus has been placed on electric vehicles the overall market share remains small. Figure 1.16 below demonstrates the growth and market share over the last few years for plug-in vehicles. With total vehicle sales worldwide totaling more than 75 million the plug-in vehicle market share represents less than 1% of vehicles sold worldwide.[52]

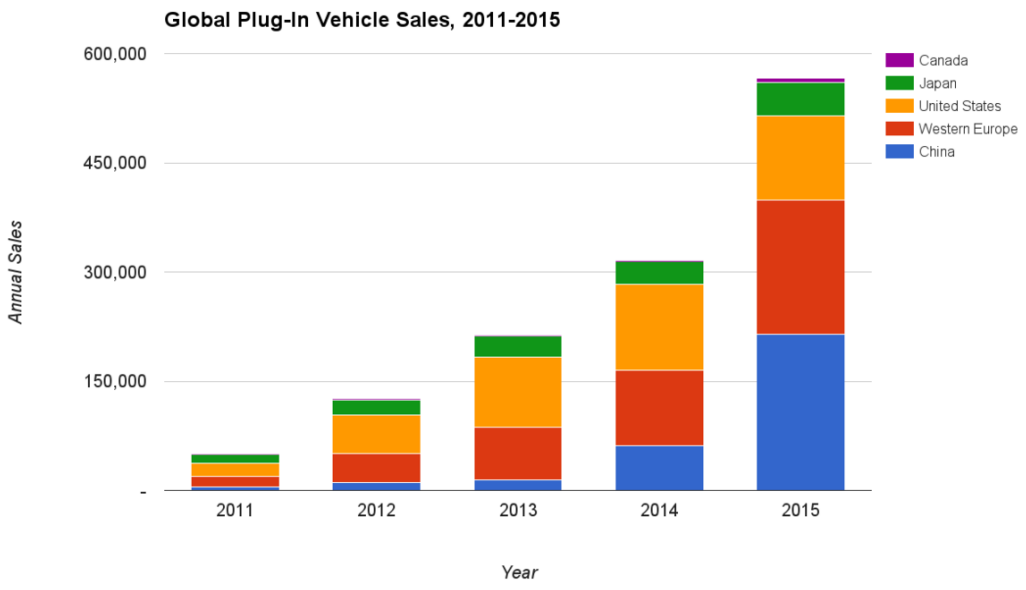

Figure 1.16: Global Plug-In Vehicle Sales, 2011-2015[26]

1.5.2 High Performance Hybrid Vehicles

Long-standing social perception have led most people to believe that hybrid and electric vehicles are underpowered. However, this perception is starting to change with the recent introduction of a number of high-performance hybrid and electric vehicles have garnered positive public recognition. A number of manufacturers including Honda, Porsche, McLaren, Ferrari, Koenigsegg, and Tesla have created hybrid and electric vehicles that rival or even exceed the performance of comparable

internal combustion engine based vehicles. With the price tag of these vehicles being substantially large, in comparison to the average price of a vehicle, one could hypothesize that these companies are using more premium price points with the intent to drive the cost of these technologies down for economical vehicles. This has openly been Tesla's strategy during the development of their vehicle line over the last decade. Table 1.4 outlines a number of high performance hybrid and electric vehicles currently available. It is interesting to note that for most of these vehicles, the electrified system is more of an assisted role rather then the predominant role. These manufacturers are most likely optimizing their design while keeping in mind the limits of the various technologies and the trade-offs made between performance and weight.

Table 1.4: Recent Hybrid and Electric Performance Vehicles[15, 16, 17, 18, 19, 20, 20, 21, 22]

Vehicle	**Total Power Output**	**Power from Electrical System**	**0 to 60 MPH Time**	**Top Speed**	**Battery Capacity**	**Year Released**	**Price (USD)**
BMW I8	357 hp	36 %	4.4 s	160 MPH	7.1 kWh	2013	$141,695
Mclaren P1	904 hp	19.6 %	2.8 s	218 MPH	4.7 kWh	2014	$1.15M
Ferrari LaFerrari	950 hp	16.9%	2.9 s	220 MPH	2.2 kWh	2013	$1.4M
Porsche 918	887 hp	31.5 %	2.5 s	218 MPH	6.8 kWh	2013	$847,000
Tesla Roadster	285 hp	100 %	3.7 s	1256 MPH	53 kWh	2008	$109,000
Tesla Model S P100D	463 hp	100 %	2.5 s	155 MPH	100 kWh	2012	$135,500
Koenigsegg Regera	1822 hp	38 %	2.8 s	250 MPH	4.5 kWh	2016	$1.9M
Honda NSX	573 hp	12.7 %	2.9 s	191 MPH	12 kWh	2016	$156,000

1.5.3 Electrified Turbo Chargers in Production Vehicles

While turbo chargers are commonplace in almost every manufacturer, electrified turbochargers have only seen one consumer application to date. The 2016 Audi TT Club sport uses an assisted compressor and a 48 volt system to reduce turbo lag. The system is not designed to recover any exhaust gases as the electric motor is only attached to a secondary compressor. A quote form Audi demonstrates the performance of the system. "Its electrically driven compressor lets it cover up to 16 meters (52.5 ft) within the first 2.5 seconds which is six meters (19.7 ft) further than a comparable car without this innovation."[32] This quote from Audi demonstrates both the impact of turbo lag on a performance vehicle and the impact of an electrified compressor on the overall performance of the vehicle.

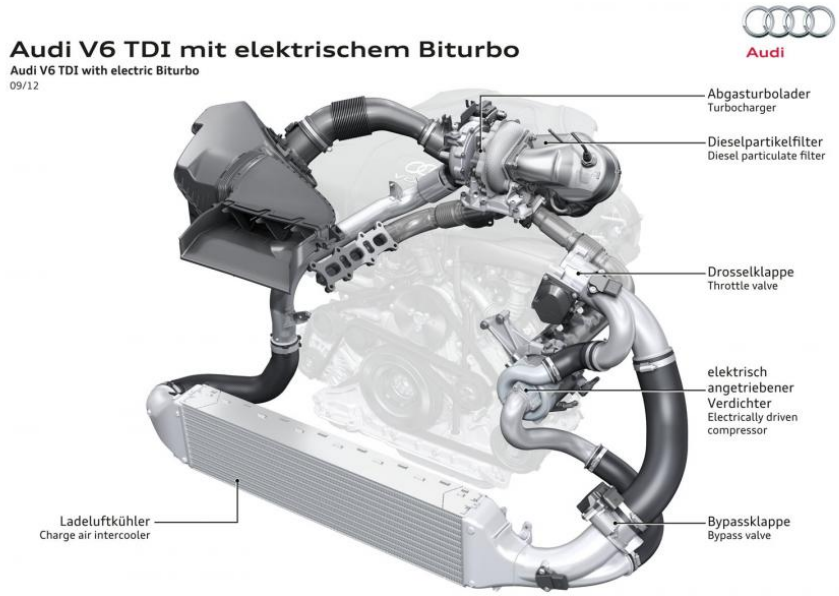

Figure 1.17: Audi Electric Bitrubo Diagram[30]

1.5.4 Formula 1 Electrification

Formula 1 (F1), for many years, has represented the pinnacle of automotive technology. F1 teams and their supporting companies are constantly innovating in part due to the continuous pressure to maintaining a technological edge over the competition Many of the technologies developed in F1 have later been applied to the consumer automotive market. Most recently, regulations placed on teams by the F1 governing body have required increased fuel efficiency on vehicles by specifying engine displacement, number of cylinders, total fuel consumption, fuel consumption rate and hybrid requirements. The use of regenerative braking and electrified turbocharger technology allows an F1 vehicle to achieve greater than 45% thermal efficiency of the fuel consumed by the vehicle. An article titled *Why an F1 car is more energy efficient than an electric car* discusses that today's electric car are only as clean as the energy used to charge their batteries. With most of the United States powered by coal at a thermal efficiency of typically 33%, the well-to-wheel efficiency of an electric vehicle in most states is less than a F1 vehicle before the electric vehicle even begins to drive.[27]

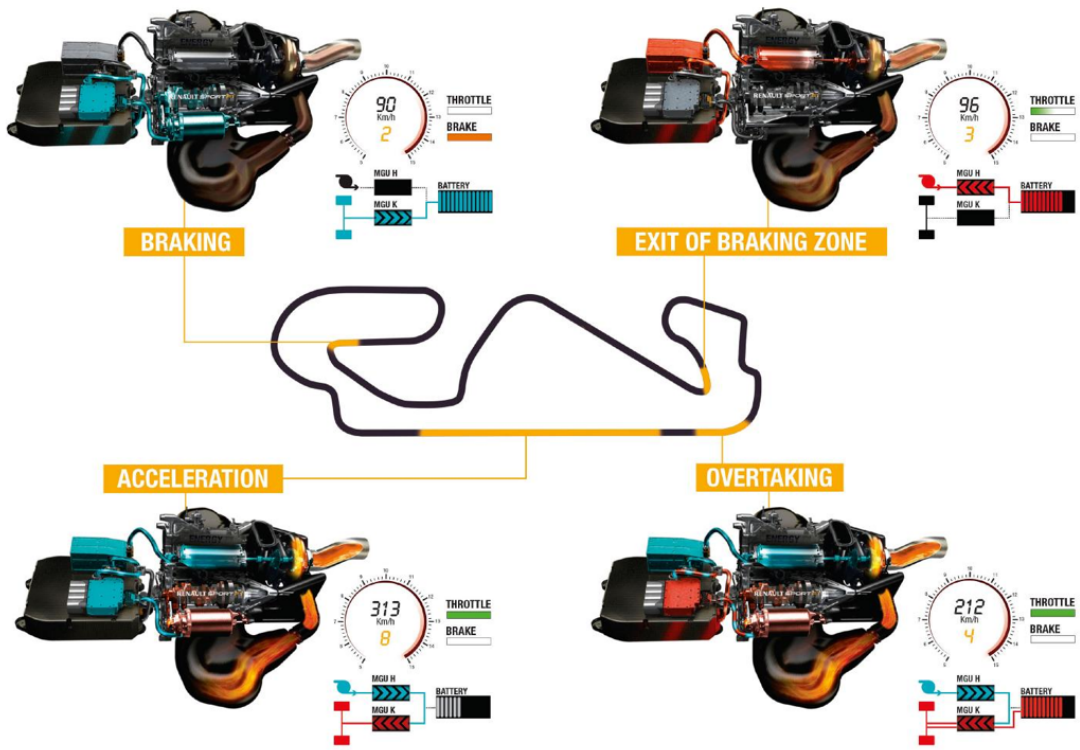

Figure 1.18: F1 Hybrid Operations[28]

The electrified turbo charger system present in F1 is a major influencing factor for investigating the effects in a consumer application. The energy recovered from the exhaust gases is sent to either a battery or electric motor, resulting an electric boost of greater than 160 hp for up to 4 MJ (1.1 kWh) per lap. Available information suggests that more than 2 MJ (500 kWh) is recovered per lap through the MGU-H (electronic turbo) system. With a typical lap lasting for roughly one minute thirty seconds, to recover that amount of energy the system must be capable of generating

greater than 60 kW of power.[46] Figure 1.19 is a picture taken at a Magneti Marelli booth of several components developed for an F1 electrical system. It can be seen in the image that Magneti Marelli advertises that the MGU-H (top left) is capable of 90 kW of power.

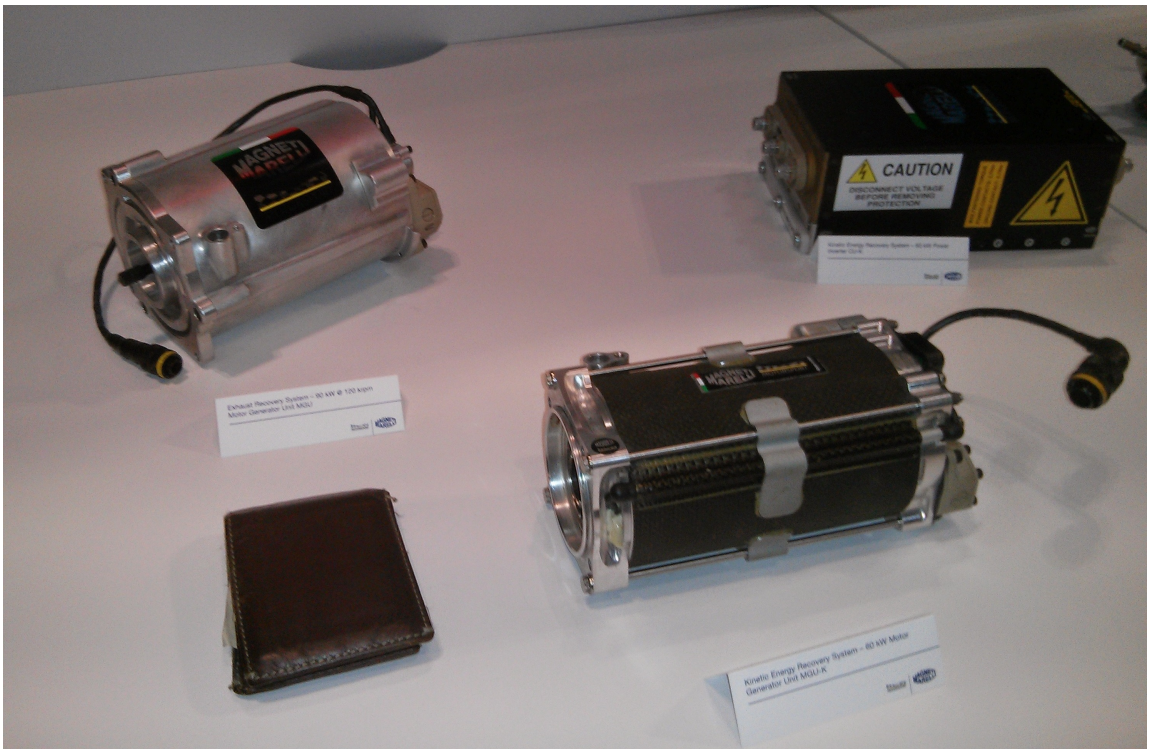

Figure 1.19: Image of F1 MGU-H and MGU-K Developed by Magneti Marelli

1.6 EcoCAR 3 Competition

The EcoCAR 3 competition, hosted by General Motors, is a student automotive design and integration competition in which 16 universities follow General Motors' vehicle design process to attempt to convert a 2016 Chevrolet Camaro into a hybrid electric vehicle. EcoCAR 3 is part of General Motors Advanced Vehicle Technology Competitions (AVTC) which has seen numerous platforms and design challenges over the last two decades. McMaster is one of the two Canadian teams currently competing in the EcoCAR competition. As a graduate research assistant working on the EcoCAR 3 project, this thesis includes work completed for this project. Many students have contributed to the project but the majority of the work discussed within the thesis has been completed independently. Every effort will be made to distinguish between independent and collaborative work throughout this thesis.

1.6.1 McMaster Selected Architecture

In the 2015/2016 Academic Year, The McMaster Engineering EcoCAR 3 Team (EcoCAR Team) was responsible for determining the architecture of the vehicle. Simulation and modeling efforts in Matlab and other applications allowed the EcoCAR Team to select both the architecture and the components to be integrated into the prototype vehicle. With a focus on performance, components were selected to achieve a final vehicle design that would rival comparable internal combustion engine vehicles. A P1-P2 Series-Parallel hybrid architecture was selected using a combination of

feasibility, expected powertrain behaviors, and cost. Figure 1.20 represents the powertrain selected by the EcoCAR Team and identifies the key components of the vehicle. With the inclusion of a clutch between the P2 motor and the engine, the vehicle is capable of running in both series, electric or parallel modes as discussed earlier.

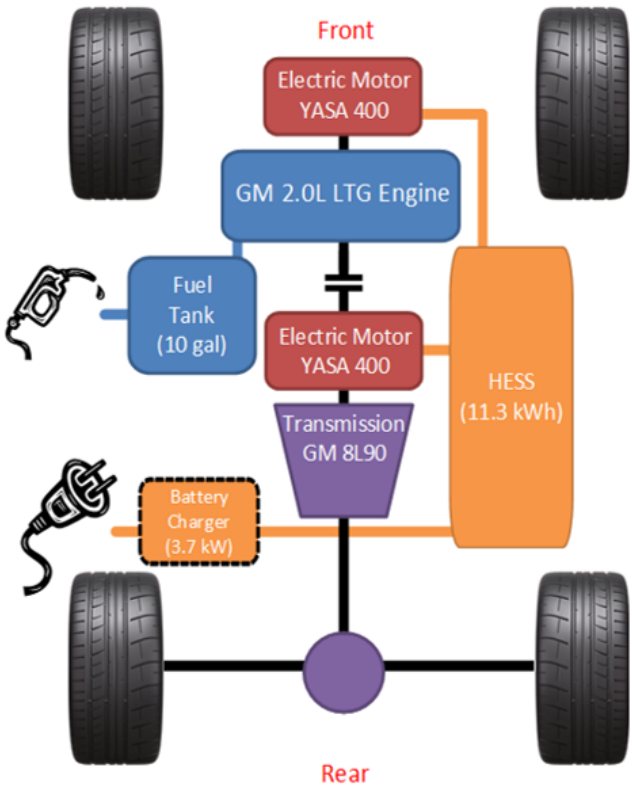

Figure 1.20: McMaster Selected Vehicle Architecture

McMaster Selected Hybrid Energy Storage System

In an attempt to allow the electrified system to contribute more to the performance of the vehicle, the EcoCAR Team opted to design and build a HESS. The intent of the HESS was to increase the power density of the energy storage system beyond that of a typical battery system, and enable the full use of the selected electric motors. The EcoCAR Team went through a separate architecture selection process for the HESS design. An ultra-capacitor battery active HESS architecture was selected as the best option for the requirements of this vehicle. The diagram below depicts the HESS that will be built for the vehicle.

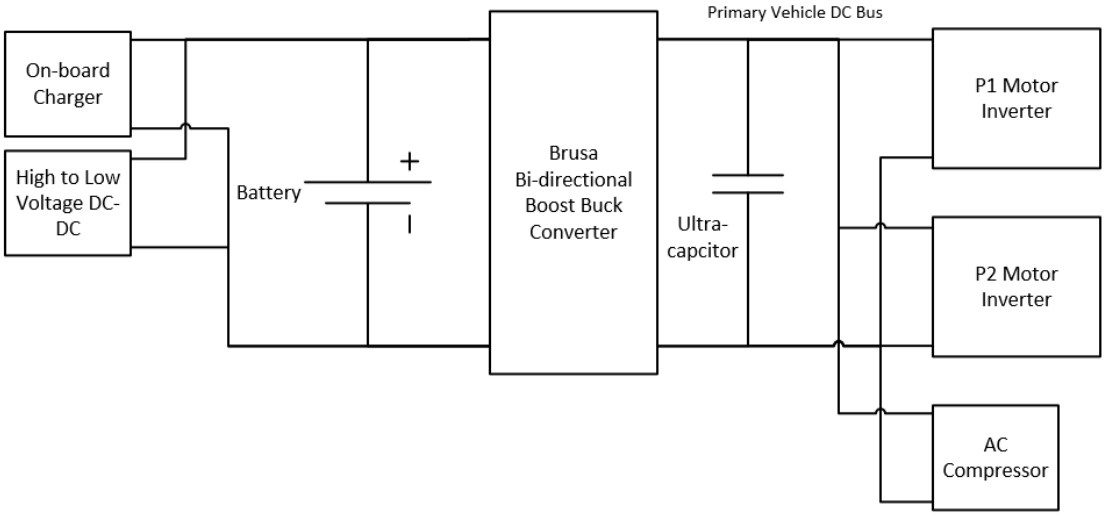

Figure 1.21: McMaster Selected Hybrid Energy Storage System Architecture

1.7 Research Objectives and Scope

The objective of this research is to assess the impact of including a Hybrid Energy Storage System or Electric Turbocharger in a performance focused hybrid vehicle. The research will attempt to identify and demonstrate the benefits of implementing both technologies. The research will also attempt The McMaster Engineering EcoCAR 3 team in developing a working hybrid energy storage system prototype for the prototype vehicle.

First, both technologies will be modeled in Matlab Simulink with the intent that these models be included in the EcoCAR Team's simulation tool and then used for to complete a comparative analysis. The models and control algorithms developed should also include methods to properly analyze the limits of this technology and be compatible with work done by other members of the EcoCAR Team. Finally, the various technologies will be compared using a simplified P1-P2 Series-Parallel architecture. This will allow the assessment of both technologies for efficiency and performance during both conventional and performance driving.

Chapter 2

Vehicle Electrification Advancements Literature Review

The purpose of the literature review is to highlight some of the work in the advancements of vehicle electrification. The intent of this literature review is to specifically look at methods and trends currently used in the research that relate to the work being done for this thesis.

2.1 Hybrid Energy Storage Systems

The use of HESS for vehicles has been the topic of research for a number of years. After reviewing literature, there are two general themes of focus when looking at

a vehicle application of a HESS. The first is the need to achieve a specific energy and power combination while the second observes the behavior of the HESS and its impact on battery life. A review of HESS systems in general also identified the use of HESS systems in other applications including grid leveling and rail systems. Siemens and ABB have both developed HESS systems for rail vehicles using a combination of ultra-capacitors and batteries.[1, 3]

2.1.1 Battery Modeling

An extensive amount of research has been conducted in the area of battery modeling for vehicle applications. This research consists of creating a representative model and the use of real life data to parameterize and simulate the battery. While numerous battery models exist, a common modeling approach uses what is referred to as a SOC-R model. This model uses equivalent electrical components in an attempt to simulate the behavior in response to electrical demands on the battery. In order to represent the transient behavior of the battery the model can be extended with an RC circuit connected in parallel (SOC-R-RC). Many resistors and capacitors can be connected in an attempt to model complex transient behavior. A voltage source in the model is dependent on the current State of Charge (SOC) which is tracked using coulomb counting. Some applications attempt to capture the changing dynamics of the capacity, resistance, and transients by varying model parameters with respect a number of additional factors. A major problem with current modeling techniques is tracking the degradation of the cell and how parameters can be updated

with time. Further examples of this type of modeling can be seen in works cited here.[31, 33, 34, 50]

When parameterizing models, the type of data is important and in some cases the lack of sufficient data results in the inability to model certain aspects of the batteries behavior. As an example the parameterization of the SOC dependent voltage source usually relies on accurate testing data of the SOC vs Open Circuit Voltage (OCV) relationship. Data of the OCV at various SOC is needed in order to recreate this relationship. In some instances, data is available from the manufacturer but this data is usually limited. The R and RC circuit components attempt to model the end series resistance and recovery time constant behavior which require different sets of data and tests to determine. Again, this information may be available from a manufacturer but will usually be limited. In some of the reviewed literature additional relationships were modeled including how resistance and energy change with temperature and cell degradation. This requires a great deal of information which is very rarely available and must be determined through advanced testing processes. An example of this type of modeling can be found in this work.[31]

2.1.2 Vehicle Applications

The majority of research into HESS systems for vehicle applications focuses on the assessment of HESS architectures. A review of the literature suggests a wide range of vehicle applications and HESS architectures have been assessed. Applications ranging in size, vehicle type and electrical demand were reviewed. In most of the research

reviewed, active HESS architectures were used, in which specific DCDC converters or power electronics were a critical element to the design of the HESS. In only one scenario a HESS was tested at the University of Campinas, Brazil. In this vehicle, ultra-capacitors and batteries were used in combination through a dual input inverter. More than half of the reviewed literature used test bench setups as a proof-of-concept of the electrical behavior of the system in combination with simulation. Cost and complexity of testing these in-vehicle proved to be a barrier to in-vehicle validation of HESS systems.[9, 14, 42, 43, 44, 51, 53, 60, 61]

The majority of the literature reviewed provided details into the control strategy used to manage energy between and from the energy storage components. While many control strategies focus on either maintaining balance or meeting peak power demand, one thesis discussed the use of real time GPS data in an effort to predict future power demands correcting the system balance to prepare for expected future events[43]. Selection and sizing process was identified by some of the research as an important aspect when designing a HESS and that not all HESS solutions perform better than a conventional ESS.[14, 43]

Research focusing on meeting peak power demand focused on the use of the Ultra-capacitors. The decoupled Battery HESS architecture was a popular choice among high power applications.[14, 42, 43, 60] For higher power demands, cost of power electronics factored into choosing HESS architectures. Some HESS systems allowed for increased regenerative capabilities of the vehicle in comparison to a conventional ESS. This was especially true in HEV and LEV containing smaller ESS systems as

not all battery systems can handle the load and the regenerative power supplied by vehicle braking.[42, 44, 53] In some scenarios, this additional regeneration can result in greater vehicle efficiencies. In research that accounted for size and weight of the system, improvements in meeting vehicle demands can be seen by a properly designed HESS system.[51]

Battery life is a primary focus of some reviewed HESS literature. Many individual research efforts quote reduced power demands, reduced cycling and reduced thermal impact as contributing factors into extending the life of the battery. The research identified battery life of EV vehicles as one of the limiting factors hindering widespread adoption. Control strategies focus on maintaining a constant load from the battery using the ultra-capacitors to manage the fluctuating power requests.[51, 60]

2.2 Electrified Turbochargers

With the trends of vehicle electrification and engine turbocharging both contributing to increased fuel efficiency in vehicles, the combination of the two technologies is an evolutionary step that has been explored over the last several years. Electrified turbochargers have recently gained research interest with publications both in the academic and private-sector becoming more prevalent. Depending on the focus of the application, the terms exhaust gas energy recovery, turbo compounding and electrified boost are used to describe various electrified turbocharger systems. There is a growing number of applications exploring exhaust gas energy recovery or turbo compounding.

The trucking industry appears to be actively exploring this application citing vehicle demands and typical use of turbocharged diesel engines as ideal candidates for this application. The use of an electrified turbochargers to reduce turbo lag is more commonly targeted at the performance segment and only few a vehicle segments exist in which the two applications intersect.

2.2.1 Electrified Turbocharger Models

Models of turbocharged engines and electrified turbocharger systems have been created using a number of different methods depending on the area of interest and desired output of the simulation. While mathematically based models can be developed there exists a number of tools available that allow expedited modeling of a turbocharger physical system. AMESim, Ricardo, Gt-Power, and Dspace all provide solutions for modeling combustion engine and turbochargers. The original intent of these tools was not to focus on electrification but tuning and development of conventional engine systems. Looking more specifically at the modeling of a turbocharger, some models exist specifically to analyze both the compressor and turbines interaction with the flow. These models focus more on designing the turbocharger as a subsystem than analyzing interaction of the turbocharger at the system level.[5, 8, 12, 29, 36, 47, 49, 54]

It is common for a system level analysis to use mean value models to investigate the averages of the major variables in the system. In these models, real life data or manufacturer performance maps are used as the basis of the simulation. If there is a lack of real life data, equations derived from thermodynamic first principles are also

used. Rarely is there an attempt to model effects of piping on flow and losses of heat through the non-major components of the model. At the highest level, these models attempt to calculate average energy in and between the system components without focusing on any one interaction at a high fidelity. [5, 29, 36, 54]

A few models attempt to go further than just the average behavior of the components. For instance the valve train of the engine, which controls the flow of air into and out of the pistons, is included in some models. This results in a more accurate representation of the flow. Some turbo charged configurations can be affected by the pulsing nature of the flow. However when manufacturer efficiency data is used the accuracy of the model may not improve by attempting to model the individual behaviors of components at higher fidelities.[8, 49]

2.2.2 Electrified Turbocharger Impact

After reviewing literature, loading conditions appear to be the most important aspect in determining whether or not an application will benefit from an electrified turbocharger. In higher load scenarios, it is possible to see efficiency increases of roughly 4 to 5 percent. Studies involving diesel trucks demonstrated the highest efficiency gains, as engine and vehicle demand cater to the ability of a electrified turbocharger to recover energy. It is interesting to note that many applications use a very basic system architecture, usually consisting a single turbo or additional turbine or compressor. Some of the literature comments on the importance of turbine and compressor sizing in ensuring effectiveness of the system.[5, 8, 29, 49]

The ability to reduce turbo lag was found in every situation in which it was studied. Some studies only looked at the use of the system to reduce turbo lag and did not include any methodology for recovering exhaust gas energy. One study in particular commented on the engine downsizing, demonstrating that a 1 liter engine could fulfill the requirements of a normally aspirated 1.4 liter engine without any noticeable lag in performance.[5, 8, 29, 36, 47, 49, 54]

Chapter 3

Vehicle Model

A vehicle model is the mathematical representation of a vehicle that can be solved over a period of time. This determines how the vehicle would perform given a prescribed situation. Generally, a vehicle model is also used to help determine the best controls methods, component selection, and systems behaviors so that the vehicle meets performance and efficiency requirements. Vehicle models can range in complexity but generally include a few key major components. A rolling chassis model represents the vehicle's dynamics including its weight, rolling resistance, aerodynamic loads and may be represented in up to three dimensions. The powertrain model includes approximate efficiency and operating behavior of primary propulsion components including the engine transmission and drivetrain. The vehicle control logic is included and are complementary to the fidelity of the model they intend to control. Simplistic strategies may be used however higher fidelity models allow for the development

of more complex control strategies. Finally, a driver model is included to act as a closed loop feedback for the vehicle when being tested against a desired event. This chapter will attempt to explain the work done by others that was used as the starting point for the research. To gain further insight into the work done by other Graduate Research Assistants (GRA) the thesis written by Joel Roleveld, Kamran Arshad and Alex Lebel can be reviewed.[8, 48]

3.1 Matlab and Simulink

While there exists a number of different software tools available to create vehicle models Matlab provides an excellent platform for both modeling and developing vehicle controls. Simulink, a component within Matlab, is especially adept at creating models using a visual block based approach through the use of a graphical user interface and a large library of predefined code and solving methods. Simscape, a component within Simulink allows for modeling of physical components in predefined domains including electrical, mechanical, and hydraulic. Simscape can simplify modeling complex physical systems and thus the process of modeling and testing systems. For controls development, Matlab provides data analysis tools, optimization tools, the ability to generate code for deployment to microprocessors, as well as providing Stateflow, a component within Simulink for creating State Machines and Flow Diagrams. All of Matlab's tools can work together seamlessly, providing an individual or team the ability to create both in-depth models and control logic for a given system. Examples of Simulink, Simscape and Matlab code will available

throughout this thesis and will be clearly identified as to which is being represented.

3.2 McMaster Simulation Tool Overview

As mentioned in the introduction the EcoCAR Team has developed a simulation tool to aid in the development of a hybrid electric vehicle. This tool is an organized platform of component models, control logic, and simulated scenarios. The tool includes modeling efforts completed by other GRAs and undergraduate students. A great deal of effort has already been placed in developing the controls for the vehicle as well as for individual subsystems. In some cases, the work completed for the EcoCAR Team's vehicle is not ideal for the comparison required in this thesis. In these situations, an explanation of the modifications made and work completed will ensure a more transparent analysis of the technologies that are the focus of this thesis. Unless otherwise noted, the models of the base vehicle have been created by other students. While some of the controls logic developed for the vehicle has been completed to optimize the vehicle's performance, in some cases these efforts have been removed and replaced by simplified control logic.

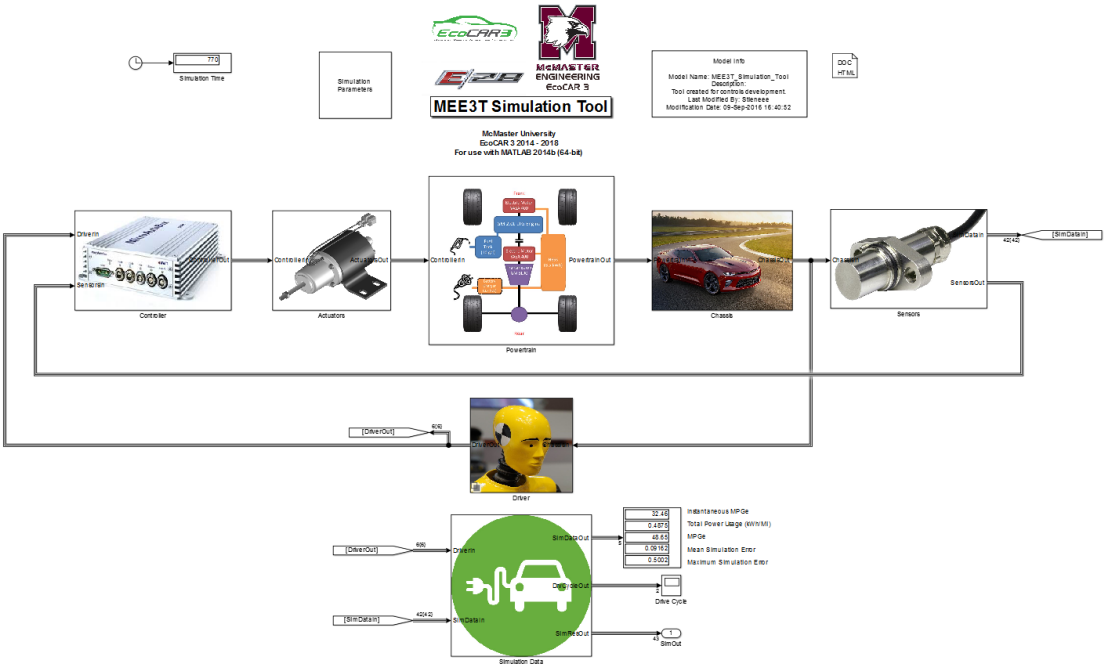

Figure 3.1: Top Level of McMaster Engineering EcoCAR 3 Simulation Tool

Figure 3.1 is an image of the top level model of the simulation tool. The tool is broken down into the various major sections of a vehicle model. As new models and control logic are developed, they can be easily interchanged by changing one of these blocks. This concept is referred to as Model Referencing in Simulink. Model Referencing has been used at a number of layers within the simulation tool and extends down into the powertrain, controller, and driver models. For this thesis, new powertrain models, controllers, and driver blocks were created containing combinations of new and old content in an effort to efficiently model and control the systems being tested.

Fidelity of a vehicle model is in part determined by the timestamps and solution method of the simulation. With the objective of maintain faster than real time simulation, a time step of 0.01 seconds was selected by the original creators of the tool as an acceptable base time step. At 100 Hz, some system behaviours are not fully simulated, including high frequency switching in the electrical systems. However, meaningful results can still be obtained without full simulation. Matlab provides both discrete and continuous methods of solving models in Simulink. However with the complexity and diversity of models and control algorithms integrated in this tool a discrete solution method is used. Closed loop information is delayed one time step where necessary including various sub models and once in the driver vehicle loop. The delay of information occurs in a similar manner to how information would be delayed as a result of sensor readings and driver reaction.

3.3 Drive Cycles

Drive cycles are prescribed speed vs time data sets that are used as the input to a vehicle model. These drive cycles are defined by outside parties and are used frequently by manufacturers and governing bodies to assess vehicles. Drive cycles range in length and complexity, but usually attempt to mimic the average driving in certain regions. Drive cycles used in this thesis include the HWFET, US06 Highway Secitons (US06H), US06 City Sections (US06C) and the DC505.[4] While the HWFET is a complete cycle, the other cycles outlined here represent sections of US06 Supplemental Federal Test Procedure Driving Schedule and Urban Dynamometer Driving Schedule (UDDS).

All the cycles listed above are defined by the Environmental Protection Agency (EPA). Typically a number of drive cycles are used to determine the overall performance of the vehicle. The McMaster Engineering EcoCAR 3 Team primarily uses a specific combination of drive cycles defined by the EcoCAR 3 competition which will be referred to as the EcoCAR 4 Cycle. The EcoCAR 4 Cycle will be used to assess the efficiency of the vehicle which is a defined weighting of these drive cycles to be used when calculating the vehicle fuel economy. The exact weightings of the EcoCAR 4 Cycle have not been included in this document as they are protected as confidential information as part of the EcoCAR project. Figure 3.2 is a graph of the four drive cycles discussed above.

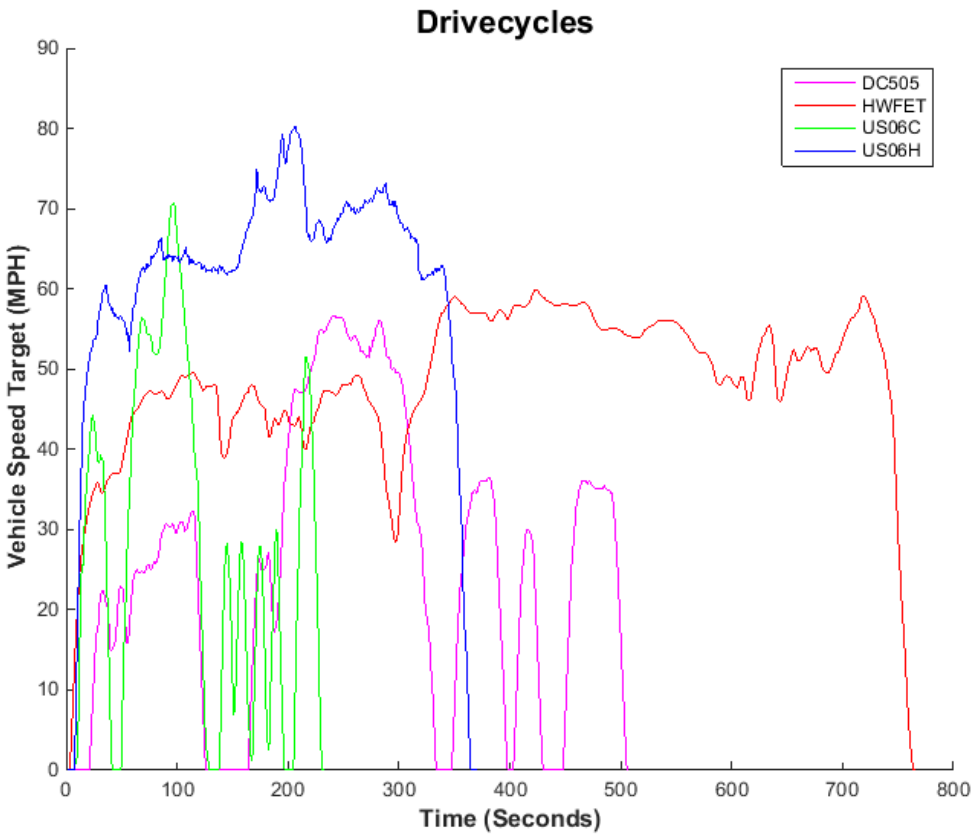

Figure 3.2: Drive Cycles Combined Plot

Table 3.1: Drive Cycle Details

Drive cycle	**Time**	**Distance**	**Average Speed**	**Top Speed**
HWFET	756 s	10.1 mi	48.2 MPH	59.9 MPH
DC505 (UDDS)	505 s	3.6 mi	25.6 MPH	56.7 MPH
US06 Highway	370 s	6.2 mi	60.5 MPH	80.3 MPH
US06 City	232 s	1.8 mi	27.4 MPH	70.7 MPH

3.4 Powertrain Model

The powertrain model is broken down into individual components. Each component has been modeled using a combination of mathematics, lookup tables, and Simscape physical modeling to accurately capture the behavior of the individual component. For this thesis, new battery, engine, and electric motor models were created. For individual tests, Model Referencing was used to select the components for a specific test to allow a quick and seamless process.

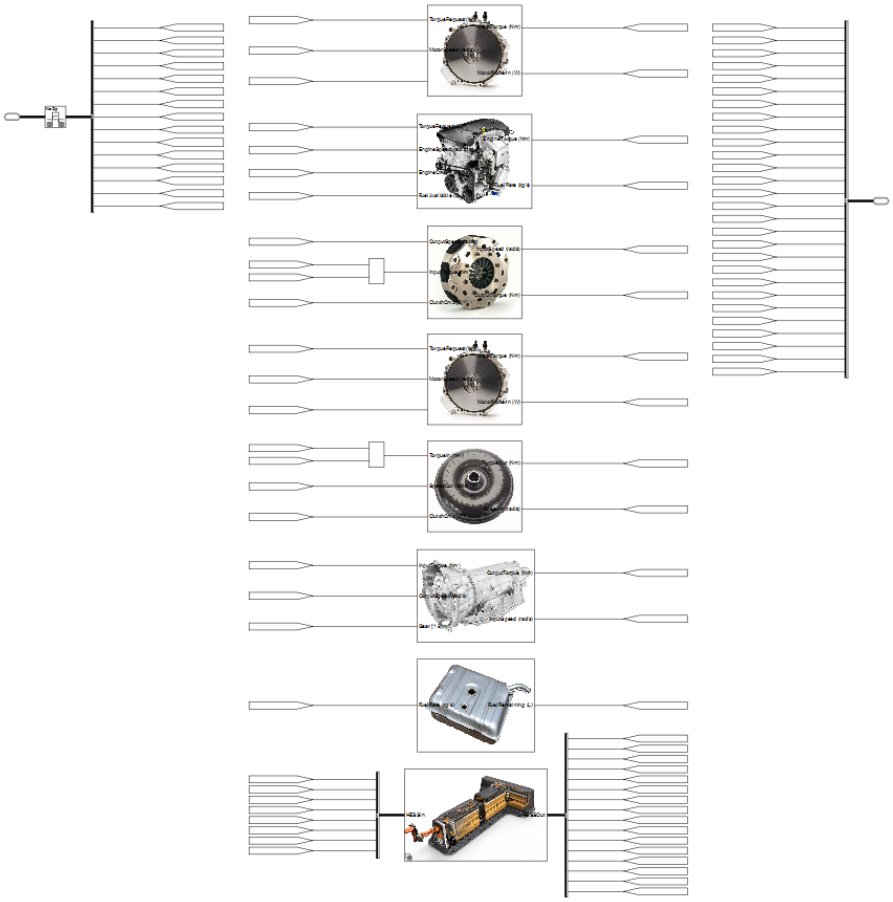

Figure 3.3: Overview Image of Powertrain Subsystem

3.4.1 Voltage Dependant Motor Model

One major contribution made to the powertrain model was an upgrade to the electric motor model. Originally, the electric motor model efficiency was only dependent on torque and speed. Voltage is a major factor in the efficiency of the electric motor selected for this vehicle. In particular, the difference in operating voltage vs voltage

range suggests that efficiency at lower operating voltages would be lower, especially as motor speeds increase. The manufacturer of this subsystem provided the EcoCAR Team with data as to how the efficiency is effected in accordance to several parameters.

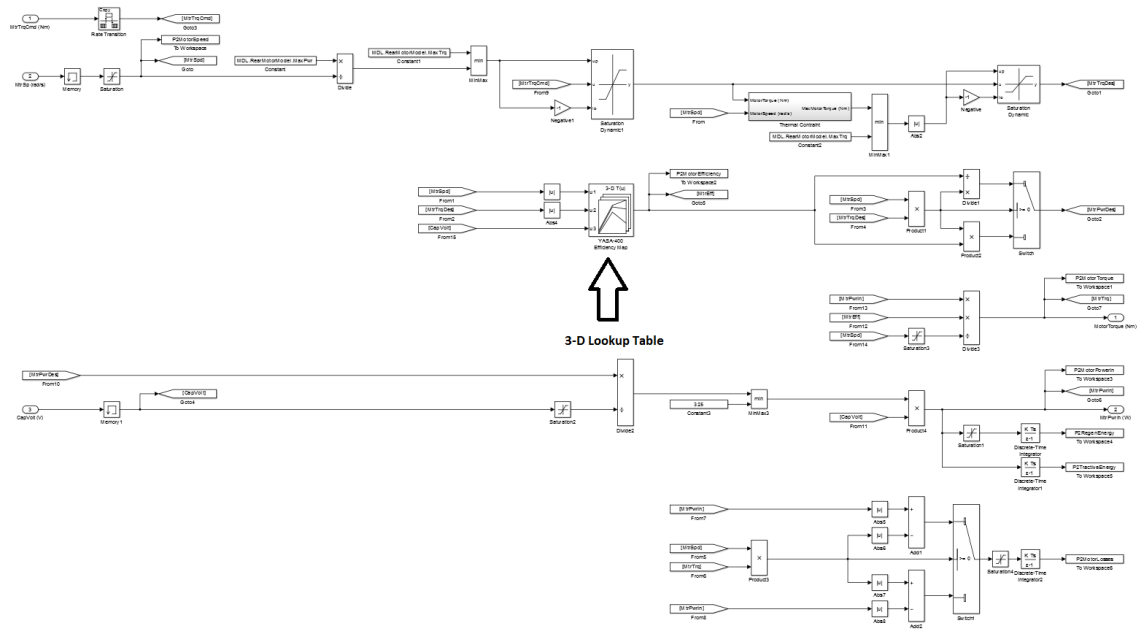

Figure 3.4: Simulink Motor Model Using 3-D Efficiency Lookup Table

To be able to bring this data into the vehicle simulation efficiency maps at various voltages were digitized using an image analysis tool to extract data points from the image. These data points were then fit to a surface and a three-dimensional look up table created by extracting points from the surface. While this method allows for errors to be introduced into the process, care is given at each step to ensure that sufficient fidelity was maintained during the processing of the data. Figure 3.5 shows

the resulting efficiency maps at 300 and 400 volts.

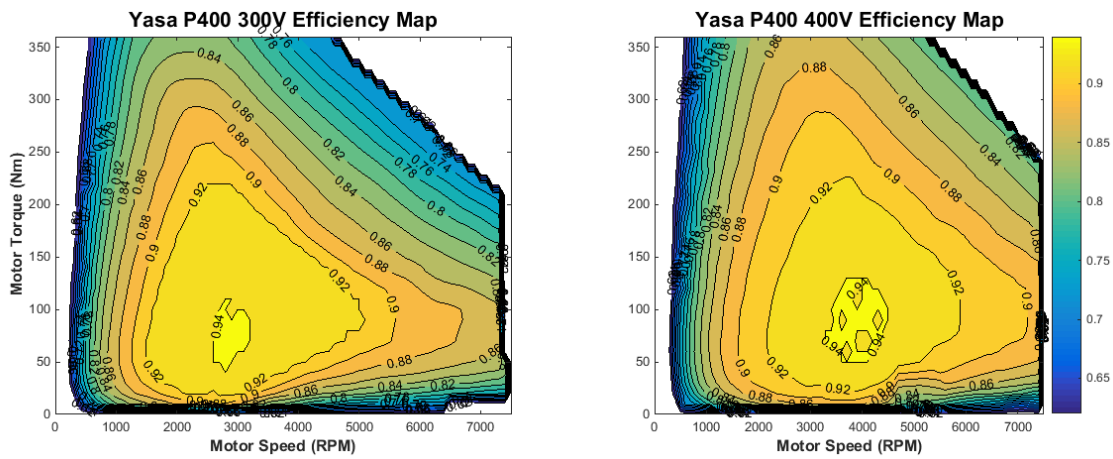

Figure 3.5: YASA P400 Post Processed Efficiency Maps

During simulation, a Simulink block uses these two lookup table to determine the motor efficiency given a particular torque, RPM and voltage. To ensure stability during simulation, a lower bound was placed on the efficiency tables. While this introduces inaccuracies it attempts to prevent the non-continuous nature of the simulation from degrading the quality of data. In the event a single iteration is solved in region of low efficiency, the resulting calculation can ripple through a simulation resulting in oscillations and other inaccuracies in the results. In general, the impact of these regions are small and represent an insignificant percentage of the final calculated values. Generating graphs of operating regions after a simulation, the time spent in these bounded efficiency regions can be quantified and the accuracy of the simulation can be judged on a case-by-case basis.

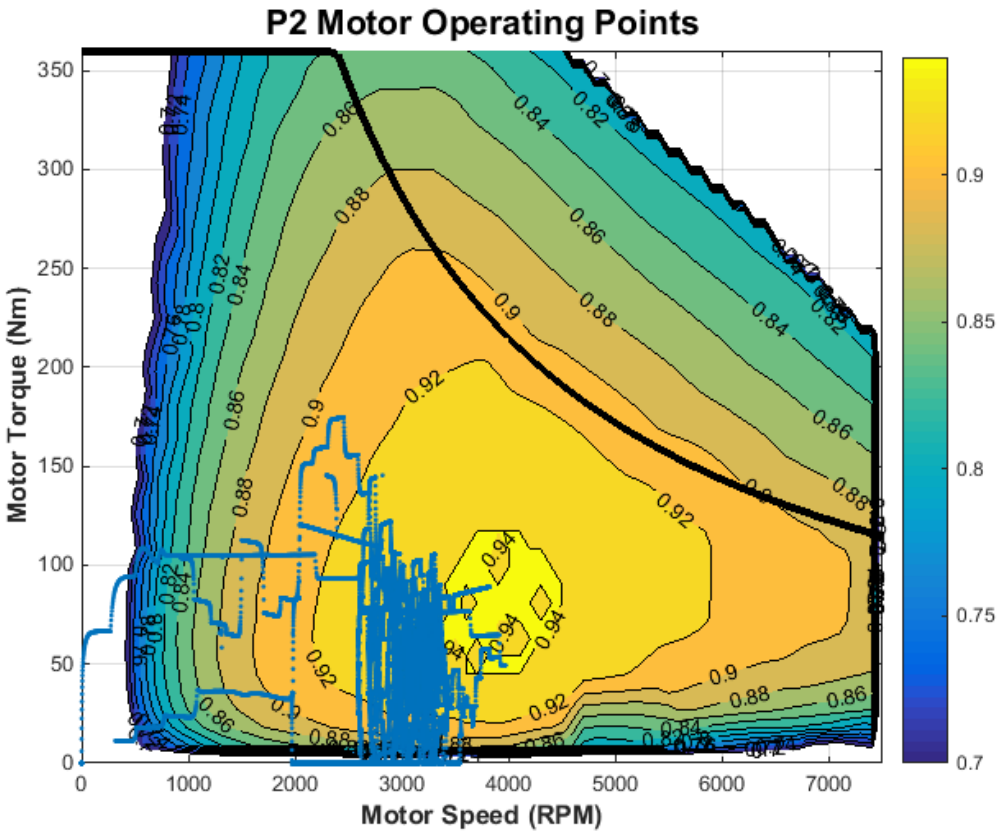

Figure 3.6: P2 Motor Operating Points During HWFET

This process of incorporating real world data into the models is common in this tool and will be used again later in this thesis. This particular improvement of the powertrain model was done in an effort to assess control strategies behavior for the vehicle's HESS. This will be further discussed in the Hybrid Energy Storage System Chapter.

3.5 Chassis Model

The chassis model included in the simulation tool was not modified for this thesis. It consists of a one dimensional longitudinal representation of the mass of the vehicle, drive line losses, and traction dynamics of the tires. The vehicle mass variable will be modified for some of the tests conducted later in this thesis which will be discussed in the descriptions of those tests.

3.6 Controller Model

The Controller Model consists of many subsystems responsible for controlling individual aspects of the vehicle. The model attempts to divide functionality into separate logic allowing for collaborative work flow and the tracking of changes. Control logic consists of a combination of look up tables, Proportional Integral Derivative (PID) controllers, Stateflow logic, and conventional coding logic. Variables are saved outside of the model in scripts which are executed during model initialization. This allows changes to variables and look up tables to be tracked using version control software as well as allowing Matlab scripts to easily alter values for testing and optimization.

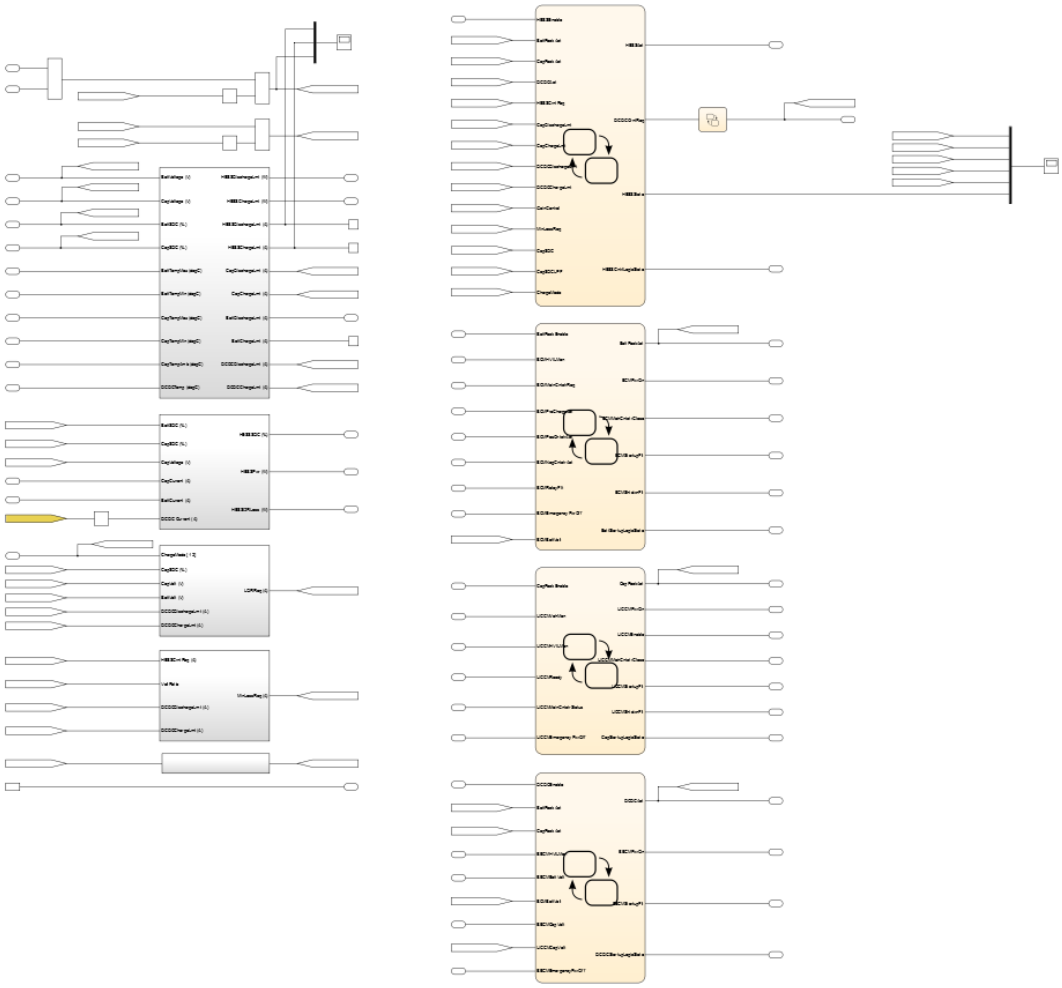

Figure 3.7: HESS Control Subsystem Containing Additional Simulink and Stateflow Subsystems

For this thesis, the torque split and drive mode logics were altered and the entirety of the HESS control logic was created. In this implementation, the vehicle operates in a number of different modes. These include Charge Depleting (CD) and Charge

Sustaining (CS) modes in which the vehicle depletes or maintains its electrical energy storage. Analysis of the vehicle is restricted to operating in two modes, electric and parallel. This simplifies the analysis during the technology comparison as the drive mode and torque split logic becomes easier to generate when this variable is removed. In parallel mode, and when positive torque is requested, the controller attempts to produce the most efficient torque request for the engine motor generator combination for the current system Rotations Per Minute (RPM). The two motors of the vehicle add or subtract torque resulting in the correct torque being delivered to the vehicle's wheels. While this is not the most efficient, it provides a simplified yet efficient and predictable powertrain response while testing other components of the vehicle. Complicated strategies for the vehicle are difficult to validate for each variant and the effects of individual component changes may be difficult to determine.

3.7 Driver Model

During conventional drive cycles, the existing PID based driver was used. This driver model takes a speed vs time profile and generates the torque request to the vehicle controller using a simulated pedal interface in a similar manner to the way a real driver would attempt to match or maintain a specific speed. It is important that the controller maintains a minimal margin of error between the vehicle speed and the drive cycle speed. This error can be caused by two major factors: error produced by the driver's PID or the failure of the controller or powertrain components to meet the drivers request. While the powertrain selected for this vehicle is relatively

powerful, the time needed to switch drive modes may slow the response of the vehicle. The adjustments to the controller model described in the previous section prevent obsessive hybrid mode switching resulting in better response of the controller and powertrain to driver input. The average and maximum error is tracked for every simulation and a plot of the vehicle's speed vs drive cycle is reviewed to ensure the validity of the simulation.

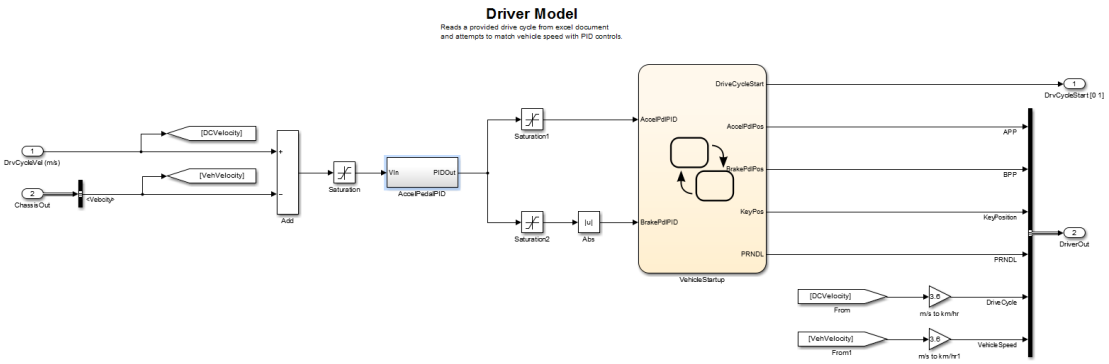

Figure 3.8: Conventional Drive Cycle Driver Model

As this thesis is also interested in accessing the driving performance a secondary method was introduced to better analyze the extremes of the vehicle's performance. New drive cycles and a secondary driver model were created to simulate the vehicles performances on a race track. OptimumLap was used to create speed vs distance drive cycles and a modified driver model attempts to complete these cycles in the least amount of time. OptimumLap is able to use a basic vehicle parameters including vehicle mass, drive type, torque curve and tire information to estimate

track performance. Decomposing a track into a series of straight and curves, it is able to determine cornering speeds and subsequently, acceleration and braking zones. OptimumLap can export these predictions as a complete speed distance profile for a given track which are then imported into Matlab. Figure 3.9 shows the results of Optimum Lap simulating the vehicle around Toronto Mosport. Due to a number of limitations of the powertrain and control logic the vehicle is not always able to perform at its peak. However, since the drive cycles are recorded as speed versus distance the failure of the vehicle to meet the profile ultimately results in the simulation taking longer while still remaining valid. One of the key performance indicators from this type of simulation is simulation time required to complete a particular distance. This directly relates to the performance of the vehicle and changes to models or control algorithms that lead to shorter simulations would also result in better real world performance.

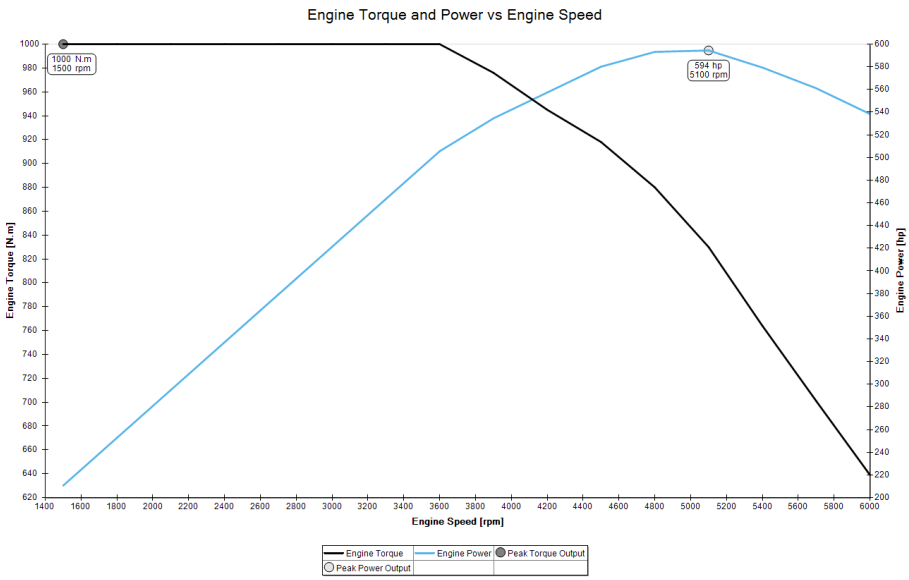

Figure 3.9: Powertrain Maximum Output Used In OptimumLap

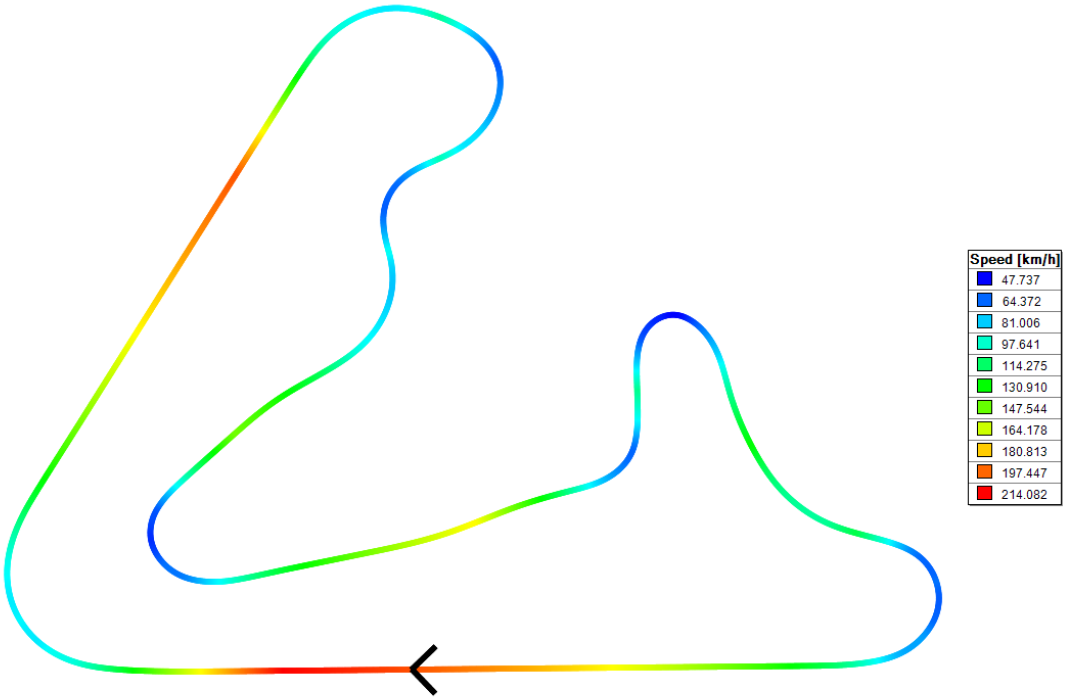

Figure 3.10: Vehicle Best Case Performance Toronto Mosport OptimumLap Result

Chapter 4

Hybrid Energy Storage System Modeling

By selecting a HESS, it was important that a more accurate representation of the system be created to allow the EcoCAR Team to better understand and develop a complete control strategy for the system. To model the HESS, it was first broken down into its major components and a modeling method for each component was determined. The developed HESS model uses a combination of basic Simulink blocks, Simscape components, look-up tables and Stateflow to model the electrical, thermal and control algorithms. It's important to note that a mean average approach was used for both thermal and electrical modeling in order to maintain reasonable simulation times. It is possible to create a more complete model but the computational time required would result in simulation time being magnitudes greater than real time. While the model

might not simulate the fast interactions between components in the high-voltage system, mean value average provides insight into the energy characteristics of the system over large periods of time.

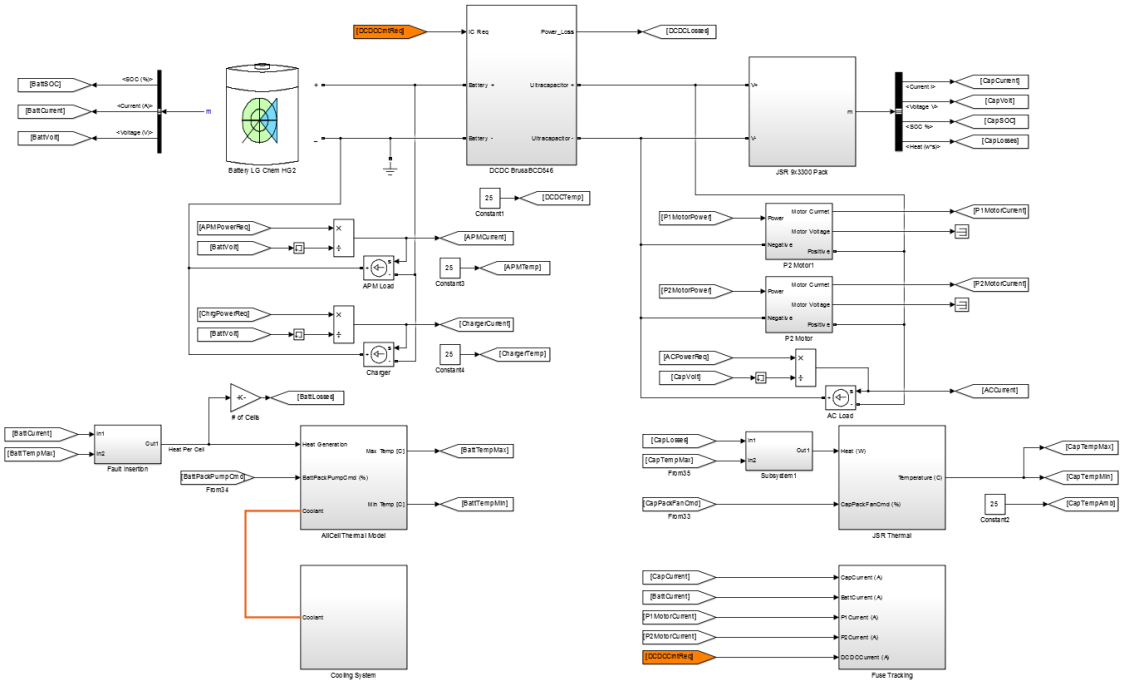

Figure 4.1: Overview of HESS Model

Figure 4.1 is a snapshot of the Simulink model created to represent the HESS. Within this image, the electrical behavior of both the energy storage systems and the power electronics excluding the motor system is represented. The thermal behavior of the two different energy storage technologies is also represented.

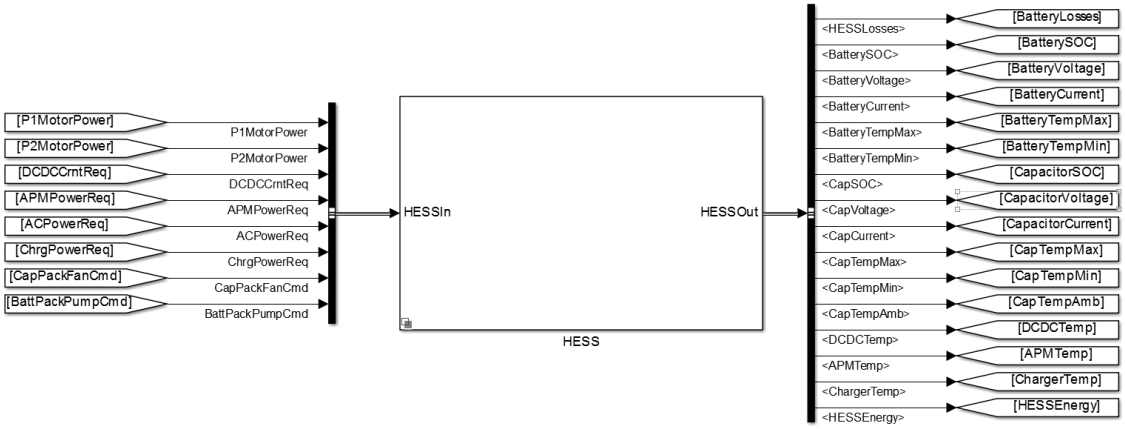

Figure 4.2: HESS Block Input and Output Variables

Table 4.1 outlines the major components that have been modeled. Each component of the HESS provided a unique challenge and as such no two components are modeled in the same manner. For convenience, the table contains a point form list of some of the unique aspects of each of these components.

Table 4.1: HESS Model Component Summary

Component	Company & Model	Electrical Model Summary	Thermal Model Summary
Ultra-capacitors	JSR Micro 9x3300 Prismatic Modules (108s)	SOC-V R mode using lookup table and manufacturer specifications.	Parameterized lumped mass thermal model.
Battery	AllCell LG Chem HG2 6 Modules in Series (84s12p)	Simscape Battery Model using manufacturer specifications and parameterized SOC-V relationship.	Thermal resistive network. Custom Simscape block modeling PCM.
DC-DC Converter	Brusa BCD546	Power balance equation with a lookup table containing manufacturer efficiency data.	Constant used for manual control system testing.
High to Low DC-DC Converter	Generic	Basic power request originating from control system.	Constant used for manual control system testing.
Fuse Model	NA	Model based off each fuse's I2C curve.	NA
Motor Model	YASA P400	Basic power request originating from the motor model. Line losses accounted for in HESS model.	Thermal model located outside of HESS model.
Charger Model	Generic	Basic power request originating from control system.	Constant used for manual control system testing.

4.1 Electrical Modeling

The electrical modeling of the system was done using a combination of Simscape SimPowerSystems components and conventional Simulink blocks. The electrical interaction between the battery, ultra-capacitor, and DC-DC converter is simulated using only SimPowerSystems components. Electrical demand of all power electronic components is calculated outside of the HESS and propagated into the HESS where the SimPowerSystems components determine the current draw on the energy storage components. For components that use voltage in determining efficiency or limits,

voltage measurements are propagated outside of the HESS model. Power demand was selected as the value type to the input to limit the dependency on delayed voltage measurements for calculations outside of the HESS model. This separation of functionality allows for independently testing of the HESS system in which power demands can be logged and used to test the HESS without the need to simulate the entire vehicle.

4.1.1 Battery Model

The battery is represented by a SimPowerSystems component specifically designed to simulate a number of different battery types. Figure 4.3 shows the block design along with the parameters that can be altered in the settings for this block. Once the cell type was selected, the manufacturer's data was used to parameterize this block to approximate the batteries behavior in simulation. While more detailed battery models could have been created. The lack of testing data and stable interaction of this block with other SimPowerSystems components resulted in the selection of this method. The equivalent circuit and equations used by this model as it is configured are below. This model is similar to the models discussed in the literature review.

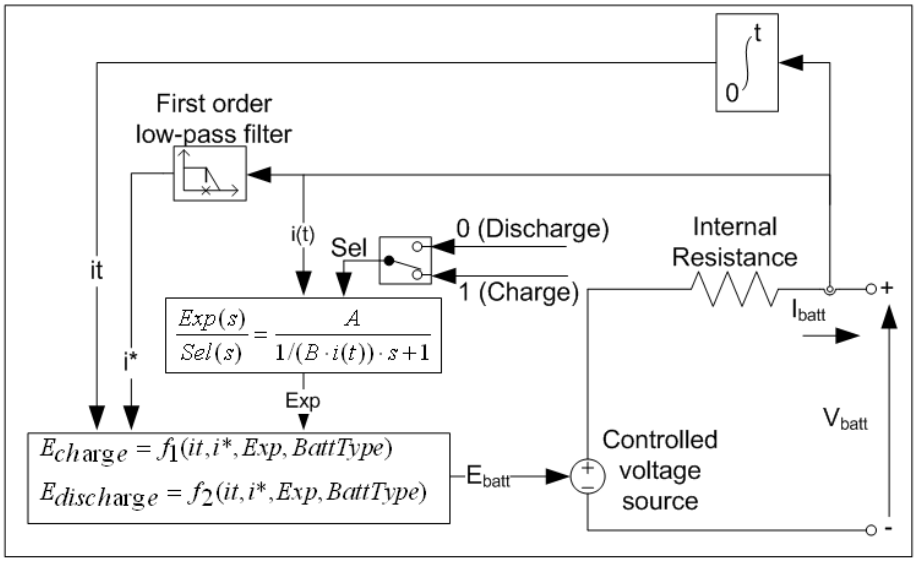

Figure 4.3: Matlab SimPowerSystems Battery Model Equivalent Circuit[37]

Matlab SimPowerSystems Li-ion Battery Model Equation[37]

$$f1(it, i*, i) = E0 - K \cdot \frac{Q}{Q - it} \cdot i * -K \cdot \frac{Q}{Q - it} \cdot it + A \cdot exp(-B \cdot it) \tag{4.1}$$

where:

it = Extracted capacity (Ah)

$i*$ = Low frequency current dynamics (A)

i = Battery current (A)

$E0$ = Constant voltage (V)

K = Polarization constant (Ah1) or polarization resistance (Ohms)

Q = Maximum battery capacity (Ah)

A = Exponential voltage (V)

B = Exponential capacity (Ah)

One of the most important relationships of a battery model is the SOC voltage relationship. This relationship was created by parameterizing a SimPowerSystems equation and the result of this can be seen in Figure 4.4. Most SOC voltage relationships appear to be similar between batteries and can be characterized by: 1)an exponential zone near the top of its SOC, 2)a flat almost linear voltage to SOC relationship through the majority of the SOC, and 3)a rapid decay of the voltage as the SOC approaches 0%. This model attempts to recreate this relationship from a few key variables expressing the size of these zones. The SOC voltage relationship provided by the manufacturer for the selected cell was uncharacteristic in the proportions and slopes of the exponential and flat zones. The parameterization of the block resulted in the exponential zone becoming elongated which can be seen in the figure below.

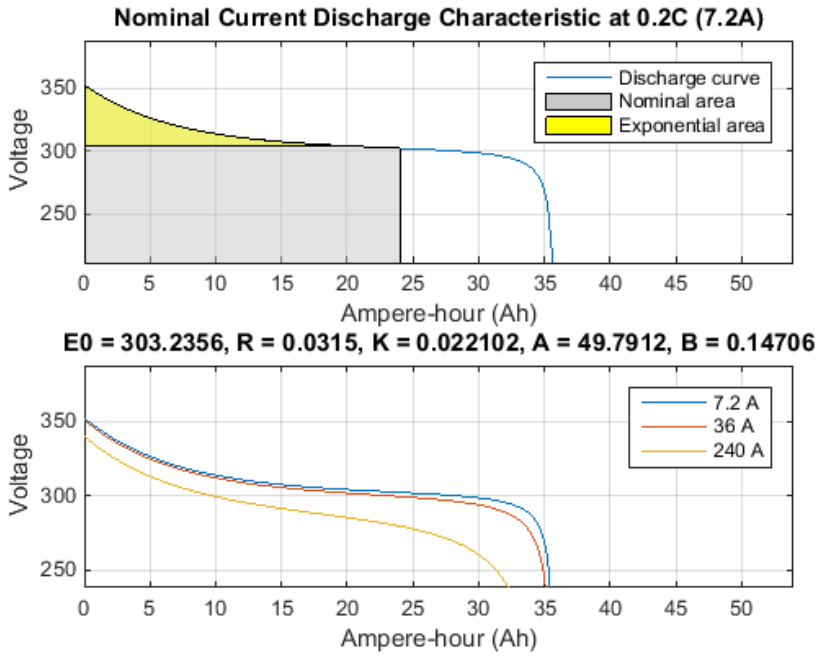

Figure 4.4: Battery SimPowerSystems Parametrization Results

4.1.2 Ultra-capacitor Model

Due to the unique nature of the ultra-capacitors selected for this HESS, Simscape did not contain a default block that would have accurately represented the behavior of the ultra-capacitors. As an alternative, a SOC-V-R model was created using components from SimPowerSystems. A simple lookup table was used to represent the linear OCV relationship while a single resistor provides the dynamic interaction of the terminal voltage. The transient response of these cells was faster than model base step time meaning any time response of the ultra-capacitors would not result in any change

to the simulation results. As the self-discharge of these ultra-capacitors is better than your typical Electric Double-layer Capacitor (EDLC), modeling di-electric loss is not required as the discharge occurs over a much greater time compared to a single simulation.

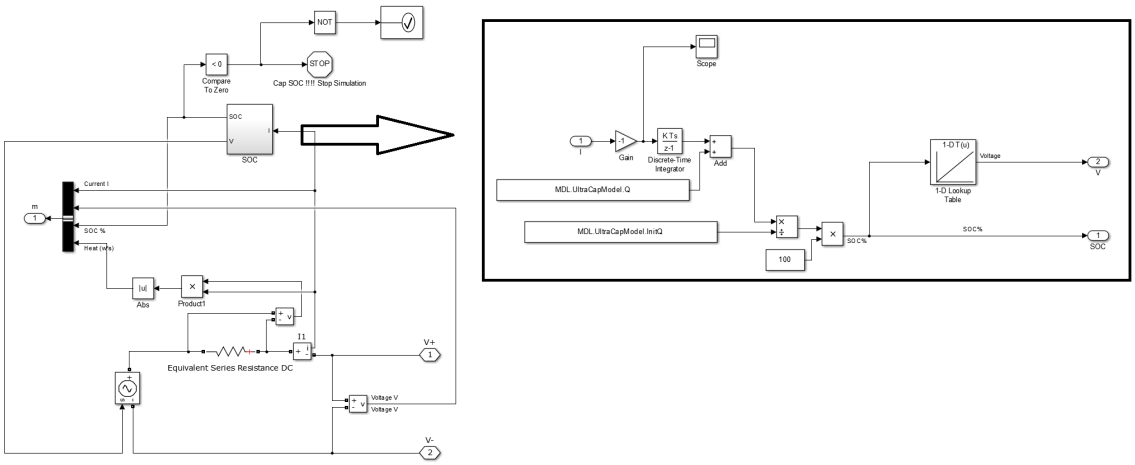

Figure 4.5: Ultra-capacitor Model

4.1.3 DC-DC Model

Two models were created to represent the DC-DC with the original model consisting of generic power balance equation with a simple series resistance to measure losses. One of the most important aspects of the overall efficiency of this HESS architecture is the efficiency of the energy transfer between the battery and ultra-capacitors. To more accurately model the efficiencies of the DC-DC converter, a lookup table was added to the existing power balance equations. The manufacturer provides a table of

efficiencies. However the table is not complete for lower currents. With the lack of information in this operating region, a number of measures and assumptions were taken. The map available from the manufacturer can be seen in the Figure 4.6. One major assumption forces the control system to avoid lower current commands to the DC-DC converter which decreases the amount of the simulation time spent in this unknown region. Typically with these types of converters, power consumption at low power plays a significant role in the device's efficiency. Therefore it is safe to assume the decreasing trend will continue with lower current. In order to create a complete map the last declared data point on both sides of the zero current line is linearly interpolated to an artificial zero crossing of 60 percent efficiency. This assumption is made with the knowledge that simulation environment will not often run the device in this region but is necessary for the efficiency to be continuous for the model to simulate.

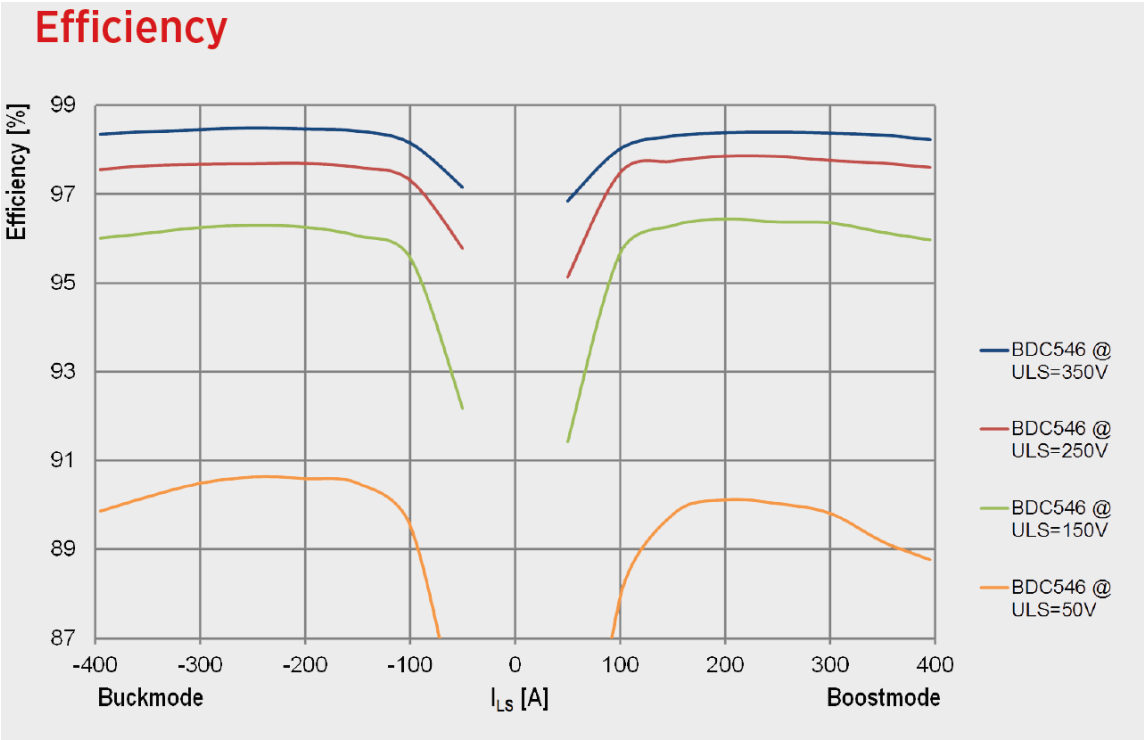

Figure 4.6: Brusa Provided Efficiency Data[13]

A unique design requirement of this particular DC-DC converter is maintaining an adequate high-side low-side voltage ratio. Due to the pack configurations this can be an issue if not properly controlled. The issue is compounded when voltage drop as a result of high currents is considered. Another possible relationship that could have been modeled is the efficiency of the system as the high-side and low-side approach their limit. Unfortunately the manufacturer did not provide details about how this behavior affects efficiency. Through bench top testing, it would be possible to more accurately model this behavior and increase the fidelity of the simulation model

simply by updating look up tables. The constraint is handled in the HESS controller and no effort was placed in the DC-DC to model this requirement.

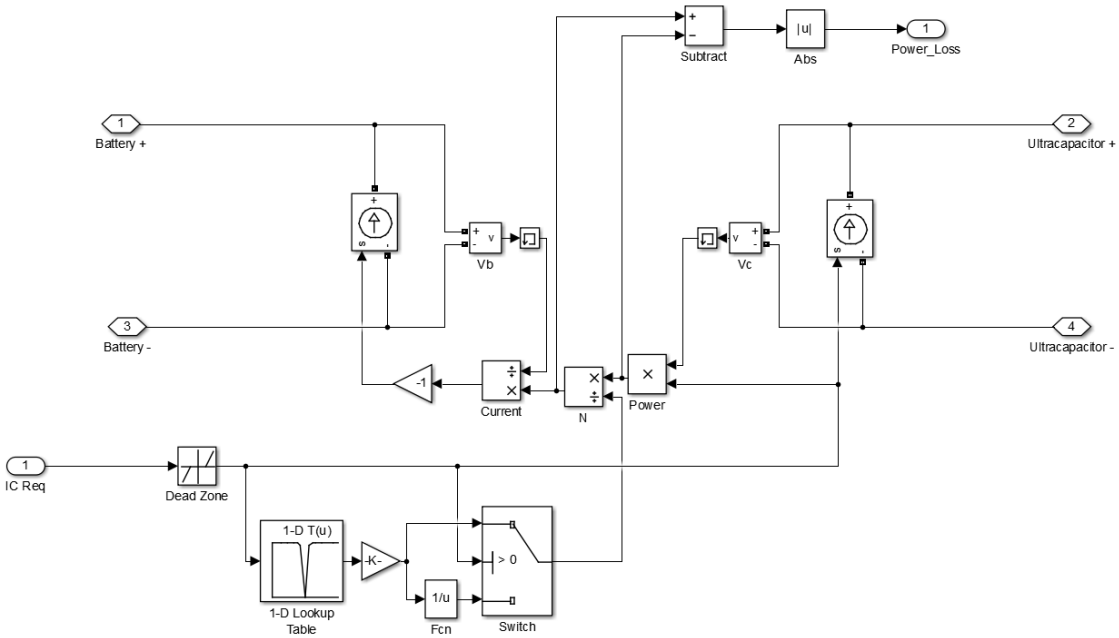

Figure 4.7: DC-DC Power Balance Model Including Efficiency Lookup Table

DC-DC Power Balance Model Equation

$$V_H \cdot I_H = V_L \cdot I_L \cdot f_{eff}(I_H) \tag{4.2}$$

where:

I_H = High side current (A)

V_H = High side voltage (V)

f_{eff} = Efficiency lookup table

I_L = Low side current (A)

V_L = Low side voltage (V)

4.1.4 Fuse Model

To validate the EcoCAR Team's fuse selection, a simple fuse model was created based off of the I2T curves of the selected fuse. Matlab's Curve Fitting Tool was used to approximate the I2T curves as a simple function. Any current passing through the fuse that violates these curves was integrated with a final condition checking to see if the fuse has reached its limit. While there are a number of inaccuracies with this method, it provides valuable insight into a success or failure of the system. These inaccuracies included the lack of individual switching behavior of components possibly resulting in the fuse failing even when the model suggests a proper fuse selection. This model does not track fuse degradation with continuous I2T violations between simulations. Therefore any violations in this model would suggest that the fuse would fail eventually after an unknown number of repeated minor violations.

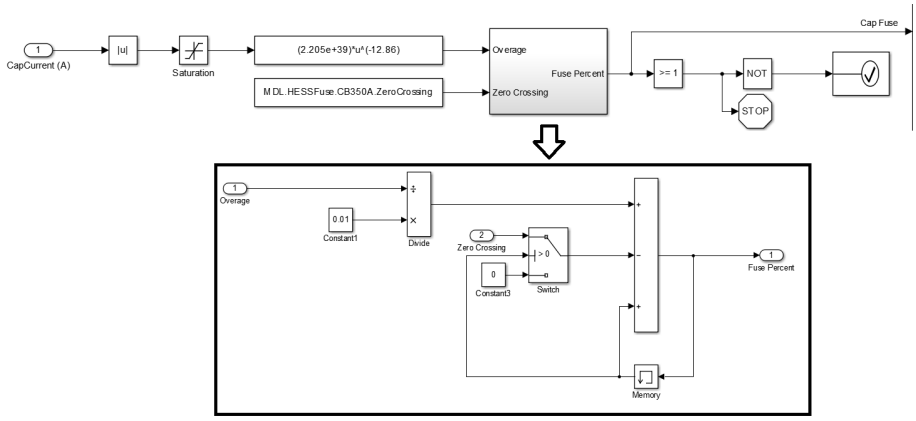

Figure 4.8: Fuse Model

4.2 Thermal Modeling

Thermal models provide insight into performance limits of HESS. With additional data and modeling efforts the effects of changes in temperature on component behavior could be include. However insufficient data is available and therefore the thermal models are only used to examine performance limits of the HESS.

4.2.1 Battery Model

The battery thermal model provides a unique challenge with the use of Phase Change Material (PCM). Every cell in a module is encased in PCM which provide both the structural and passive thermal management of the batteries. A unique property within the material goes through a solid to solid phase change process absorbing a

large amount latent heat energy. This phase changes occurs at a temperature below the thermal operating limits of the cells and well above average ambient temperature. This effectively provides a large amount of passive thermal storage that must be filled before the cells can reach temperature limits. Figure 4.9 and 4.10 are two images from the manufacture's (AllCell) documentation presented with the intent to help visualize both the mechanical configuration and thermal behavior.

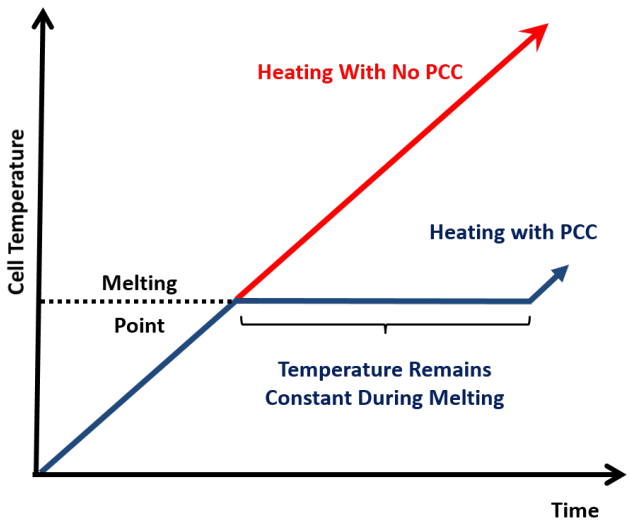

Figure 4.9: Phase Change Material Thermal Behavior[6]

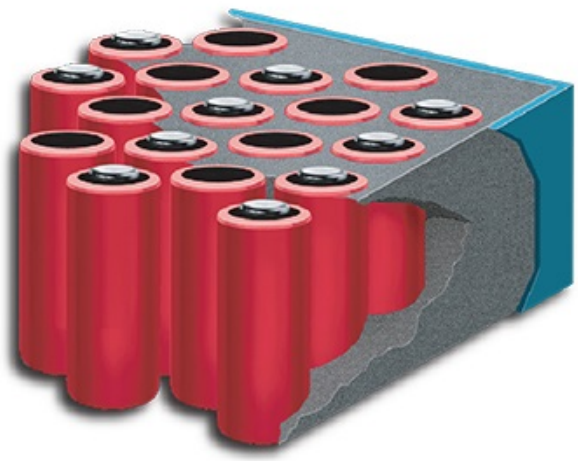

Figure 4.10: Cells Encased in Phase Change Material[7]

Using provided CAD models and thermal properties, thermal simulation of the modules were first completed in collaboration with other students using NX Thermal Analysis Tool. NX Thermal Analysis is a finite element analysis tools with the ability to analyze PCM. The specific properties of the batteries and phase change material provided by the manufacturer were imported into NX and tested using several constant heat generation simulations. Figure 4.11 shows the result of one of these simulations after approximately half a day of computation time. While this provides excellent insight into the thermal behavior of a module, there is no efficient method of connecting this type of stimulation to the Matlab vehicle model. This type of simulation is also not capable of being run in real time and therefore would be impractical for repetitive use. This particular simulation includes the assumption that cooling plates are present on both sides of the module to remove heat over time.

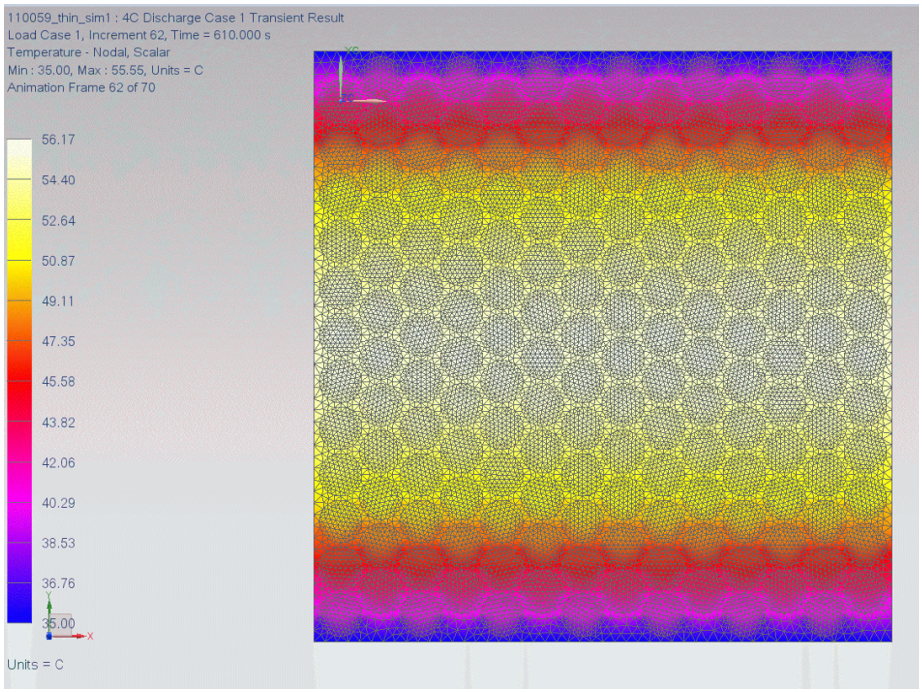

Figure 4.11: Battery Module NX Thermal Simulation Result

Examining the results of the simulation, a decision was made to create a one-dimensional thermal resistive network using Simscape Thermal. To accurately model the phase change material, a custom Simscape block was coded with the generalized behavior of how a mass of PCM would interact in a thermal network. An assumption was made in the creation of the custom Simscape block where all of the latent heat absorption occurs at a particular temperature in a similar fashion to the Figure 4.11. In actuality, the latent heat abortion occurs over a temperature range of a few degrees. It was decided not to attempt to model this behavior as the custom block represents a large mass of phase change material and on average would react as the block behaves. The code for this custom Simscape block can be found in Appendix C.

To create a representation of a module in one dimension, the module is broken into 24 identical rows each containing battery mass and PCM mass. These masses were connected to each other with a conductive heat transfer block containing the average distance between the masses as well as the area connecting them. Each row is then connected with two conductive heat transfer blocks representing the average areas of battery and PCM and average distances between centers of each row. Figure 4.12 demonstrates the custom PCM block and represents 1/24th of a module.

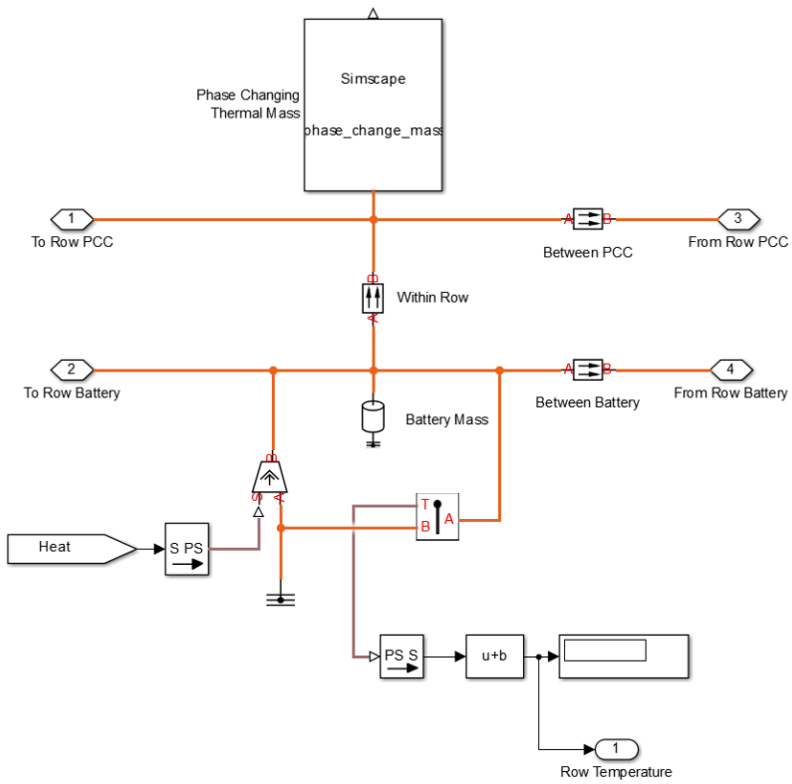

Figure 4.12: Simscape Thermal and Custom Simscape Block Representing 1/24th of a Battery Module

The results of the NX Thermal Analysis and the created Simscape thermal network were compared with respect to cell temperature rise, and thermal energy flow across the module. While there are several minor discrepancies between the two environments, both environments agree during intensive heating profiles. The result is a Simscape Thermal network that provides a reasonable estimate of the modules thermal behavior within the expected simulation time.

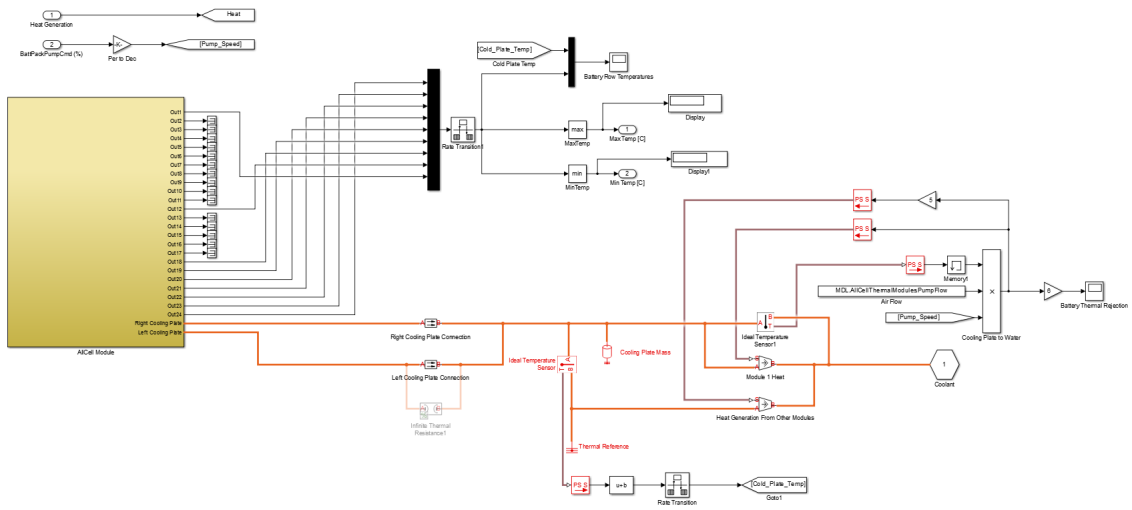

Figure 4.13: Battery Thermal Model Top Level

Cooling Solution Testing

The Matlab thermal network was used to test a number of different cooling solutions. Analysis included: placement and number of cooling plates, effects of coolant flow and temperature, and compressor based cooling solutions. A solution was selected

which allows the vehicle to perform within the thermal limits of the battery. While PCM provides excellent passive thermal storage, the thermal conductivity is quite low resulting in the inability to remove generated heat. It was determined that cooling plates placed on both sides of the module would be adequate to control the removal of thermal energy from a module for all but the most extreme scenarios. The PCM provides almost enough thermal Mass to absorb all of the thermal energy that can be generated from a full pack with the caveat being the temperature rises above the thermal charging limit due to aggressive discharge.

4.2.2 Ultra-capacitor Model

Thermal modeling for the ultra-capacitor modules was considerably simpler in comparison to the battery model. Due to a limitation of the module design, the only strategy that can be used for cooling the ultra-capacitors is a forced air strategy. A simple lumped mass model was created to represent the modules with basic airflow cooling calculations. Each module has a number of small tubes running between the cells allowing for air flow to come into direct contact with the cells. The manufacturer provided test data showing a series of continuous load demands with a known air flow and ambient temperature value. Using Matlab's Parameter Estimation Toolbox, and the data provided by the manufacturer, a simple airflow heat model was parametrized.

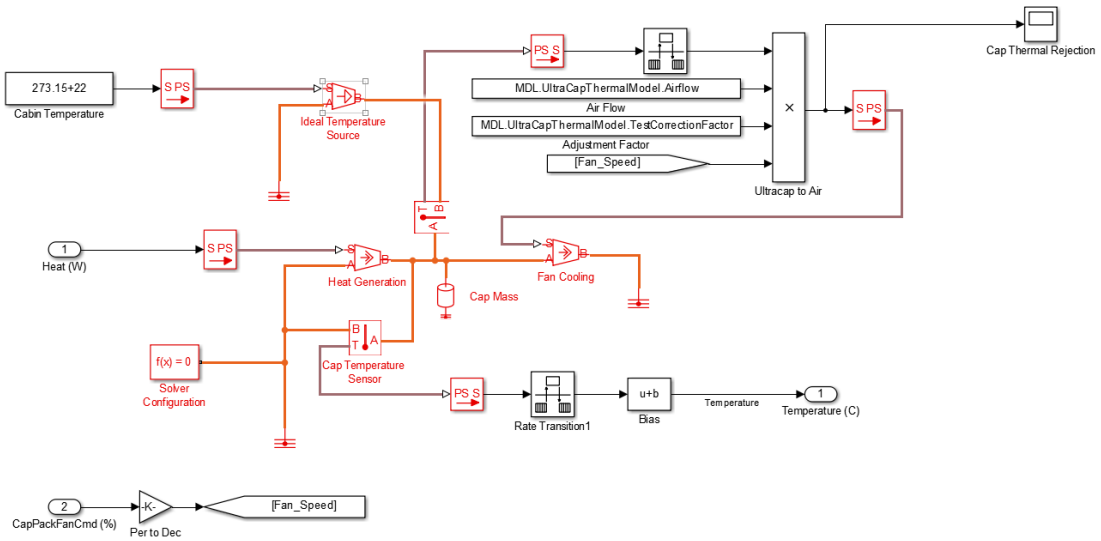

Figure 4.14: Ultra-capacitor Thermal Model Top Level

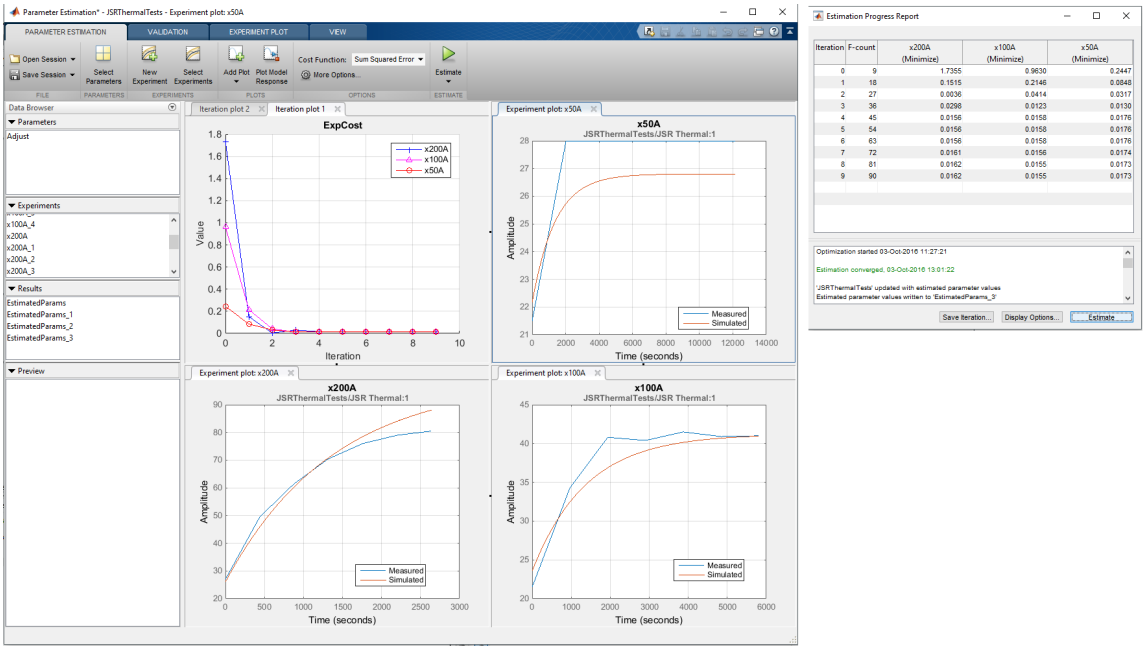

Figure 4.15: Ultra-capacitor Parameter Estimation Results

Fan Equivalence Validation

To ensure adequate airflow in the full sized pack, a Flowmaster compressible flow simulation was created in order to compare the flow rate in the manufacturer's test bench to the expected flow rate in vehicle. The Flowmaster simulation is set up in block line manner with each module as a series of rectangular tubes. The number and size of these tubes was measured directly from the modules. The pressure vs. flow curves for the test fan and in vehicle blower were inputted into Flowmaster and used to compare flow rates between a single module setup and the multi-module setup

that will be present in the vehicle. The Flowmaster model suggests that there will be a slightly higher flow rate in-vehicle due to the strong pressure curve of the blowers selected for the vehicle.

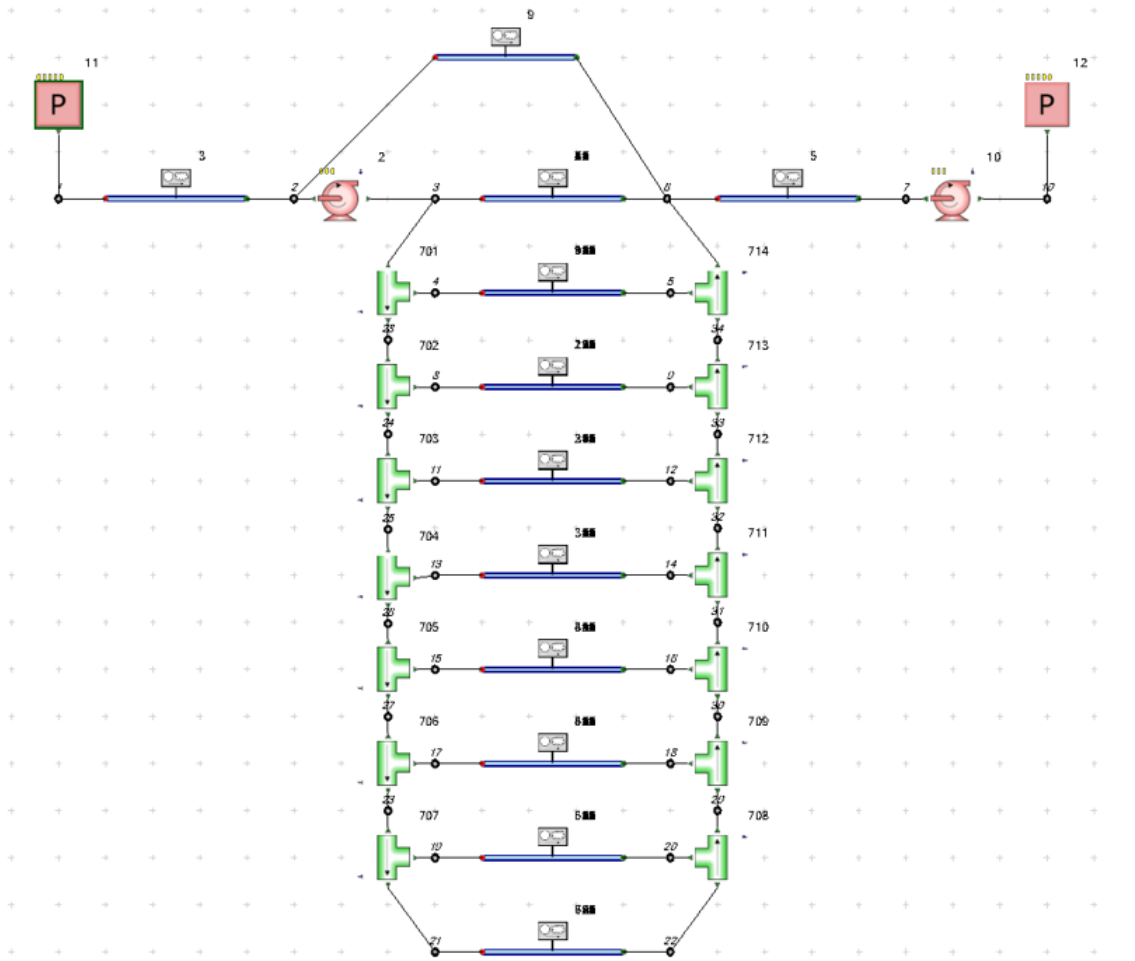

Figure 4.16: Flowmaster Model

4.3 Controls Development

As discussed in the introduction, a HESS can add an additional variable to the overall control and optimization of a vehicle. In addition, the control of this selected HESS architecture is critical to the proper functionality of the overall vehicle. Vehicle level optimization completed by the EcoCAR Team to date does not consider the HESS. As a result some of the work done for this thesis looked at the optimization of the HESS separately. The complexity of the optimization problem at the vehicle level is non-trivial and excluding the HESS from vehicle level development has allowed others to focus on optimizing critical powertrain behavior. This HESS architecture, with such a small amount of energy on the primary vehicle bus requires a controller that maintains a proper energy balance and respecting component limits. Due to limitations placed on the system by the operation of the DC-DC converter, and the architecture of the vehicle itself, it is also important that a high ultra-capacitor SOC always be maintained as this is a crucial factor when starting the vehicle and successfully changing drive modes.

There are several requirements that must be met by the HESS controller which include: protecting components, meeting power requests, maintaining a proper balance and finally operating efficiently. While the priority of these demands change in some situations the safe operation of the system overrides all other requirements. Looking at the HESS and the balance of energy and power on both sides of the DC-DC converter, it can be assumed that the majority of the controllers efforts will be in maintaining a balance in the system. However, for the vehicle to reach its full electrified potential,

the control strategy must also contain logic to ensure that maximum power can be reached when the propulsion system places the demand on this energy storage system.

4.3.1 HESS Limits

One of the most important aspects of the developed HESS controller is the continuous calculation and respecting of the limits of all components. These limits are not only used by the rest of the HESS strategy but are also passed on to the vehicle's control logic. It is important that both controllers abide by these limits for the safety of the vehicle and its occupants. A number of lookup tables were created using manufacturer provided data to determine which variables are the current limiting factors for the HESS. In some cases, a small safety factor has been included to ensure that manufacturer's safety limits are not violated and other safety systems do not intervene in the vehicle. The HESS limits block was extensively tested to ensure that it correctly outputs the right limits in all scenarios. Figure 4.17 below shows a portion of the the HESS limits calculations as the entire logic is too large to represent in this document. Limit calculations are cascaded to determine system level limit. Equations 4.3, **??**, and **??** help depict how limits of components are cascaded to determine system limits. The objective of these examples is to demonstrate the method and therefore does not provide complete insight into the entire set of limit calculations.

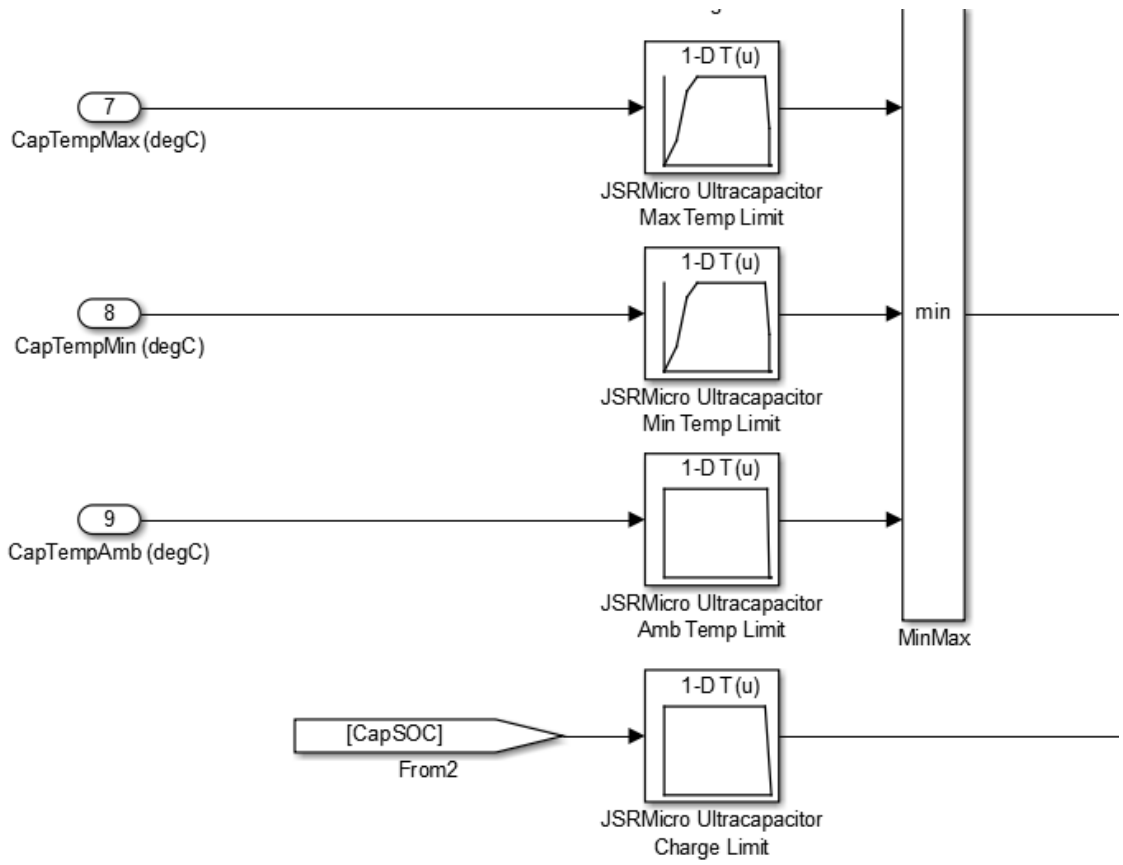

Figure 4.17: HESS Limits Example Showing Lookup Tables Containing Operational Limits

Example HESS Limits Cascading Calculations

$$f_{BattDis}() = min(f_{BTemp}(T_{BMax}), f_{BTemp}(T_{BMin}), f_{BSOC}(SOC_B)) \tag{4.3}$$

$$f_{DCDCDis}() = min(f_{BattDis}() \cdot \frac{V_{HS}}{V_{LS}}, f_{DCDCTemp}(T_{DCDC}), f_{DCDCVolt}(V_{LS}, V_{HS})) \quad (4.4)$$

$$f_{HESSDis}() = f_{DCDCDis}() + f_{CapDis}() \quad (4.5)$$

where:

T_{BMax} = Battery maximum temperature (C)

T_{BMin} = Battery minimum temperature (C)

SOC_B = Battery SOC (%)

V_{HS} = Ultra-capacitor bus voltage (V)

V_{LS} = Battery bus voltage (V)

T_{DCDC} = DCDC temperature (C)

$f_{Description}()$ = Limit determining function

Currently, the limit calculations assume perfect knowledge and timely arrival of information. When this logic is brought into the vehicle, an assessment of the potential faults and delays in information needs to be completed to ensure the limits are calculated correctly for the vehicle.

4.3.2 Gain Control

One of the simplest methods for balancing a system is gain control. To create a gain controller, two methods were explored which will be discussed in this section. The first of these methods involved the development of a Linear Quadratic Regulator (LQR). An LQR is a multi-input multi-output optimized response gain controller. This was done in collaboration with other students however it is no longer being used as part of the HESS control. The second method was a scheduled gain controller which is similar to a number of individual gain controllers that run independently during certain operating regions. A scheduled gain controller provides a high degree of flexibility while still being relatively simple to integrate, validate, and optimize.

Matlab provides a toolbox for calculating LQR controllers from an equivalent State-Space model. A cost function represents arbitrary values of the LQR controller that is used to tune its behaviour. For more information on the work done please reference[24].

Observing the behavior of the LQR, it became apparent that the continuous nature of this control method may not be optimal for an entire vehicle system. For this reason, a gain scheduled controller was investigated. Figure 4.18 demonstrates the overall function of this gain scheduled controller. Vehicle mode and ultra-capacitor SOC are two of the most influential variables in the control of a HESS and became the primary focus of the gain scheduled controller. The gain scheduled controller also allows for bang-bang control behaviour. When the extreme limits of Ultra-capacitor SOC are reached, the controller effort is maximized which in this scenario provides a

favorable control response. The optimization of this controller will be discussed later in this section.

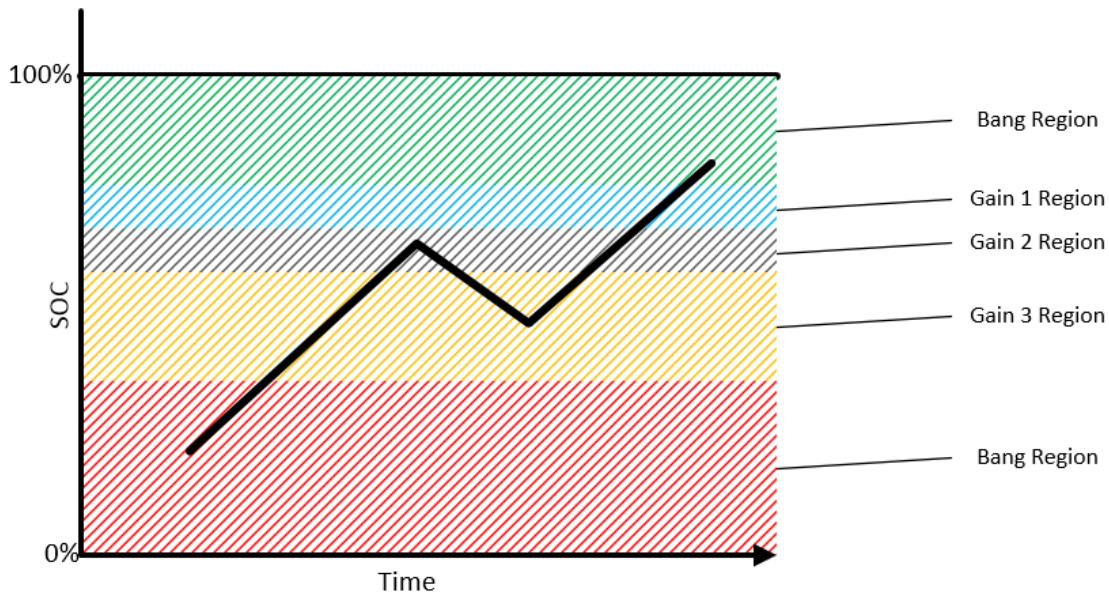

Figure 4.18: Schedule Gain Control Diagram with Bang-Bang Behavior

Gain Schedule Controller Represented as a Function

$$I_{dcdc} = f_{gsc}(SOC_C, DM) \tag{4.6}$$

where:

$f_{gsc}()$ = Pre-calculated gain schedule lookup table

I_{dcdc} = Current request to the DCDC (A)

SOC_C = Ultra-capacitor SOC (SOC)

DM = Vehicle Drive Mode (Enumerated)

4.3.3 Minimized Loss Request

In an attempt to find greater efficiencies while operating the HESS, the most efficient mathematical control action is also calculated. As losses in both energy storage systems are proportional to the current squared, the most efficient momentary control can be calculated by determining the appropriate split between the two packs. The result of this calculation will be referred to as the Minimized Loss Request (MLR). Using a simple resistive model for the DC-DC converter, a simple mathematical equation can be used to determine which control action would result in the least energy losses while meeting the current request. While following this controller would result in immediate highest efficiency, it does not consider the long-term state of the two systems. With the energy balance not being mathematically equal to the most efficient control action, in most scenarios, the capacitor SOC would become the limiting factor preventing the system from operating. The equation below represents the base equation that could be used in determining the MLR.

$$\underbrace{(I_{\text{dcdc}}(V_{\text{cap}}/V_{\text{batt}}))^2}_{\text{Battery Current}} R_{\text{batt}} + I_{\text{dcdc}}^2 R_{\text{dcdc}} = \underbrace{(I_{\text{hess}} - I_{\text{dcdc}})^2}_{\text{Ultra-capictor Current}} R_{\text{cap}} \tag{4.7}$$

When attempting to calculate the MLR with a non-linear DC-DC converter model, it becomes a less trivial task to determine the MLR. Using Matlab's Optimization Toolbox, a dead zone and a simple quadratic function 4.8 was parameterized in an attempt to realize an accurate MLR. While this does not provide the truest MLR, it does provide a relatively efficient instantaneous request and response to a request to the HESS. Figure 4.19 shows the losses generated from the different current split scenarios. This includes meeting the vehicle requests entirely from the ultra-capacitor, battery, or MLR. The next section will discuses how the MLR is integrated with the gain controller to provide a more efficient control method.

MLR Parametrized Quadratic Function

$$I_{dcdc} = Ax^2 + Bx + C \tag{4.8}$$

where:

I_{dcdc} = Current Request to the DCDC (A)
x = Current Demand on the HESS (A)

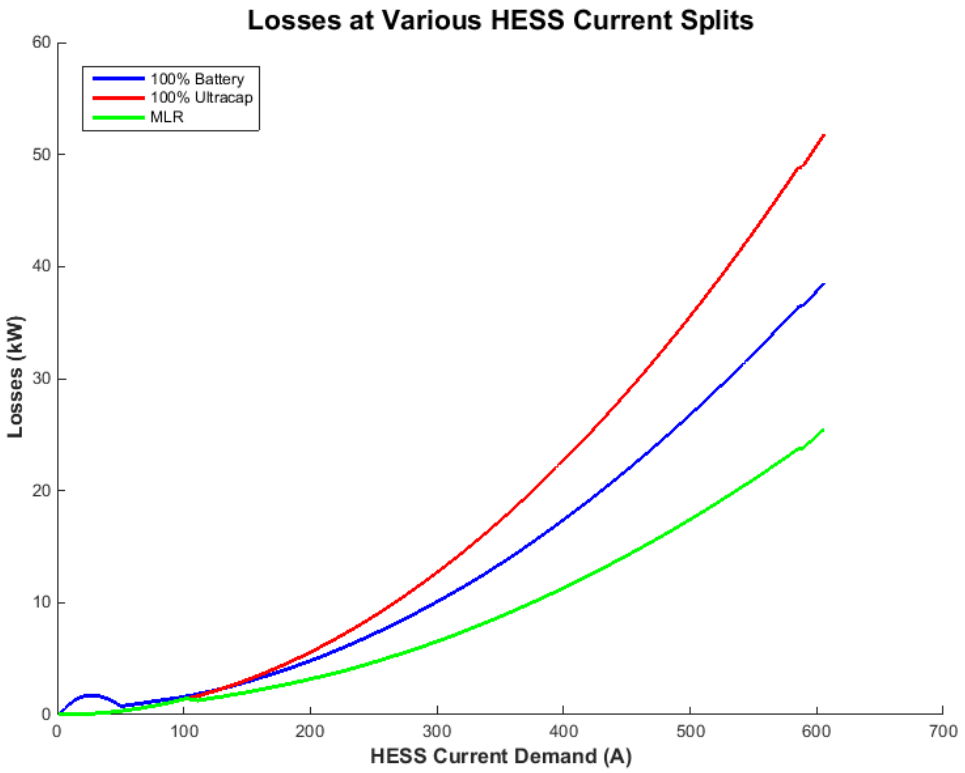

Figure 4.19: HESS Losses Comparing Ultra-capacitor, Battery or MLR Fulfillment

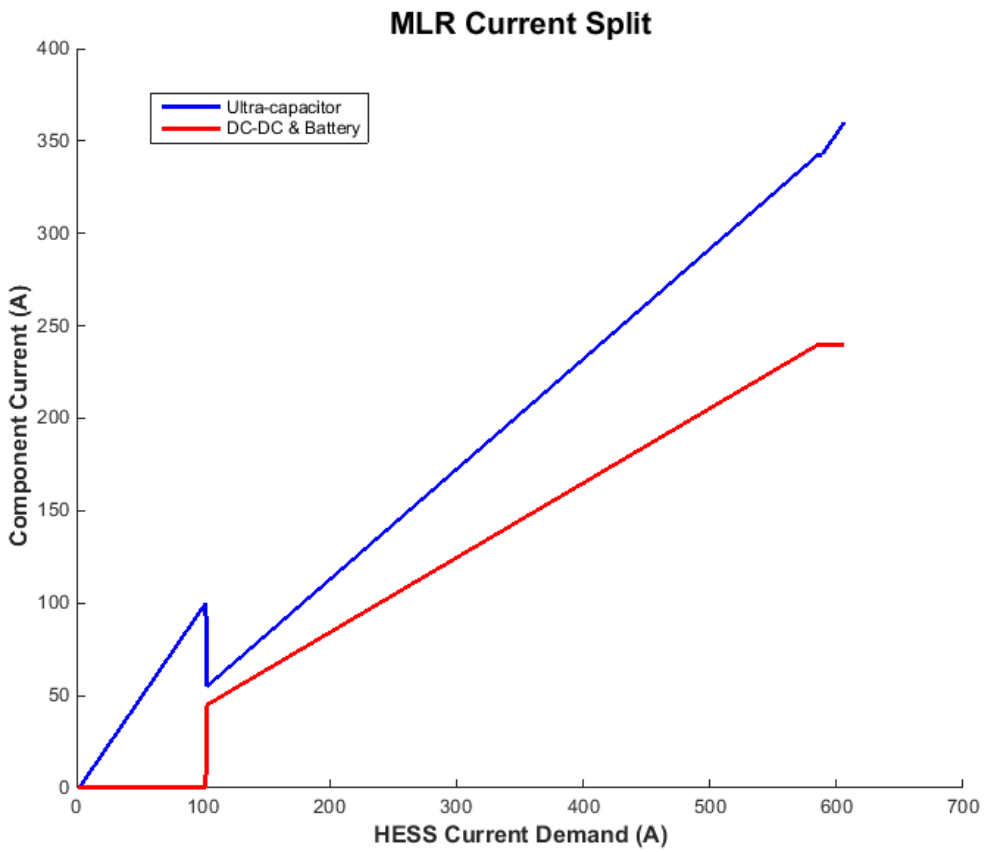

Figure 4.20: MLR Component Current Split

4.3.4 Rules Based Controls Blending

When examining the power request to the HESS, there are several high level conclusions that can be made. Firstly, vehicle modes have a large impact on demand. Driving on CD only has comparatively larger continuous and peak power demands on

the HESS while providing little regeneration. Both modes experience periods of long continuous power demands with peak demands being intermittent and correlating to the vehicle's acceleration. Another unique situation arises when the vehicle is driven at its maximum performance where the electrified system becomes ultimately limited by the continuous power output of the DC-DC converter. In an attempt to achieve efficient operation in all possible vehicle situations, a rules based controller taking input from the gain controller and MLR controller was developed. This rules based controller also ensurers the extreme demand on the HESS would not violate the safe operating of any of the components while following the current gain or MLR commands. Many variants of the rules based strategy outlined in the state flow diagram below were tested, this variant was selected for its simplicity and effectiveness.

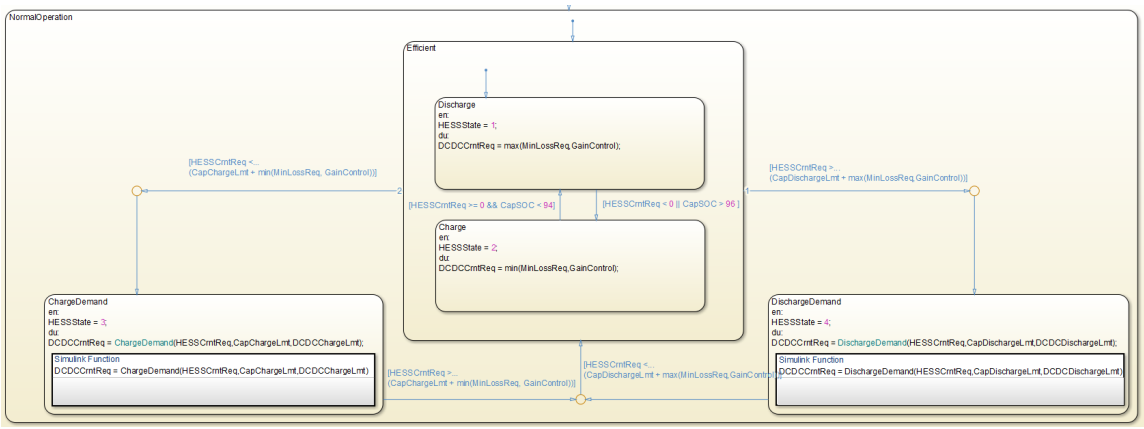

Figure 4.21: HESS Rules Based Controller Stateflow

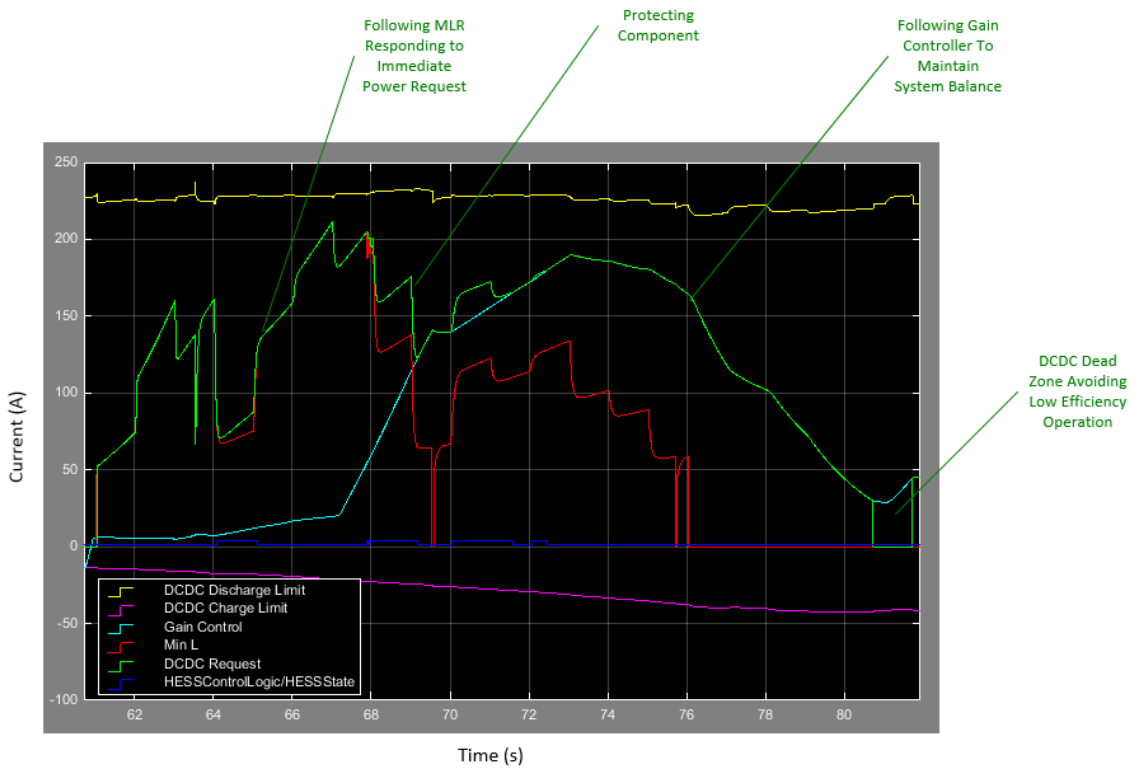

Figure 4.22: Simulink Scope Showing the Various Behaviors of the Rules Based Controller

4.3.5 Optimization

While the work discussed to this point is primarily focused at the subsystem level control, the gain controller provides an avenue for vehicle level optimization. HESS control can impact the overall vehicle efficiency in a number of different ways. These include energy used to balance the HESS and control of system voltage which effects

the efficiency of other components. As discussed in the vehicle model chapter, a motor voltage sensitive efficiency model was created in preparation for this level of analysis. The optimization discussed in this section looks to make adjustments in the gain controller to improve efficiency when the vehicle is driven against a series of prescribed drive cycles. In particular, the EcoCAR 4 Cycle was selected as this is the metric that the vehicle will eventually be tested against.

To optimize the gain controller, Matlab's Optimization Toolbox was used and the vehicle model was encapsulated in function. The function's inputs adjust the vehicle parameters and then simulated the adjusted vehicle against all drive cycles to finally return the weighted vehicle energy usage. To increase the effectiveness of this function, Matlab's Parallel Computing Toolbox was used to run the drive cycles in parallel. Adjusting the level logging in the stimulation environment, and leveraging the Parallel Computation Toolbox, the execution time was only a few minutes. This allowed the function to be called numerous times. In contrast, a single drive cycle simulation can take just as long when the environment is in its most data intensive settings. The function is calling the vehicle model and startup initialization scripts in at a high level. As a result, extending this method of optimization to other variables in the vehicle requires little effort.

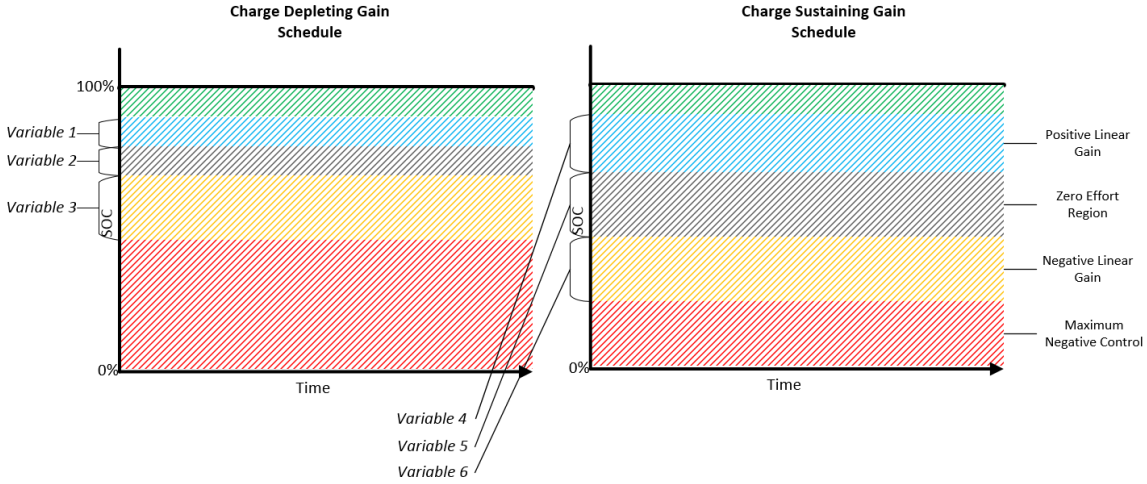

Figure 4.23: Diagram Showing Gain Regions, Variables and Resulting Trends for the Gain Schedule Optimization

For this optimization, the gain schedules were adjusted using 6 variables. These variables correlate to the size and location of both positive and negative linear and zero controller effort regions of the DC-DC current control. This is detailed in the figure 4.23. To ensure the stability of the controller, the optimization was not given the ability to affect the bang-bang regions of the gain schedule. This ensure the system would still operate correctly regardless of the variables being tested. During this test, all other variables of the vehicle were held constant. The optimization is only valid for particular calibration of the torque split and charge sustaining behaviors of the propulsion system as changes in the propulsion system control will result in a different demand placed on the HESS.

```
Function Time: 364946.63

    8       35       0.863417             1     Refine Mesh

input =

    13     9     5     5    29     5


CD =

     0    68    73    82    95   100


CS =

     0    51    56    85    90   100

Completed Drive Cycle (4 of 8)
    Simulation Time: 59.45 sec; Total Elapsed Time: 59.55 sec
Completed Drive Cycle (5 of 8)
    Simulation Time: 77.46 sec; Total Elapsed Time: 77.55 sec
Completed Drive Cycle (3 of 8)
    Simulation Time: 42.20 sec; Total Elapsed Time: 101.78 sec
Completed Drive Cycle (6 of 8)
    Simulation Time: 113.21 sec; Total Elapsed Time: 113.31 sec
Completed Drive Cycle (2 of 8)
    Simulation Time: 115.19 sec; Total Elapsed Time: 115.28 sec
Completed Drive Cycle (7 of 8)
    Simulation Time: 42.17 sec; Total Elapsed Time: 119.96 sec
Completed Drive Cycle (8 of 8)
    Simulation Time: 53.88 sec; Total Elapsed Time: 155.87 sec
Completed Drive Cycle (1 of 8)
    Simulation Time: 68.95 sec; Total Elapsed Time: 184.26 sec
Post Processing Simulation Results ... Displaying Results

---- VTS-Related Information --------------------------
Charge Depleating Range:                  29.20 km
Total Energy Consumption:                 0.87 kWh/km
Total Fuel Consumption:                   0.49 kWh/km
```

Figure 4.24: Console Output During Optimization Showing Setup, Simulation and Final Calculation Results

Matlab offers a number of different optimization algorithms for these types of problems. Computation time is an important factor in selecting optimization algorithms that are feasible for the time and resources available. Complexities and number of non-linearities within the vehicle means that a number of local minimums are possible throughout the solution space. For this particular problem, a pattern search algorithm was used with a number of different initial points. A pattern search starts from a location and varies each of the variables to determine a gradient at a point. The

search variation is random and repeated in an attempt to defeat local minimums. There is no guarantee that the solution finds the global minimum.

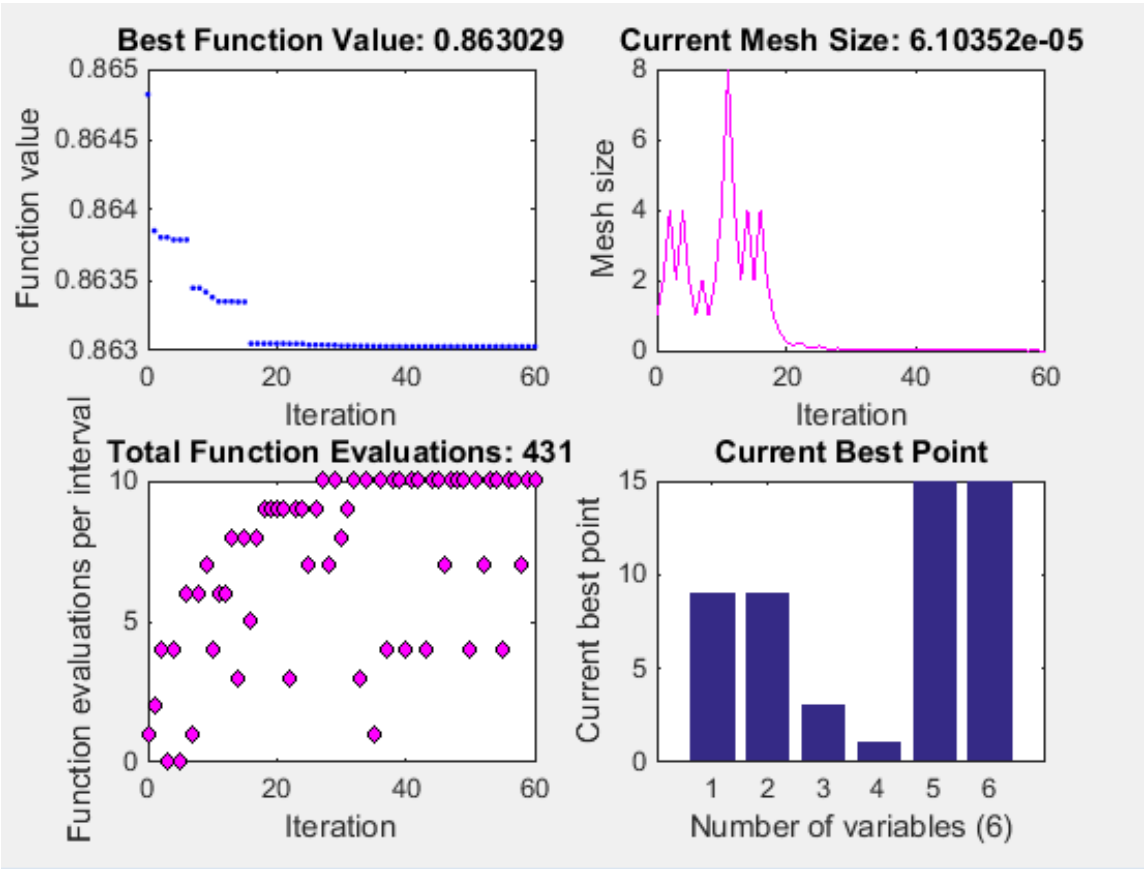

Figure 4.25: Optimization Toolbox Pattern Search Results

The results of the optimization are reasonable and logical for each situation. Looking at the differences in the gain schedules between the CD and CS drive cycles, the effects of both maintaining correct bus voltage and over balancing can be seen. During CD, the gain controller can be described as aggressively maintaining bus voltage as

this allows the motors to operate more efficiently. During CS drive cycles, the gain controller relaxes and introduces a larger zero operation range allowing for a larger deviation of ultra-capacitor SOC and spending less effort to maintain the balance.

Chapter 5

Electric Turbo Charger Modeling

As discussed in the literature review and, in the work by Kam Arshad[8], there are a number of different tools and methods that can be used to model an electrified turbocharger system. Focusing on the objectives of this thesis, an electrified turbocharger model was created in Matlab Simulink with the necessary fidelity to examine average behavior of such a system in a vehicle. The fidelity of this model is such that a reasonable approximation of the systems behavior can assess the impact of the system on the vehicle's performance and efficiency. While the particular modeling details of the various components and controls is not as refined as the HESS system, there are no plans to see the system integrated into a vehicle. The purpose of this exercise is to compare the effectiveness of this system against the HESS. With very little data to validate the correct behavior of the model, it is important that the results are looked at with a degree of suspicion. One major question while planning

this model was determining the effects of the turbo model on the original engine model. While it would be possible to predict changes in engine response time, the original engine model did not assume a delay in the engine response. It was decided that the engine model remain unchanged and that this model would only examine the potential energy benefits of including this system in a consumer performance application.

5.1 Engine Model

In an effort to provide a fair comparison between the two technologies, it was decided that the engine model remain static and be a separate entity that will not achieve closed loop behaviour with engine dynamics. The current engine model provides sufficient information to be able to determine the behavior of the electronic turbo System by making a few assumptions. Given the RPM, fuel rate and an assumed Air Fuel Ratio (AFR), the mass flow and energy flow of the engine can be approximated. While a constant AFR is not an ideal assumption as an engine does not operate at a constant AFR during loaded events. At high engine loads an Engine Control Unit (ECU) will attempt to maintain a desired air fuel ratio. Selecting a reasonable AFR for this type of turbo charged engine application provides a reasonable approximation of the average operating AFR. If additional engine data was available it would be possible to use values for volumetric efficiency or AFR throughout the operating range of the engine to increase the accuracy of this model.

5.2 eTurbo Modeling

Figure 5.1 is an overview of the electronic turbocharger model created for this thesis. Primarily using Simscape pneumatics, information from the higher-level engine block is used to approximate an electronic turbocharger system. The architecture used for this system can be seen in Figure 1.15 and will be referred to as an eTurbo. Major components of this model consists of subsystems representing the compressor, engine flow, turbine, exhaust system, waste-gate, and bypass valves. In addition, a simplified representation of an electric motor has been added to the shaft connecting the compressor and turbine.

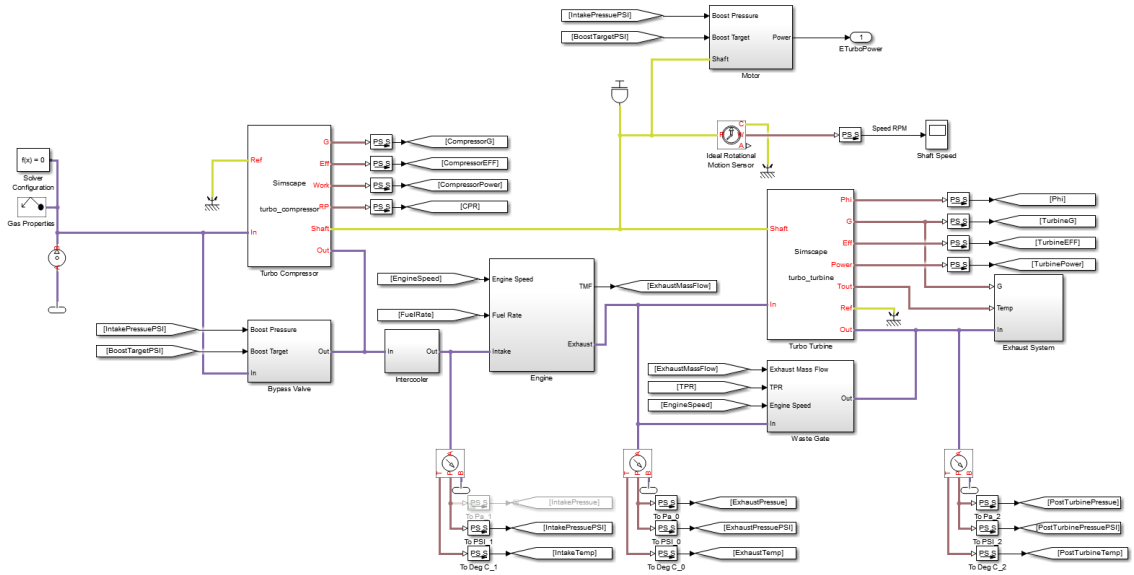

Figure 5.1: Electric Turbo Charger Model Overview

For this application, an appropriate turbine and compressor were selected from Borg Warner. The manufacturer provides information on these components including efficiency and performance maps which are the basis of this model. Borg Warner was selected for their ease of access of information and sizing tools allowing for proper component selection. While the selected components are not optimized, the selection provides a reasonable starting point for this analysis. The turbocharger components selected from Borg Warner are appropriately sized for the engine. A great deal of work from collecting turbine and compressor data to estimating system behavior would be required in order to make an optimized selection.

5.2.1 Simscape Pneumatics

While no ideal Simscape physical domain existed to model this type of system, Simscape Pneumatics offers a physical domain that should provide a sufficient platform for this level of analysis. Simscape pneumatic is intended to model a wide range of gaseous applications using the Ideal Gas Law and conservation of energy between pneumatic and mechanical systems. It will provide the basic platform needed to create the desired model. While the basic equations accurately represents some of the model, more specifically the components before the engine, adjustments to these calculations will have be made to account for the non-ideal gas characteristics of exhaust gases. Overcoming this limitation will be discussed when describing the individual components ability to calculate exhaust gas energies. Figure 5.2 from Matlabs documentation is the fundamental equation used to solve relationships in

Simscape Pneumatic networks.

Fundamental Equations

The energy balance for a control volume [1] is

$$\frac{dE_{cv}}{dt} = Q_{cv} - W_{cv} + \sum_i \left(m_i \left(h_i + \frac{v_i^2}{2} + gz_i \right) \right) - \sum_o \left(m_o \left(h_o + \frac{v_o^2}{2} + gz_o \right) \right)$$

where

E_{cv}	Control volume total energy
Q_{cv}	Heat energy per second added to the gas through the boundary
W_{cv}	Mechanical work per second performed by the gas
h_i, h_o	Inlet and outlet enthalpies
v_i, v_o	Gas inlet and outlet velocities
g	Acceleration due to gravity
z_i, z_o	Elevations at inlet and outlet ports
m_i, m_o	Mass flow rates in and out of the control volume

Figure 5.2: Matlab Simscape Pneumatics Fundamental Equation[38]

Matlab offers a turbine engine example in Simscape pneumatic which provided basic insight on how to create both turbine and compressor models. The equations and relationships between components in this example are basic and the resulting turbocharger model uses some of the same fundamental equations. There are several major differences between Matlab's model and the model created for this thesis. None of the blocks used in this example are used in the final model. Equations 5.1, 5.2 and 5.3 below are the basic fundamental enthalpy conserving equation for a turbine and compressor that used in conjunction with lookup tables to create the eTurbo model.

The implementation of these equations into custom Simscape block can be found in specific appendix corresponding to each component of the system.

Compressor Equation

$$CW = G \cdot c_p \cdot (T_B - T_B) \cdot n_{eff} \tag{5.1}$$

where:

CW = Compressor Work (J/s)

G = Flow Rate (kg/s)

c_p = Specific Heat (J/kg/K)

T_B = Temperature After Compressor (K)

T_A = Temperature Before Compressor (K)

n_{eff} = Compressor Efficiency

Turbine Equations

$$TW = G \cdot c_p \cdot (T_B - T_B) \cdot n_{eff} \tag{5.2}$$

$$\frac{P_B}{P_A} = (\frac{T_B}{T_A})^{\frac{gam-1}{gam}} \tag{5.3}$$

where:

TW = Turbine Work (J/s)

G = Flow Rate (kg/s)

c_p = Specific Heat (J/kg/K)

T_B = Temperature After Turbine (K)

T_A = Temperature Before Turbine (K)

P_B = Pressure After Turbine (Pa)

P_A = Pressure Before Turbine (Pa)

gam = Specific Heat Ratios

n_{eff} = Turbine Efficiency

5.2.2 Compressor

To represent the compressor, a custom Simscape block was created. A unique feature of this block is its internal use of lookup tables in which data from Figure 5.3 was imported. Being one of the first components created for this model, the compressor was a testing ground and a learning experience as to creating a Simscape component using lookup tables and of this complexity. Several iterations of the block were created and tested before the desired behavior was accurately captured in Simscape.

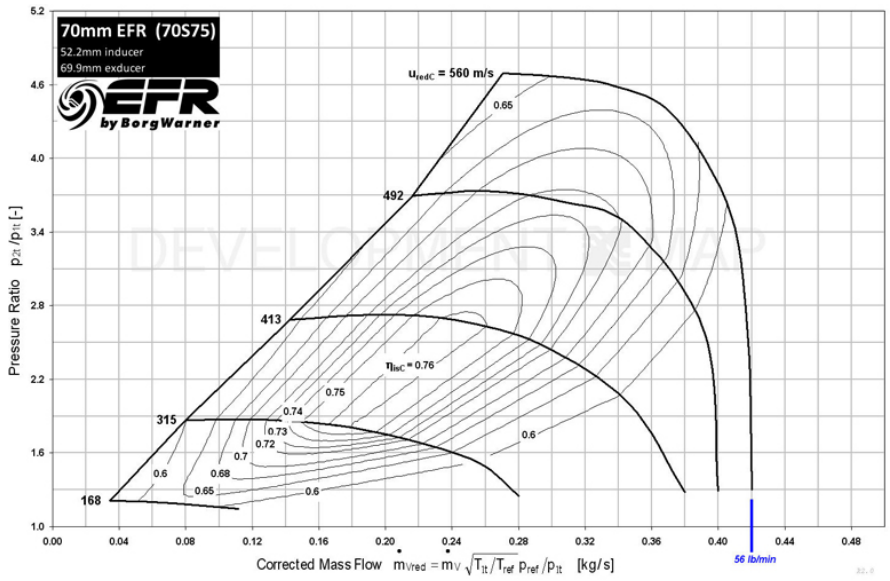

Figure 5.3: Borg Warner Compressor Performance and Efficiency Map[56]

Similar to the methodology used when creating the voltage motor model, images containing data on the selected compressor were digitized and brought into Matlab Simulink. This process first involved plotting key points on the map, fitting the points to a surface and finally sampling the points into an organized table that can be used by Simscape. Due to restrictions in Simscape's data processing, it was necessary to re-sample the digital points to a high enough fidelity such that linear interpolation can be used for solving points between discrete points within the lookup table. For the compressor, two 2-D lookup tables were created to represent compressor angular speed, pressure ratio, mass flow and efficiency. The relationship between flow and efficiency variables determined from lookup tables have been programmed into the block using a number of equations. The internal variables of the block are outputted

and can be monitored during the simulation. Figure 5.4 shows Matlab's Curve Fitting Tool fitting the raw data to a quadratic surface. The Matlab code for this compressor block can be found in Appendix E.

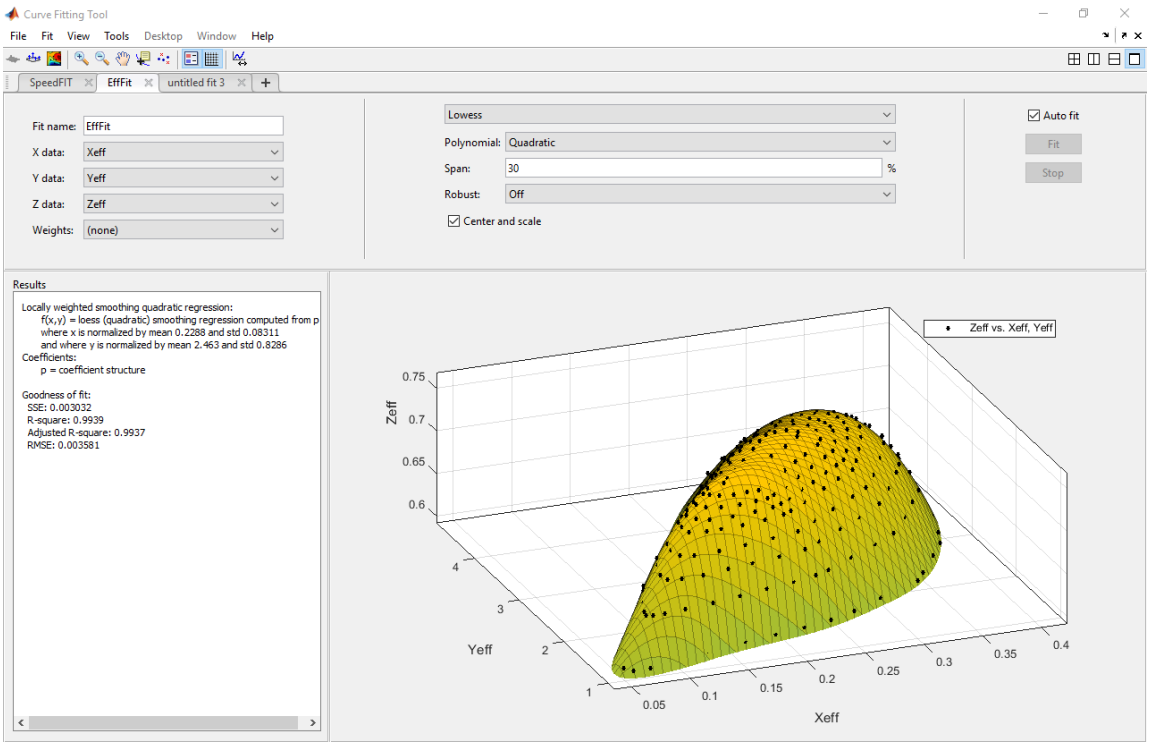

Figure 5.4: Digitized Compressor Map Surface Fit

5.2.3 Engine Flow

Using information originating from the engine model as well as previous AFR assumption, a custom mass flow Simscape block was created representing the engine

stage of the turbocharger system. This model properly accounts for the added energy and mass added to the flow between intake and exhaust manifolds. The image below shows the custom and standard Pneumatic and Thermal blocks used to approximate the engine and exhaust manifold.

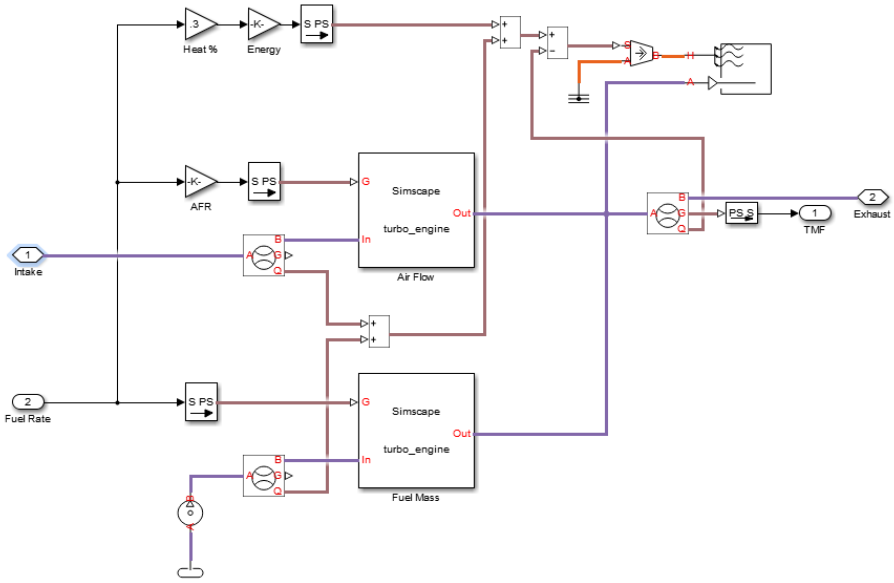

Figure 5.5: Electrified Turbo Model Engine Mass and Heat Flow Model

5.2.4 Turbine and Exhaust System

One of the most difficult aspects of creating this model was accurately modeling the behavior of the turbine, exhaust system and the exhaust system's interaction with the outside world. To model the turbine, a map from Borg Warner provided the data for a lookup table describing the relationship between the pressure ratio, efficiency, and the expected mass flow. Figure 5.6 is the data provided by Borg Warner. The

available information for the turbine is not as extensive as the information provided for the compressor. It is common for turbocharger manufacture to only provide this relationship. The efficiency and behavior of the turbine is dependent on the piping and housing implementation for a specific application. In comparison compressors are not as sensitive to changes in final installation. As a result the efficiency map had to be estimated. A conservative estimate of the pressure ratio vs efficiency relationship was made after reviewing information on this topic.[55]

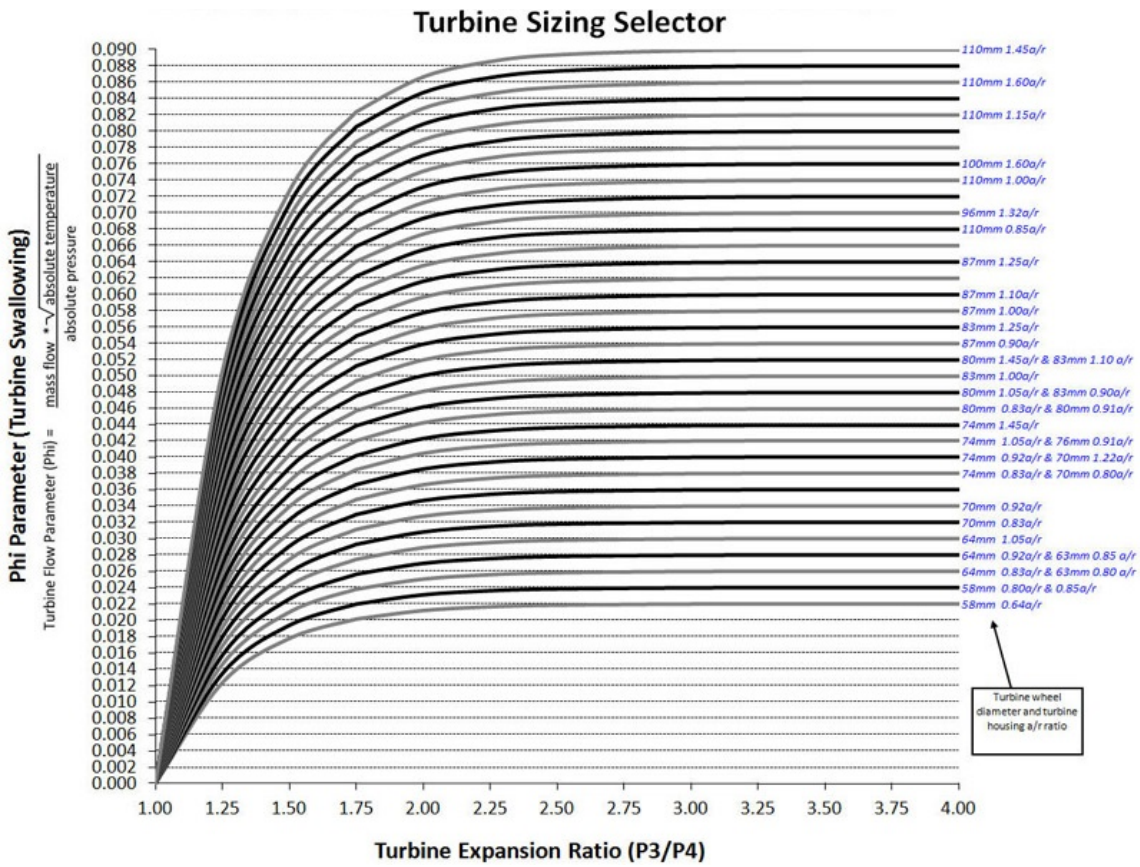

Figure 5.6: Borg Warner Turbine Performance Map[56]

Basic Simscape blocks do not provide a simple method to represent a gas being vented to atmosphere as the fundamental equation of Pneumatic network must conserve energy between every component. A simple atmosphere source block connected to the exit of the turbine would result in Simscape assuming all energy is being absorbed by the turbine. While a turbine converts energy in exhaust gases to mechanical energy, typical exhaust temperatures at the exit of an exhaust system are still in the order of hundreds of degrees. Creating the correct relationships in the turbine, the data stored in the lookup table can sufficiently estimate the energy converted by the turbine. Exit flow rate and temperatures are then passed from the turbine block to the exhaust system block which determines back-pressure on the turbine and handles the removal of waste energy from the network. This is a unique use case for a Simscape Pneumatics as a Pneumatics Network usually requires a chamber in between every component in order to solve pressure and temperatures. The two blocks were interconnected in this way to allow the turbine block to set the specific heat ratio for the exhaust gas. Adjusting this ratio is important to the turbine equation as the specific heat ratio is part of the thermodynamic equation. The approximate exhaust back-pressure is estimated by a lookup table in which reasonable values for an exhaust system were assumed. The code for both the turbine and the exhaust system can be found in Appendix G and H.

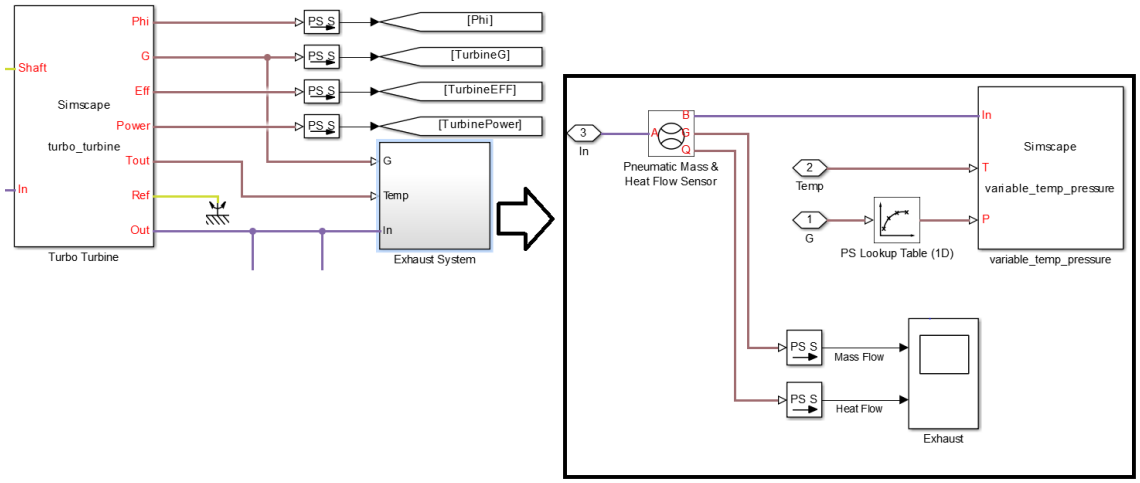

Figure 5.7: Turbine and Exhaust Model Showing Additional Physical Signal Dependence

5.2.5 Bypass and Waste-gate Valves

Finally, for completeness and stability of the model, simple bypass and waste gate valves were created. Simscape provides a variable area orifice which was used to create these two valves. One limitation of this block is that it requires constant flow therefore these valves are never completely closed. A small enough area was used to ensure flow through both these valves remain insignificant when closed. Simple PID controllers were tuned to ensure pressures in the intake and exhaust manifolds remain within acceptable ranges and perform their respective functions. It is interesting to note that in a typical application a waste-gate is controlled to regulate the amount

of flow through the turbine to prevent excessive amounts of boost being created in the intake. When the eTurbo model is functioning correctly the waste-gate no longer opens as the additional energy is captured by the electrical system. The image below shows the configuration of these valves in the model.

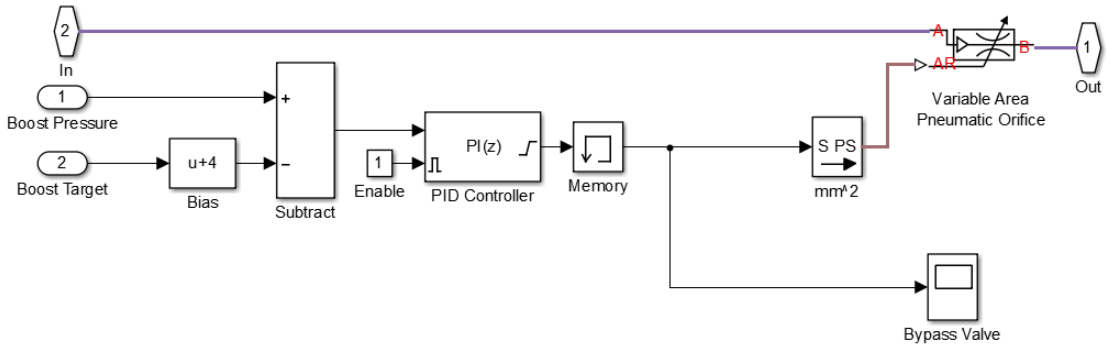

Figure 5.8: Bypass Valve Model

5.3 Electrical Modeling

A simple mathematical approach is used to model the conversion from mechanical to electrical energy. The intent of this model was not to aid in the design of the system but merely to assess the impact of the eTurbo on performance and efficiency. The particular details of the systems electric motor have been omitted. While a number of proposed electric motors meet the requirements of an electronic Turbo

System, a search into a suitable commercially available motors did not identify any candidates. Due to the high speed nature of this application, motors meeting the requirement typically are designed specifically for an application and therefore not commercially available. The papers cited here all provide a solution suitable for this system.[11, 23, 35, 45]

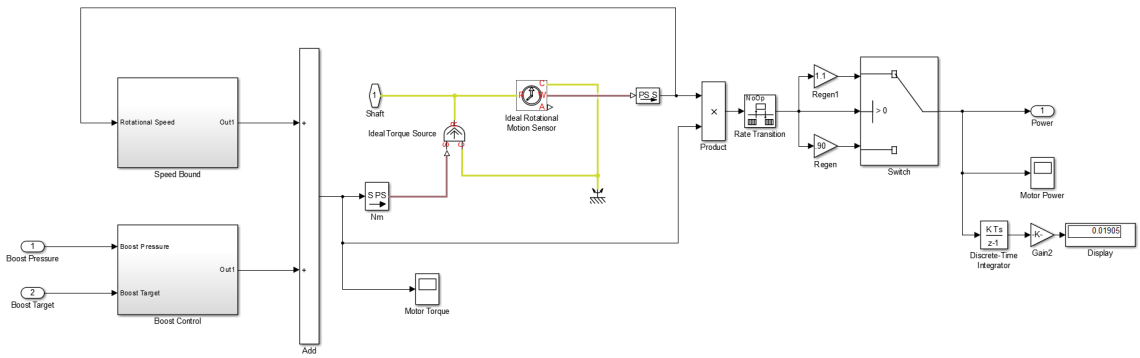

Figure 5.9: Simple Electric Motor and Controller for Electric Turbo

5.4 Control Logic

A review of recent literature demonstrated a numbered of different control methodologies that can be used to provide control. While an advanced control strategy considering all aspects of the vehicle could aid in determining the control action of the eTurbo system, a simple strategy will be used for this model. An example of more advance controls development is discussed in detail in the following masters

thesis.[49] A comparison of 3 simple control strategies was made for a similar system in which the primary control variables were exhaust gas temperature, turbocharger speed, and engine boost.[5] Using information learned from this comparison, a control method using engine boost pressure was selected as the primary method of control. To extend this control further a top speed bound was placed on compressor speed in a basic attempt to keep the compressor in an optimized region of the compressor map. Looking back at Figure 5.3 it can be seen that efficiency drops off at the highest rotational speeds and that the compressor's peak efficiency is met for a wide mass flow range corresponding to a narrow speed range.

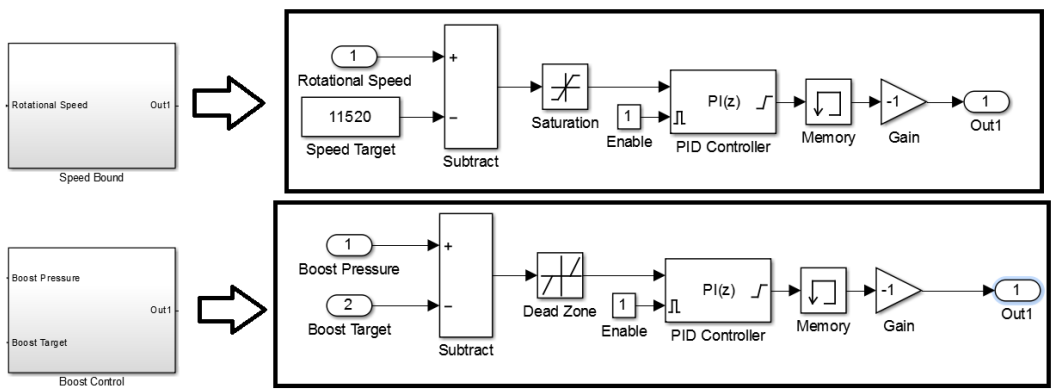

Figure 5.10: Electric Turbo Controller Details

The designed controller begins with a lookup table which provides the relationship between engine speed, engine load, and required boost pressure. The required boost

pressure is compared to the current intake boost pressure which is fed into a PID while a small dead-band around the zero crossing of this signal provides stability during low boost targets. Additional testing of this controller was done with the positive torque control region removed essentially eliminating the turbo lag reduction behavior of the system. The difference in response of the system can be seen in Figure 5.11, in which the intake pressure and pressure targets have been plotted with and without the aid of the electrified system. Without the aid of the eTurbo system in some scenarios the intake pressure drops below atmosphere suggesting that a major turbo lag behavior of the engine would be observed.

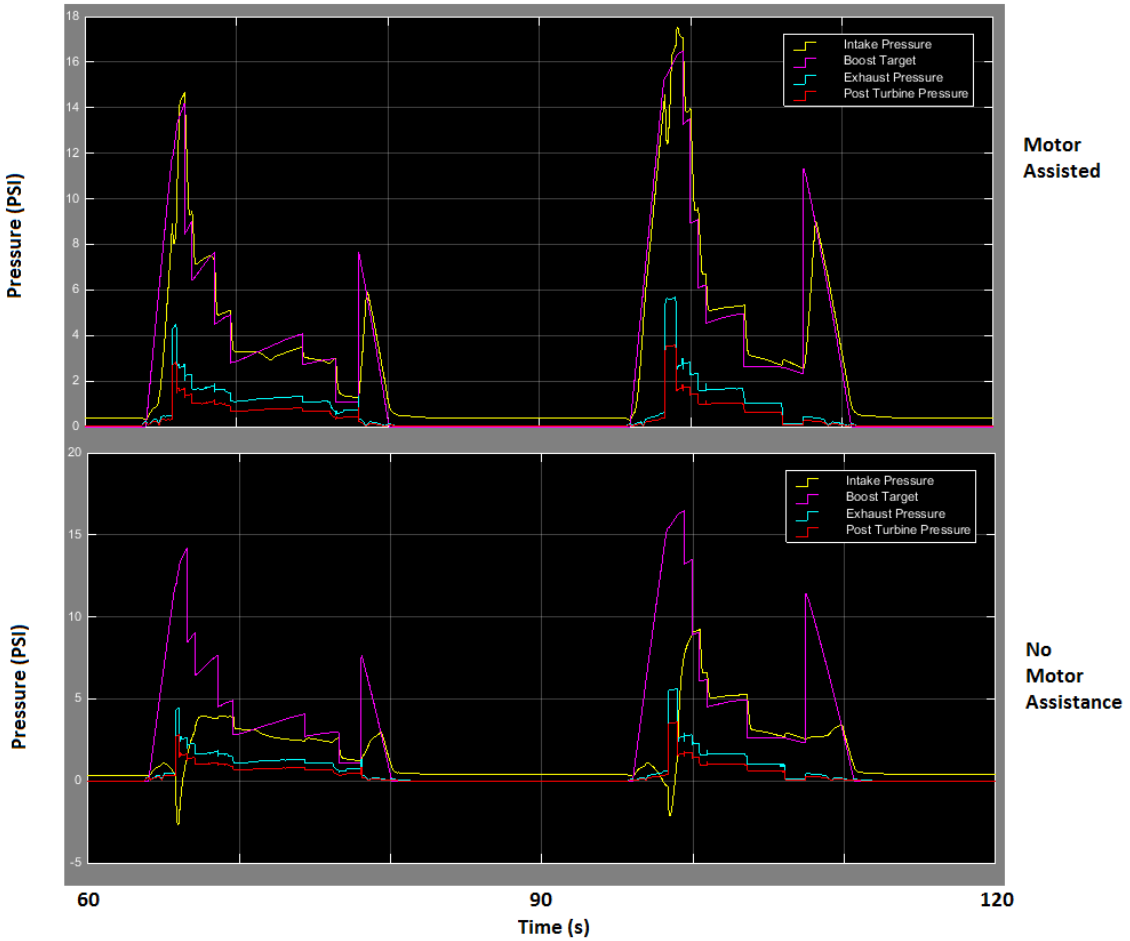

Figure 5.11: Intake Pressure Response Comparison

5.5 Resulting System Available Power

One of the most important aspects of this system is the surplus power between the turbine and compressor at the various operating points of the engine. This surplus

determines how fast the turbo shaft will accelerate and how much power is available for the system to recover. To determine this power, the model was run through a very basic test independently of the vehicle model. Programmed inputs effectively ran the model through a dynamometer test holding the engine at full load while controlling the operating speed. Figure 5.12 demonstrates surplus power available at the various operating points once the system has achieved steady-state. It can be seen that this model suggests that this engine, compressor and turbine combination is capable of generating an additional 30 kW of power from the exhaust gases at approximately 6000 RPM. Additional graphs of the various variables from within the model during this test are available in Appendix I. These graphs provide insight into the overall performance of this system at various operating points. However this data represents the system at steady-state and therefore neglects the time-variant behaviour of the system.

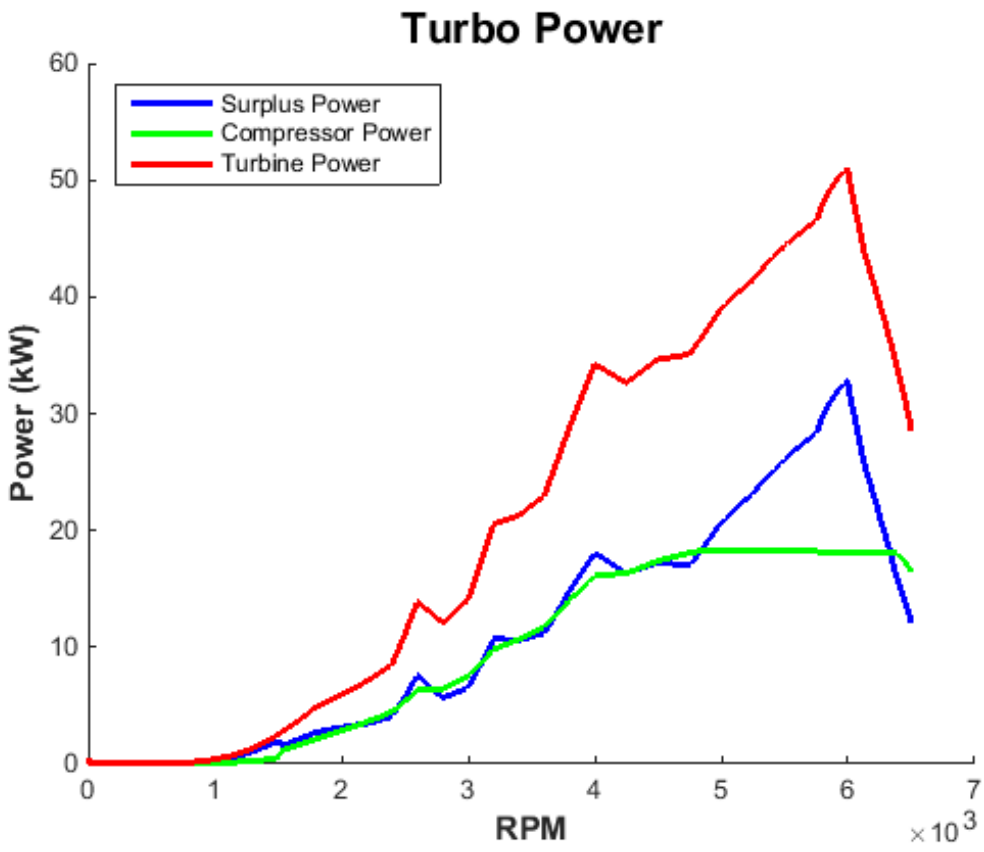

Figure 5.12: eTurbo Surplus Power

Chapter 6

Selection of Architectures and Controllers for Comparison

The final objective of this thesis is the comparison of impact a HESS and an eTurbo have on a performance hybrid vehicle. Each technology was simulated using the P1P2 Series-Parallel architecture available in the vehicle model. To complete this task, several steps had to be taken in order to allow each technology to be simulated independently and in an effort to ensure a fair comparison between the two technologies. This chapter will discuss the changes made to the modeling tool in order to make this comparison.

6.1 Overview of Method

Three different vehicle variants were created within the simulation tool. The tool provides some flexibility for altering components while retaining the same system behavior and controlled limits. The objective was to compare the impacts of these two technologies in a performance application. It was decided to use peak system power as the metric that must be held constant when varying the electrified aspect of these systems. While the different subsystem behaviors will influence differently, performance peak power is a metric used by individuals to measure performance of a vehicle. The EcoCAR Team conducted an intensive study during the architecture selection process investigating the feasibility, cost, efficiency and performance of a number of architectures. Some of the knowledge gained during this process supports the feasibility of the selected variants as similar subsystems changes were deemed feasible by the EcoCAR Team.

One of the most important aspects of this comparison is that the underlying vehicle including engine, motors, and control behavior will not be altered. There are two possible approaches that are equally valid when attempting to compare these two technologies. The first is modifying every aspect of the vehicle design in attempt to develop the best platform to showcase the technology. While modifying system components and behavior may be beneficial to a particular variant, the effort required is beyond the scope of this work. The second valid approach and ultimately the approach used is to alter as little as possible between the vehicle variants. In addition, the same battery cells will be used between each application which will result in

the predictable scaling of battery performance. Eliminating unnecessary variations between each variant will allow an individual to compare the technology without having to consider the differences in underlying subsystems. The difference between each vehicle's battery pack will be discussed throughout this chapter and in the results. In the sections to follow, the details on any minor adjustments made to models and controls to accommodate vehicle variants will be outlined.

6.2 Selected Architectures

6.2.1 P1P2 Series-Parallel with Basic Battery

This vehicle represents a conventional approach to the P1P2 Series Parallel Hybrid and provides a baseline to compare each technology. This vehicle uses the torque split strategy discussed in the Vehicle Model chapter.

Battery Overview

Using Model Referencing, a conventional battery model composed of LG Chem HG2 cells replaced the HESS model in the simulation tool. While the model still produces a signal for ultra-capacitors, as required by Model Referencing, these signals are set to zero during model initialization, simulation and post processing. In an effort to meet the power demand of the system it was necessary to use approximately 2.8 times the number of cells as the battery pack located in the HESS. Looking at the

peak charge rate, it would be necessary to have approximately 8 times the amount of cells in the pack to have a comparable momentary charge rate of the HESS. As the performance of the vehicle is more heavily weighted to the discharge power a battery pack containing 3 times the number of cells as in the HESS was selected. As the density and weights of the two packs in the HESS are approximately equal, this results in the pack being 50 percent larger and heavier when directly compared to the HESS packs. However as the battery no longer requires the DC-DC converter. The overall weight impact is approximately an additional 30kg to the vehicles gross weight. This additional weight will be updated in the vehicle model during simulation. Figure 6.1 outlines the basic battery model created for this vehicle variant.

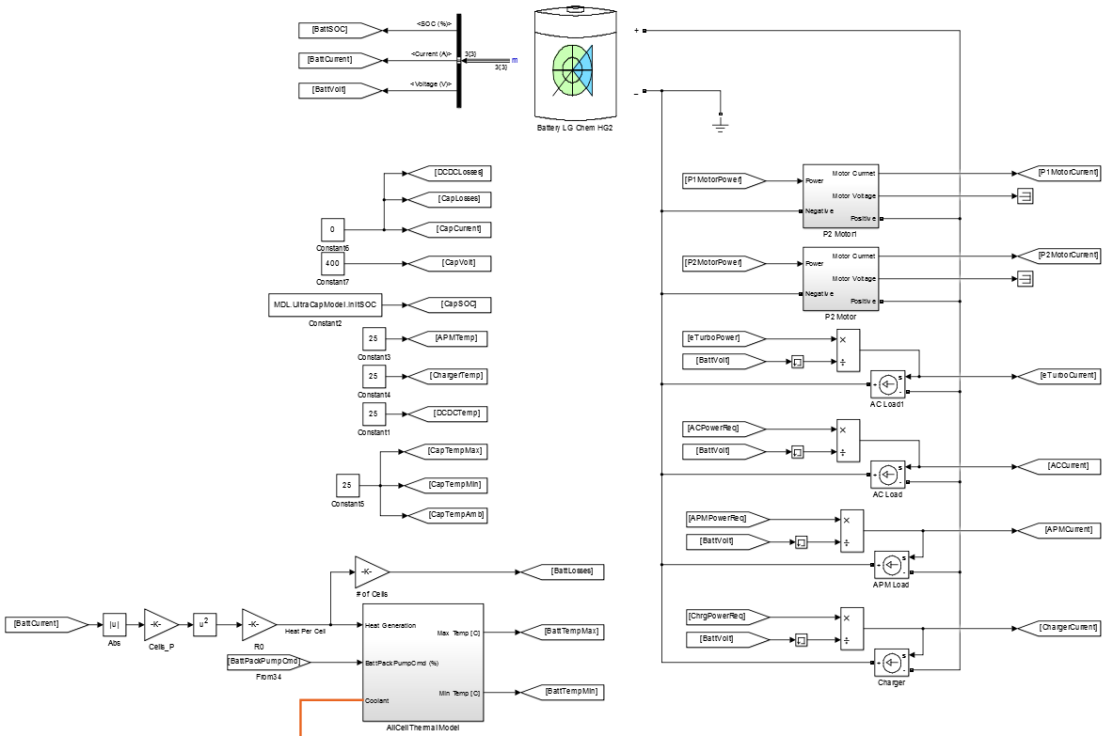

Figure 6.1: Basic Battery Model

Supervisory Controller Logic

Changing the battery requires the limit calculations and HESS controls to be modified. As there is no longer an active control of energy in the ESS, all DC-DC converter controls were removed and all limit calculations were updated to reflect the system.

6.2.2 P1P2 Series Parallel with HESS

This vehicle represents the vehicle as is specified by the EcoCAR 3 Team. All modifications to the vehicle model and controls discussed in the Vehicle Model and HESS Chapters are applied to this configuration of the vehicle.

6.2.3 P1P2 Series Parallel with eTurbo

Powertrain Overview

Using Model Referencing a different engine block was created that contains the eTurbo as a sub-model. In order to represent this new demand on the Battery Block, the power demand of the eTurbo motor was propagated out of the engine model and into Battery block.

Battery Overview

In an effort to achieve equivalent performance with the eTurbo system, several system level behaviors have to be considered. The first of these behaviors is the maximum power generated by the system. This is highly correlated to the engine output power and therefore to the powertrains operating RPM.

In sizing a battery to achieve similar performance the change in the engine response from decreased turbo lag should also be considered. Since the model created cannot

accurately compare this effect it is difficult to quantify. To match peak power without providing 30kW from the eTurbo system, the battery needs to be 2.5x the size of the battery in an HESS. In the interest of compensating for the engine response and the continuous nature of the eTurbo a battery 2 times the size of the battery pack in the HESS was selected for this vehicle variant. While this solution provides reduced peak power in comparison to the other vehicle variants the continuous peak power post battery depletion is larger. The same battery model created for the basic vehicle variant was used and the parameters of the number and arrangement of cells was updated.

Supervisory Controller Logic

For this vehicle, the battery limits were updated. Since the eTurbo model will not be used by the EcoCAR Team moving forward, no effort was made to integrate the eTurbo controls into the controller model. Therefore, the controls for the eTurbo remain embedded in the eTurbo model. To ensure a valid simulation a minor modification to the controller ESS limits was made to account for the power demand of the eTurbo. The ESS power limits logic is complex and spans many subsystem with a hierarchy of priorities and remediating actions. Due to time constraint, it was decided that the eTurbo power demand be placed before all others simply reducing the power available to all other systems when required by the eTurbo. This solution requires the least amount of controls rework and in reality, would not be far from a fully developed implementation. No feedback was propagated to the eTurbo controller. As a result

it assumes it is free to operate without limits. With its power demands being small relative to the operating limits of the battery, the chance of the system violating the safe operating boundaries during normal operation is minimal. During all tests, the battery operating limits were checked to ensure the eTurbo did not violate the ESS operating limits.

6.2.4 Testing Vehicle Summary

The table below summarizes the three vehicle variants. A detailed discussion can be found in the previous section.

Table 6.1: Vehicle Comparison Summary

Vehicle	**Energy Storage System**	**Additional Electrical**	**Electrical Peak Power**	**Energy Storage**	**Weight**
P1P2 Series Parallel	84s36p LG Chem HG2		250 kW Discharge 50 kW Charge	32.4 kWh	Base + 25 kg
P1P2 Series Parallel with HESS	84s12p LG Chem HG2 108s JSR Micro Ultimo 3300		240 kW Discharge 160 kW Charge	11.3 kWh	Base
P1P2 Series Parallel with eTrubo	84s24p LG Chem HG2	30 kW Peak eTurbo with Turbo Lag Reduction	200 kW Discharge 34 kW Charge	21.6 kWh	Base

6.3 Drive Cycles and Testing Metrics

Each of the vehicle variants were driven through a number of drive cycles. All changes discussed above were made to each vehicle and the changes were tested ensuring correct behavior. The results of the drive cycles were post processed and some of the most interesting performance metrics were compared. While it would be possible to

compare moment-by-moment performance, the presented metrics are restricted to high level results to avoid momentary bias.

6.3.1 Traditional Driving

There are several metrics that were recorded and analyzed that provide an understanding of the efficiency of the variants. The overall vehicle fuel efficiency was calculated using the EcoCAR 4 Cycle. This will provide the greatest insight to the impact of the various components. This analyses will be further broken down into energy consumption in CD and CS mode of the powertrain. For larger calculated CD ranges the vehicle may prove to be more fuel efficient over its lifetime depending on the owners typical driving and plug in charging habits. Behavior and performance metrics of the HESS and eTurbo system were also analyzed. Finally the efficiency of each ESS was calculated as this is important in understanding the difference between each electrified system.

6.3.2 Performance Driving

There are two distinct metrics that can be compared using the performance model and drive cycles. The first of these is the vehicle's CD maximum performance where the vehicle is unrestricted in its use of energy. The second major performance metric looks at long term performance where the vehicles continuous to operate in CS. In addition, the thermal limitations were recorded. The behavior of the HESS and eTurbo system

will also be analyzed. Finally the SOC over time of each ESS system was examined as well as the ESS limits and impact of these limitations on performance.

One additional note that must be made relates to the process used to generate the drive cycle for this analysis. The drive cycle generated by OptimumLap was generated using a specific vehicle weight and a generic weight balance assumption. Each of these vehicles will have different gross weights and weight distributions which would result in a different drive cycle result from OptimumLap. However, the margin of error in these estimations were larger than the estimated difference calculated by OptimumLap. Therefore the same drive cycle was used for each of the vehicles. It would be more accurate to perceive this simulation not as a track simulation but a series of braking, speed limited and unlimited zones in a single dimension. This essentially provides a more targeted assessment of the powertrains performance when comparing these different vehicle platforms. Adjusting the gross weight in the chassis model provides some adjustment towards assessing the vehicle's actual performance. The full extent of the impact is difficult to assess using this approach.

Chapter 7

Hybrid Powertrain and Controller Variations Simulation Results

This chapter contains the results from the simulations detailed in the previous chapters. Two distinct tests were performed with each of the vehicles as such this chapter first examines the results of conventional driving followed by performance driving. This chapter also includes recommendations for future work and potential improvements to the models and processes.

7.1 Traditional Driving

7.1.1 Energy and Fuel Consumption

Table 7.1: EcoCAR 4 Cycle Fuel Economy Result for Each Vehicle Variation

Vehicle	**CD Fuel Economy MPGe (L/100km)**	**CS Fuel Economy MPG (L/100km)**	**CD Energy Consumption kWh/Km**	**CS Energy Consumption kWh/Km**	**CD Range Mi(Km)**
P1P2 Series Parallel	59.0 (4.0)	30.2 (7.8)	0.355	0.694	68 (110)
P1P2 Series Parallel with HESS	50.8 (4.6)	30.8 (7.6)	0.412	0.679	19 (31)
P1P2 Series Parallel with eTurbo	53.2 (4.4)	31.2 (7.5)	0.394	0.671	42 (68)

Using the EcoCAR 4 Cycle the fuel economy of each vehicle variant was calculated. The important aspect of this comparison is not the results in comparison to regular fuel economy ratings, but the differences between each vehicle. Governing bodies like the EPA use a different combination of driving scenarios to determine fuel economy. While the EcoCAR 4 Cycle provides a mixture of drive cycles, no analysis between this set of cycles and standard EPA test have been completed. It is also important to note that no accessory loads or HVAC loads have been including in the energy demand during this analysis.

The results show the larger battery solution performs best during CD which can be explained when the ESS efficiencies are examined later in this chapter. It is interesting to see that both the HESS and eTurbo outperform the larger battery during CS. This could be the result of a number of factors including the weight difference and subsystem behaviors.

7.1.2 eTrubo Impact

Figure 7.1 is a composite graph containing all CS drive cycles of the eTurbo based vehicle. The most immediate observation is the limited operation time of the eTurbo system. This is primarily caused by the average low RPM operation of the engine during the majority of CS operation. Two enhanced sections of the figure provide insight to the behavior of the eTurbo during these driving cycles. Power consumption (positive) is generally larger and shortly followed by some generation (negative). This is the result of the eTurbo being used to reduce the turbo lag and increase the intake pressure faster when the engine load is increased. Engine load increases are usually shortly followed by a load decrease resulting in a higher than needed boost pressure. The eTurbo then recaptures a proportionally smaller amount of energy than used to build pressure. In general, the engine fails to operate at sufficient RPM and load for the system to produce more energy than it demands.

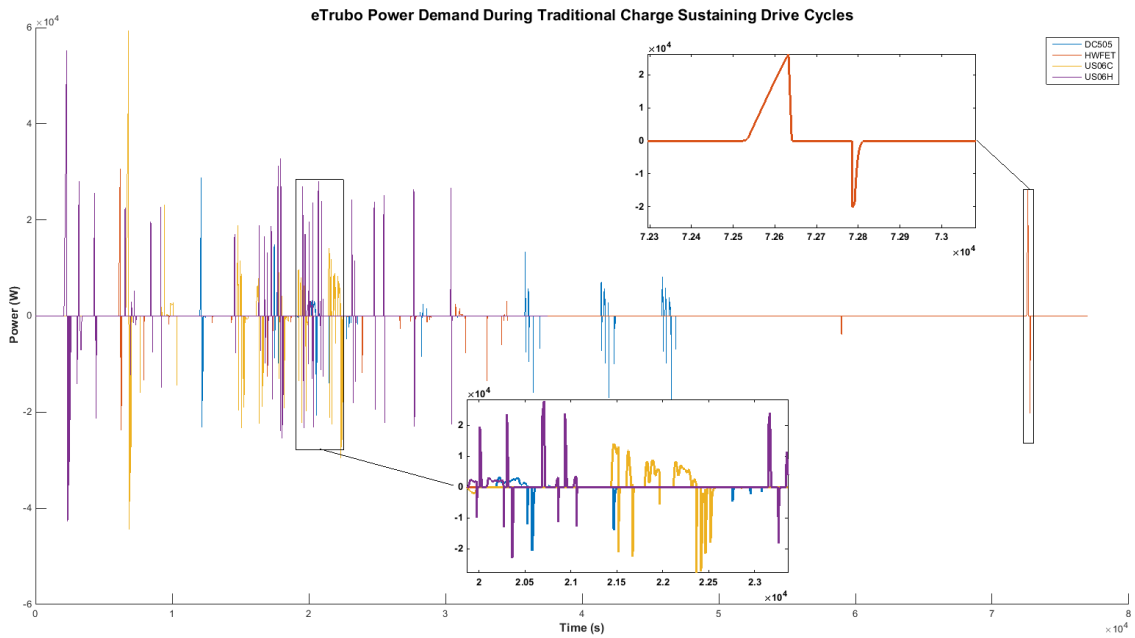

Figure 7.1: eTurbo Power Demand

Table 7.2 summarizes the energy consumed by the eTurbo system during CS cycles. For two of the CD cycles the engine does not operate resulting in a zero power demand from the eTurbo system. The more demanding cycles result in larger, more frequent engine loads ultimately resulting in a larger energy consumption.

Table 7.2: eTurbo Energy Consumption

Drive Cycle	**Charge Depleting Energy (Wh)**	**Charge Sustaining Energy (Wh)**
DC505	0	7.7
HWFET	0	4
US06C	19.9	20.2
US06H	30	31

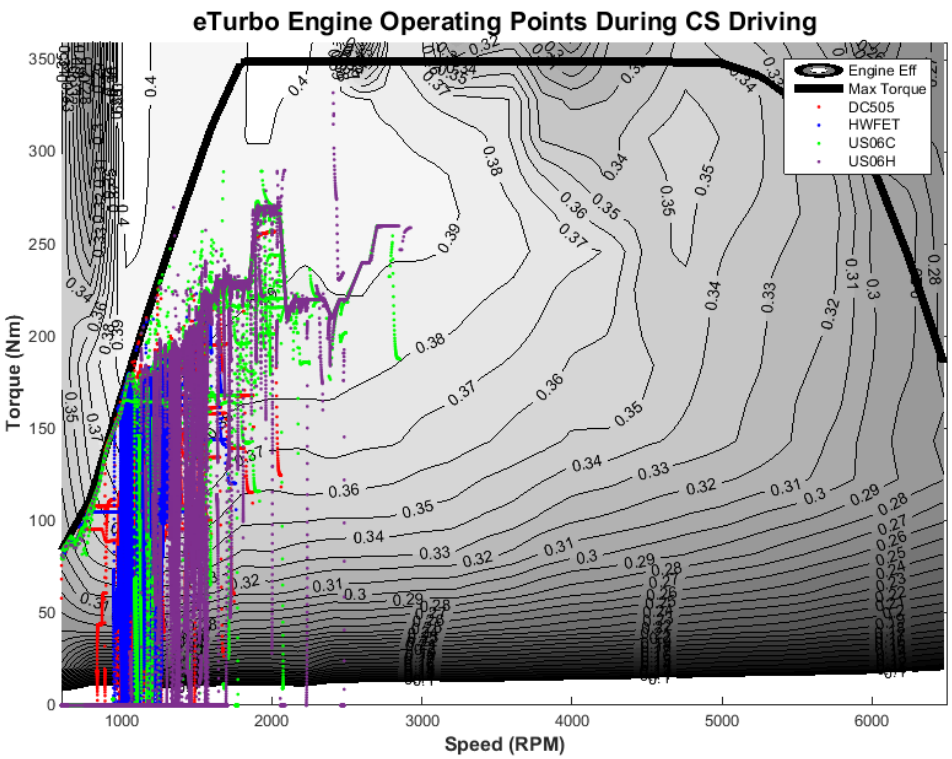

Figure 7.2: eTurbo Engine Operating Points During CS Driving

Figure 7.2 contains a plotted point for every engine operating point during all CS drive cycles. This supports the conclusion that the engine fails to sustain high enough RPM and loads to support significant exhaust gas energy recovery. This identifies a sizing mismatch in the system in which the powertrain is too powerful to be stressed during conventional drive cycles. This suggests that placing an eTurbo in a performance application will result in the system being underutilized during conventional driving.

7.1.3 HESS Balance

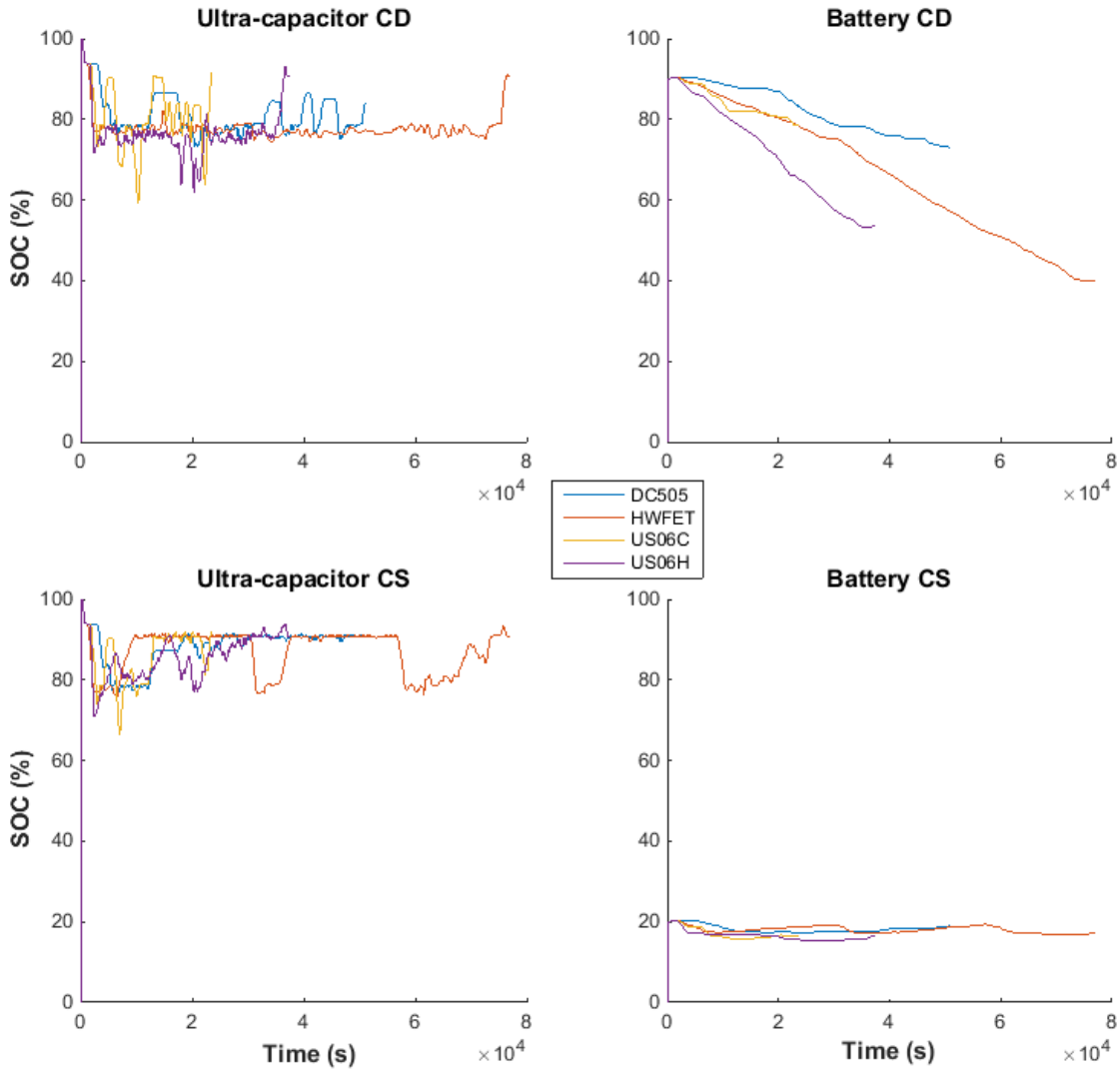

Figure 7.3: HESS Component SOCs for all Drive Cycles

Figure 7.3 above outlines the behavior of the HESS over all drive cycles. The results of the work on the HESS control and optimization can be seen here with the SOC of the ultra-capacitor being maintained depending on the drive mode.

7.1.4 ESS Efficiencies

Table 7.3: Energy Storage System Efficiencies

Vehicle	**DC505**	**HWFET**	**US06C**	**US06H**	**EcoCAR 4 Cycle Weighted**
P1P2 Series Parallel	98.4%	98.5%	96.4%	97.1%	97.5%
P1P2 Series Parallel with HESS	91.7%	90.5%	89.4%	89.4%	90.2%
P1P2 Series Parallel with eTurbo	97.8%	97.4%	94.1%	95.3%	96.1%

One of the major contributing factors to a vehicle's CD energy consumption was the efficiency of the ESS system. There is a significant difference in efficiency between the HESS when compared to the two larger battery options. Considering that during CD operation, energy stored in the battery must first pass through the DC-DC converter, the HESS efficiency is reduced. In addition the DC resistance of the ultra-capacitor pack is higher than the larger battery options. For identical current the HESS is less efficient. One difference in system efficiency that is not represented here is the result of the HESS's ability to regulate bus voltage. This results in higher electric

motor efficiency and lower current for a given power demand. From the fuel economy results, we can conclude that the improvements in efficiencies of other components does not outweigh the efficiency losses within the HESS resulting in an overall less efficient vehicle. We can also conclude that the basic vehicle variant is more efficient in part due to the greater efficiency of larger battery.

7.1.5 Suggestion for eTurbo Future Work

With many possible methods of integration for an electronic turbocharger this particular implementation represents a performance oriented solution. Having tested alternative options of the eTurbo controller, energy recovery instead of consumption can be achieved even at lower operating conditions. The caveat with this alternative control is that the system would not compensate for turbo lag and with the additional inertia of the electric motor the turbo lag could significantly increase. This may not actually be a problem to the overall operation of the engine. However a more advanced model would be required to properly investigate this hypothesis. In addition the effects of engine back pressure at lower boost pressures would need to be considered. Alternatively, designing a system containing a second turbine and motor may allow for better energy recovery. This secondary system could focus on capturing energy during low load and RPM regions of operation. A model that is capable of assessing the impact on engine response would allow for the further development of the system with a focus on energy recovery during conventional operation.

In addition, an opportunity to downsize the system further and create a complete

solution for series hybrid or range extended EV is possible. This model could be scaled to assess the feasibility of such a system. Only requiring a new engine, compressor and turbine maps it would interesting to see the effects of an eTurbo in a system level design targeted at efficient operation and not performance.

7.2 Performance Driving

7.2.1 Lap Time

Figure 7.4 provides the most comprehensive view of vehicle performance. Each stem represents the lap time of the vehicle with first lap being a traditional standing start lap and all subsequent laps carrying the speed from the previous lap. With so many dynamics affecting performance, additional figures are required to explain these results but clear differences can be seen between the vehicles.

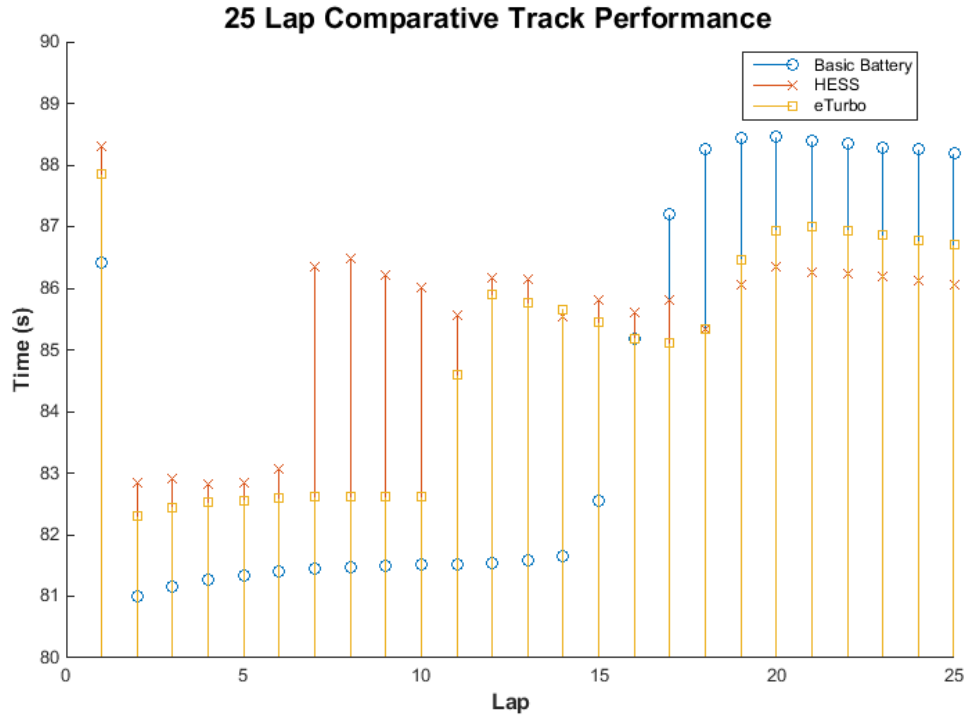

Figure 7.4: Vehicle Track Time Comparison

Treating this simulation as a race, the resulting order of the race would be basic battery placing first, eTurbo second and finally the HESS variant placing third. Although not presented here, additional simulations testing different environmental scenarios suggest that the final result may not always be similar to the results presented. As the ending of this figure and subsequent figures will demonstrate, long term performance will result in the HESS system eventually out performing the other systems. In a higher temperature environment, thermal limits of the HESS could result in the

eTurbo variant outperforming .

7.2.2 eTrubo Impact

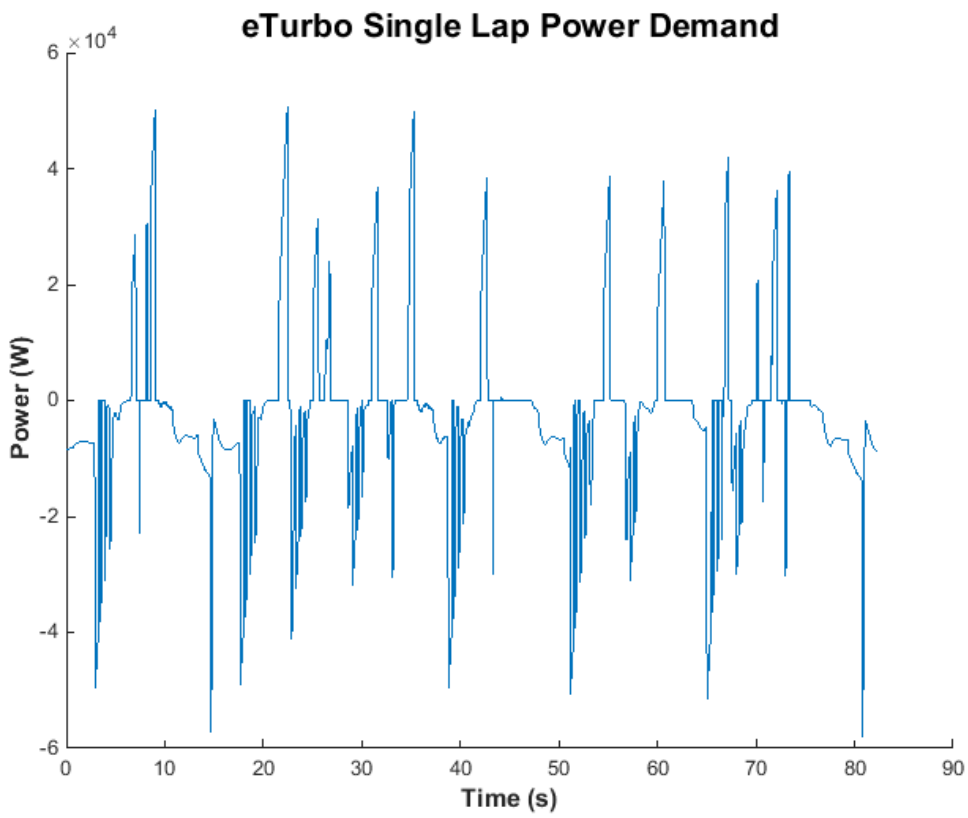

Figure 7.5: Single Lap eTurbo Power Demand

In contrast to traditional driving, the power demand of the eTurbo system during performance driving appears very different with the system actively consuming or

producing energy for the majority of the vehicle operation. It can also be seen in Figure 7.5 that the system is spending a considerable amount of time recovering energy. Over the course of the 25 lap simulation, the system recovered approximately 4.6 kWh of energy. Producing up to 20 kW of power during vehicle wide open throttle events, the estimated surplus through the steady state test was an optimistic assessment in comparison to the dynamic generation of the system.

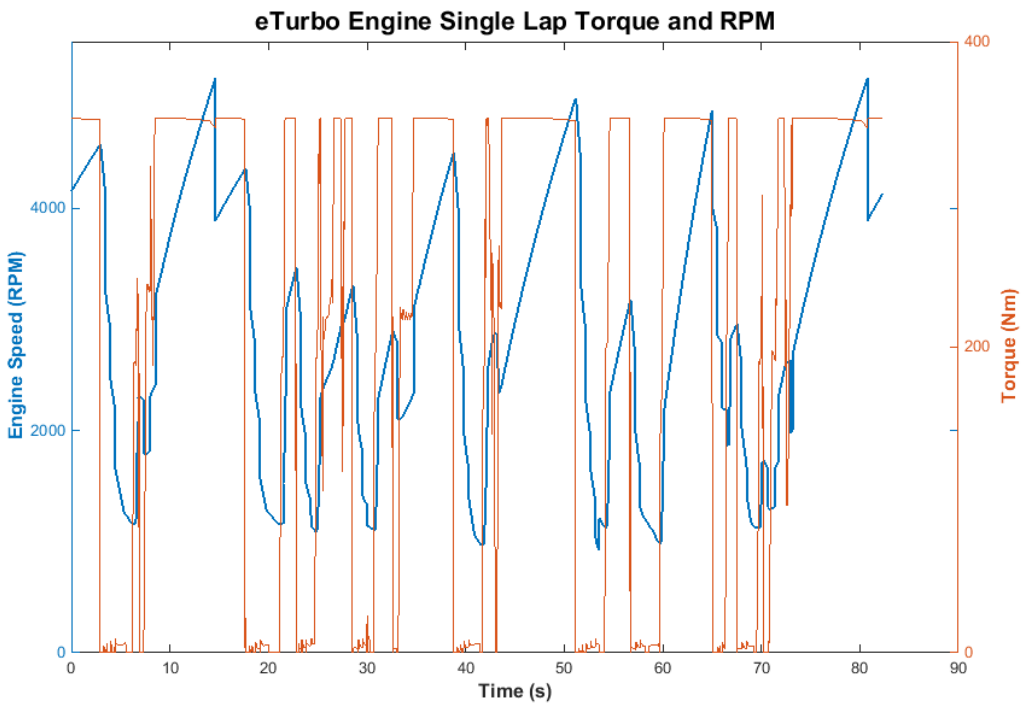

Figure 7.6: eTurbo Engine Single Lap Torque and RPM

The simplistic shifting schedule used during this testing is aggressive in shifting to

higher gears. This was developed initially in attempt to achieve better efficiency of the electric motors. The current shifting schedule also shifts earlier than the speed limit of the system in attempt to keep the engine motor combination in its peak power zone. This logic is not dynamic and has not been adjusted for the eTurbo system. A more performance orientated shifting schedule with higher RPM should result in the eTurbo system recovering more energy at higher powers. Performance improvement during CD and CS could be realized with improvements to powertrain controller.

7.2.3 HESS Balance

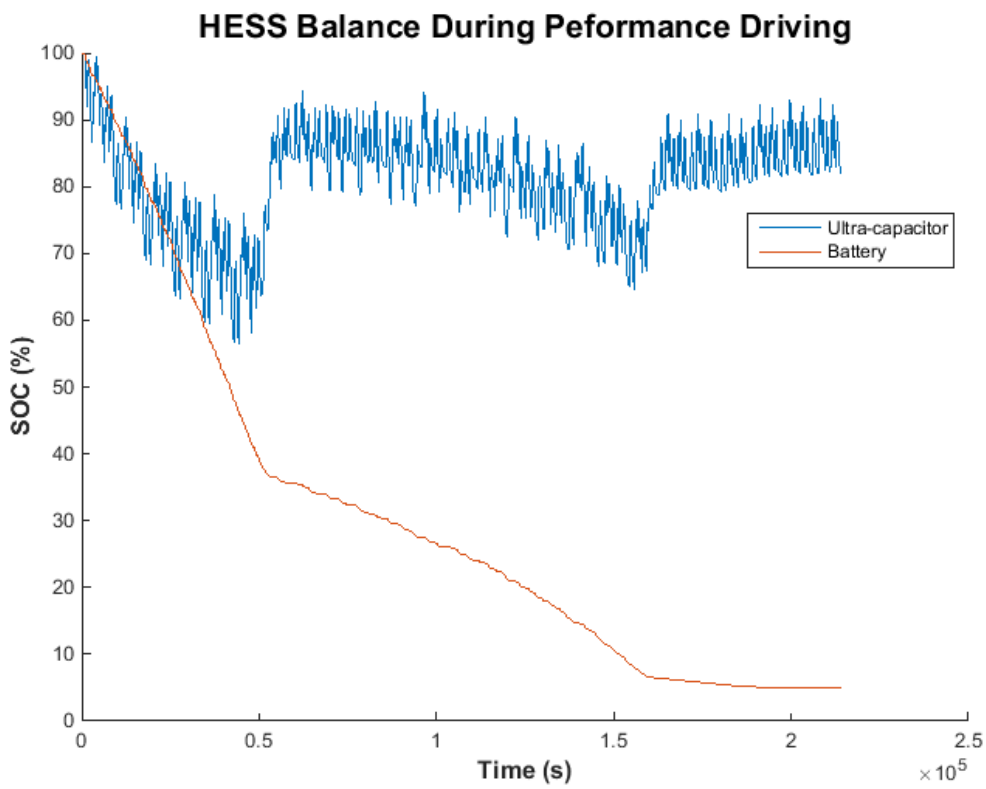

Figure 7.7: HESS Performance Driving Behavior

The resulting HESS SOC plot (Figure 7.7) demonstrates several interesting behaviors of the system. The first being the constrained nature of the ultra-capacitor SOC. This is due to the high-side low-side voltage relationship limit of the DC-DC converter. Maintaining adequate voltage difference is important to the proper operation of the HESS. It can also be seen that when the thermal limit and SOC limit is reached,

the SOC must recover to a higher value before aggressive cycling of ultra-capacitors continues. This smae behaviour occurs again when the SOC limit of the battery is reached. This is a result of the battery terminal voltage increasing when the current from the battery is reduced. This explains the sudden drop in performance on lap 7 of the 25 lap performance test. Figure 7.8 is the terminal voltage of the two packs. With the exception of a few momentary artifacts, a result of the time step and delay of information around the model, and adequate voltage separation is maintained throughout the simulation.

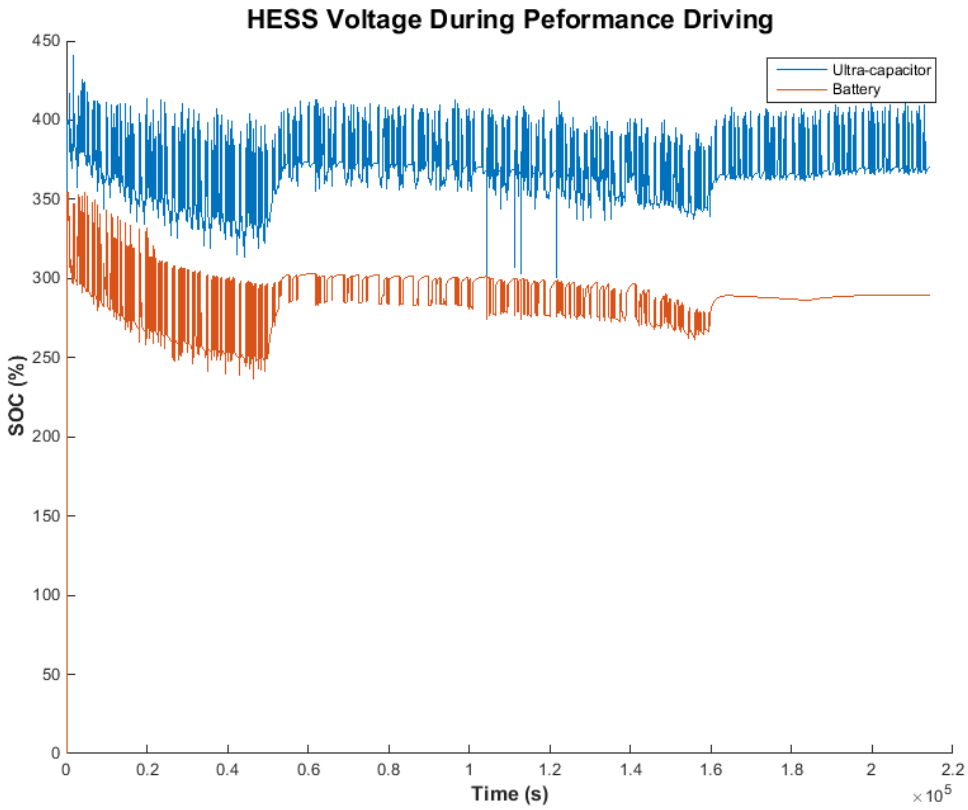

Figure 7.8: HESS Voltage During Performance Driving

7.2.4 ESS SOC

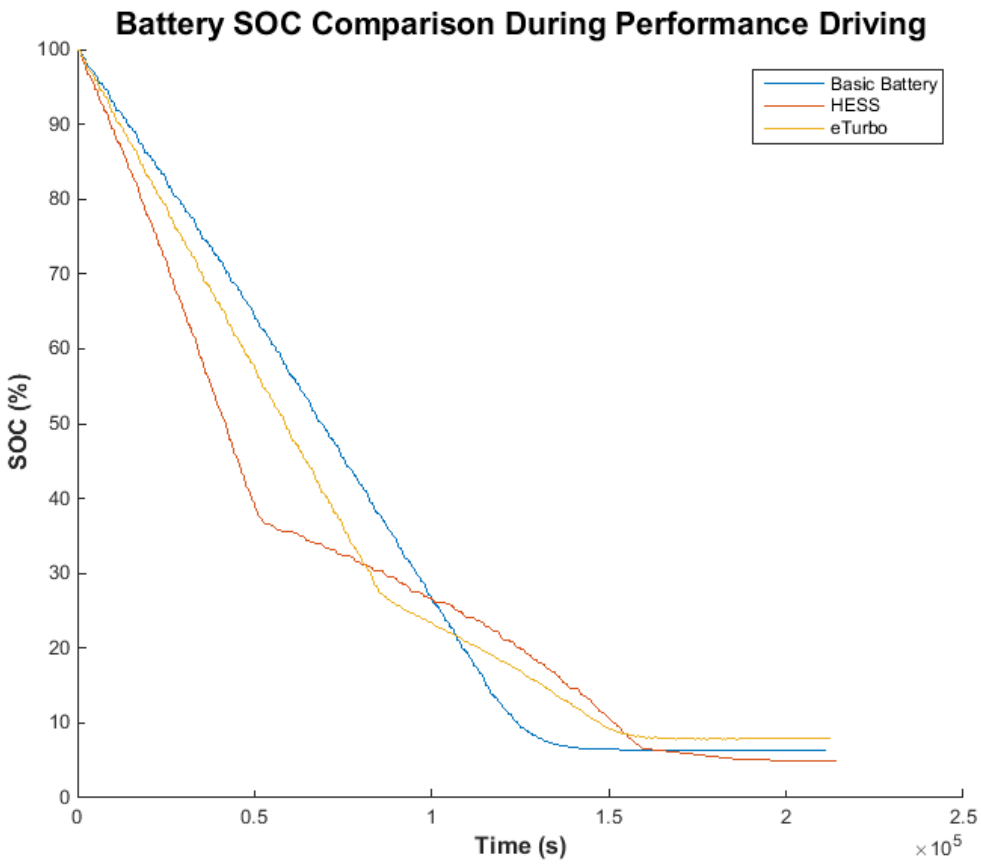

Figure 7.9: ESS SOC Depletion Comparison

Figure 7.9 demonstrates the impact on size of the battery over the course of the race. We can understand that continuous power output of these packs over this period must be proportional to their energies. This explains the basic P1P2 Series-Parallel's advantage during the first half of the simulation. Its high continuous power rate of

the larger battery. The non-linear discharge curves of the HESS and eTurbo vehicles hints at the next factor in the performance of these systems.

7.2.5 ESS Thermal

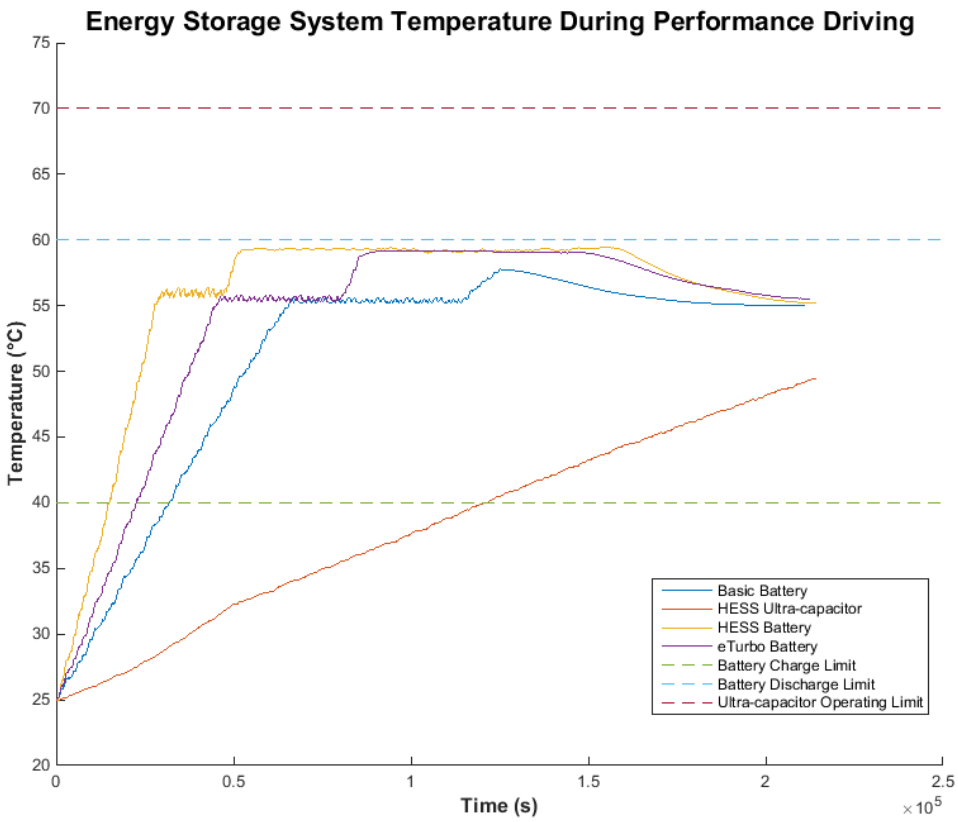

Figure 7.10: ESS System Temperature During Performance Driving

Figure 7.10 presents expected peak ESS cell temperatures during this drive cycle This figure also demonstrates when the limits of these components have been reached. There are several key factors that can be observed from this figure. These include, the difference in heat generation due to the discharge rates. The HESS's battery usage appears to be more aggressive resulting in thermal limits being reached earlier in the simulation. A more comprehensive view of the temperature across the battery module during this simulation can be seen in Appendix A. In addition we can also conclude that the power supply of the eTurbo and size of the basic vehicles battery result in less heat generation per mass during CD driving. The behavior of the phase change material can be observed with temperature plateaus occurring in each of the systems. For two of the systems the PCM is completely saturated in the center rows of the pack resulting in the heat reaching the discharge limit and the control system limiting discharge until the pack is exhausted. The heat generation rate for the basic pack is scaled back such that the heat is managed successfully by the system resulting in the SOC limit being reached before thermal limits are reached.

In all vehicles, the thermal charge limit of the battery pack is reached resulting in disable battery charging for the majority of the simulation. For the basic and eTurbo variants, this results in regenerative braking being completely disabled. Due to the high operating limits of the ultra-capacitors, regenerative braking remains active through the entire simulation. Comparing this the CS performance of the vehicle we can conclude that energy captured through regenerative braking during CS operation is greater than the energy recovered by the eTurbo. This results in the HESS out performing all vehicles once the battery SOC limits have been reached.

7.2.6 Suggestion for Future HESS Performance Work

Having analyzed the behavior of the powertrain and HESS systems there exists an opportunity to further improve the HESS performance. With the additional thermal capacity of the ultra-capacitors the powertrain of the vehicle could recover additional energy into the HESS during braking and non peak load demands. Not only could this improve CS performance by making more energy available to the powertrain during acceleration. It would also reduce the load on the battery during the CD performance driving. The additional benefits from an improved control algorithm would result in improved HESS performance during the entire simulation at the cost of additional fuel consumption.

Chapter 8

Conclusion

Three vehicle variants were created using the simulation tool developed by the McMaster Engineering EcoCAR 3 Team and models of a Hybrid Energy Storage System and an electrified turbocharger. By holding the powertrain and vehicle level control algorithms constant, the vehicle variants were simulated over several traditional and performance drive cycles.

The traditional driving analysis demonstrated that a vehicle containing a large battery argumentatively outperformed the innovative vehicle variants when observing vehicle efficiency. ESS efficiency was the largest differentiating factor between each vehicle. The HESS with an efficiency of only 90% performed the worst when comparing vehicle fuel economy. Although the designed eTurbo system has the ability to recover up to 50 kW of power, no fuel economy benefit was observed by including this system. The performance orientated nature of the vehicle resulted in an underutilization

of the internal combustion which in turn resulted in poor electrified turbocharger performance.

During performance driving the larger battery offers improved short term performance while the HESS provides the best long term performance. Although effort was spent in developing controls for both innovative systems, improvements to vehicle and system level control strategies could further increase the impact of both innovative technologies. With these two technologies there exists the potential to create a high performing hybrid vehicle that is not as susceptible to the energy and thermal limits of its battery for today's performance consumer market. The ability for these systems to offer better power densities also provides a level of attractiveness when considering the importance of size and weight in a performance application.

Overall, no one vehicle variant was superior. The choice to incorporate one of these technologies is reliant on target vehicle specifications and expected driving scenarios. While both of the technologies bring unique benefits the conventional approach of carrying a large battery can still be an effective choice.

Bibliography

[1] ABB (2014). Septa advances energy efficiency goals with unique hybrid energy storage system from abb. http://www04.abb.com/global/usabb/usabb045.nsf!OpenDatabase&db=/global/usabb/usabb049.nsf&v=1A6E&e=us&url=/global/seitp/seitp202.nsf/0/749EFC2C93DEE20A85257C5D004B8B12!OpenDocument.

[2] Administration, N. H. T. S. (2016). Cafe - fuel economy. Online; accessed October 12, 2016, http://www.nhtsa.gov/Laws-&-Regulations/CAFE-%E2%80%93-Fuel-Economy.

[3] AG, S. (2010). Sitras hes. https://w3.usa.siemens.com/mobility/us/Documents/en/rail-solutions/railway-electrification/dc-traction-power-supply/sitras-hes-en.pdf.

[4] Agency, E. U. E. P. (2016). Dynamometer drive schedules. Online; accessed September 12, 2016, https://www.epa.gov/vehicle-and-fuel-emissions-testing/dynamometer-drive-schedules.

[5] Algrain, M. (2005). Controlling an electric turbo compound system for exhaust

gas energy recovery in a diesel engine. In *2005 IEEE international conference on electro information technology*, pages 6–pp. IEEE.

[6] AllCell (2016a). Pcc thermal management. Online; accessed September 14, 2016, `https://www.allcelltech.com/index.php/technology/pcc-thermal-management`.

[7] AllCell (2016b). Phase change composite (pcc) thermal management material. Online; accessed September 14, 2016, `https://www.allcelltech.com/index.php/products/thermal-management-material`.

[8] Arshad-Ali, S. K. (2015). *Suitability of Hybrid Electric Powertrains with Electric Turbocharger*. Master's thesis, McMaster University.

[9] Avelino, W., Garcia, F., Ferreira, A., and Pomilio, J. (2013). Electric go-kart with battery-ultracapacitor hybrid energy storage system. In *Transportation Electrification Conference and Expo (ITEC), 2013 IEEE*, pages 1–6. IEEE.

[10] Batterybros.com (2015). Lg hg2 review (20a, 3000mah). Online; accessed September 7, 2016, `https://batterybro.com/blogs/18650-wholesale-battery-reviews/57179459-lg-hg2-review-20a-3000mah`.

[11] Besharati, M., Pullen, K., Widmer, J., Atkinson, G., and Pickert, V. (2014). Investigation of the mechanical constraints on the design of a super-high-speed switched reluctance motor for automotive traction. In *Power Electronics, Machines and Drives (PEMD 2014), 7th IET International Conference on*, pages 1–6. IET.

[12] Brito, I. H. (2007). *Modeling and Control of Wastegate Equipped Turbocharged Engines*. Master's thesis, The University of New Mexico.

[13] Brusa (2016). Bdc546 - bidirectional 750 v dc/dc-converter. Online; accessed September 14, 2016, `http://www.brusa.biz/fileadmin/template/Support-Center/Datenbl%C3%A4tter/BRUSA_DB_EN_BDC546.pdf`.

[14] Cao, J. and Emadi, A. (2012). A new battery/ultracapacitor hybrid energy storage system for electric, hybrid, and plug-in hybrid electric vehicles. *IEEE Transactions on Power Electronics*, **27**(1), 122–132.

[15] caranddriver.com (2014). 2014 mclaren p1. Online; accessed September 9, 2016, `http://www.caranddriver.com/mclaren/p1`.

[16] caranddriver.com (2016a). Acura nsx. Online; accessed September 9, 2016, `http://www.caranddriver.com/acura/nsx`.

[17] caranddriver.com (2016b). Bmw i8. Online; accessed September 9, 2016, `http://www.caranddriver.com/bmw/i8`.

[18] caranddriver.com (2016c). Ferrari laferrari. Online; accessed September 9, 2016, `http://www.caranddriver.com/ferrari/laferrari`.

[19] caranddriver.com (2016d). Koenigsegg regera. Online; accessed September 9, 2016, `http://www.caranddriver.com/koenigsegg/regera`.

[20] caranddriver.com (2016e). Porsche 918. Online; accessed September 9, 2016, `http://www.caranddriver.com/porsche/918`.

[21] caranddriver.com (2016f). Tesla model s. Online; accessed September 9, 2016, http://www.caranddriver.com/tesla/model-s.

[22] caranddriver.com (2018). 2008 tesla roadster. Online; accessed September 9, 2016, http://www.caranddriver.com/reviews/2008-tesla-roadster-road-test.

[23] Chayopitak, N., Pupadubsin, R., Karukanan, S., Champa, P., Somsiri, P., and Thinphowong, Y. (2012). Design of a 1.5 kw high speed switched reluctance motor for electric supercharger with optimal performance assessment. In *Electrical Machines and Systems (ICEMS), 2012 15th International Conference on*, pages 1–5. IEEE.

[24] Chemali, E., McCurlie, L., Howey, B., Stiene, T., Rahman, M. M., Preindl, M., Ahmed, R., and Emadi, A. (2015). Minimizing battery wear in a hybrid energy storage system using a linear quadratic regulator. In *Industrial Electronics Society, IECON 2015-41st Annual Conference of the IEEE*, pages 003265–003270. IEEE.

[25] Continental (2016). electrification. Online; accessed September 7, 2016, http://www.continental-automotive.com.

[26] Daniel.Cardenas (2016). Global plug-in vehicle sales, 2011-2015. Derived from http://energy.gov/; Online; accessed September 7, 2016, https://commons.wikimedia.org/w/index.php?curid=47932154.

[27] Edmondson, L. (2016). Why an f1 car is more energy efficient than an electric car. Online; accessed October 1, 2016, http://www.espn.co.uk/f1/story/_/id/15152695/why-f1-car-more-energy-efficient-electric-car.

[28] Evolution, A. (2016). Renault details new formula one engine. Online; accessed October 1, 2016, http://s1.cdn.autoevolution.com/images/news/gallery/renault-details-new-formula-one-engine-photo-gallery_7.png.

[29] Frigo, S., Pasini, G., Marelli, S., Lutzemberger, G., Capobianco, M., Bolognesi, P., Gentili, R., and Ceraolo, M. (2014). Numerical evaluation of an electric turbo compound for si engines. Technical report, SAE Technical Paper.

[30] Holloway, H. (2012). Audi reveals electric turbocharger technology. Online; accessed September 7, 2016, http://www.autocar.co.uk/car-news/motoring/audi-reveals-electric-turbocharger-technology.

[31] Huria, T., Ceraolo, M., Gazzarri, J., and Jackey, R. (2012). High fidelity electrical model with thermal dependence for characterization and simulation of high power lithium battery cells. In *Electric Vehicle Conference (IEVC), 2012 IEEE International*, pages 1–8.

[32] INGOLSTADT/REIFNITZ (2015). Audi tt clubsport turbo technology concept car set to debut. Online; accessed September 7, 2016, https://www.audiusa.com/newsroom/news/press-releases/2015/05/audi-tt-clubsport-turbo-technology-concept-car-set-to-debut.

[33] Jackey, R., Saginaw, M., Sanghvi, P., Gazzarri, J., Huria, T., and Ceraolo, M. (2013). Battery model parameter estimation using a layered technique: An example using a lithium iron phosphate cell. Technical report, SAE Technical Paper.

[34] Jackey, R. A., Plett, G. L., and Klein, M. J. (2009). Parameterization of a

battery simulation model using numerical optimization methods. Technical report, SAE Technical Paper.

[35] Kachapornkul, S., Somsiri, P., Pupadubsin, R., Nulek, N., and Chayopitak, N. (2012). Low cost high speed switched reluctance motor drive for supercharger applications. In *Electrical Machines and Systems (ICEMS), 2012 15th International Conference on*, pages 1–6. IEEE.

[36] Li, Y., Zhao, C., Zhu, Z., Wu, F., Guo, F., and Zhang, Z. (2012). Investigation on the control strategy for the compound cycle of turbo diesel engine. In *Computer Distributed Control and Intelligent Environmental Monitoring (CDCIEM), 2012 International Conference on*, pages 385–389. IEEE.

[37] Matlab (2016a). Mathworks documentaiton - battery. Online; accessed September 13, 2016, `http://www.mathworks.com/help/physmod/sps/powersys/ref/battery.html;jsessionid=5e90812b32222d88be91ccc079ac`.

[38] Matlab (2016b). Mathworks documentaiton - modeling pneumatic systems. Online; accessed September 16, 2016, `http://www.mathworks.com/help/releases/R2014b/physmod/simscape/ug/modeling-pneumatic-systems.html`.

[39] Maxwell (2016). Dadasheet k2 ultracapacitors. Online; accessed September 7, 2016, `http://www.maxwell.com/images/documents/K2_3V_DS_3001423_EN_1.pdf`.

[40] Micro, J. (2014). Ultimo prismatic cell. Online; accessed September 7, 2016, `http://www.jsrmicro.com/index.php/lp-prismatic-cell`.

[41] Micro, J. (2016). The electrochemical difference. Online; accessed September 7, 2016, http://www.jsrmicro.com/index.php/EnergyAndEnvironment/LithiumIonCapacitor/.

[42] Mikkelsen, K. B. (2010). *Design and Evaluation of Hybrid Energy Storage Systems for Electric Powertrains*. Master's thesis, University of Waterloo.

[43] Moshirvaziri, M. (2012). *Ultracapacitor/Battery Hybrid Energy Storage Systems for Electric Vehicles*. Master's thesis, University of Toronto.

[44] Nielson, G. and Emadi, A. (2011). Hybrid energy storage systems for high-performance hybrid electric vehicles. In *2011 IEEE Vehicle Power and Propulsion Conference*, pages 1–6. IEEE.

[45] Novák, M., Novák, J., Cerovskỳ, Z., and Chyskỳ, J. (2011). Dynamic properties of high-speed electrical motor supercharger. In *Industrial Technology (ICIT), 2011 IEEE International Conference on*, pages 153–158. IEEE.

[46] Petrny, M. (2014). How formula one's amazing new hybrid turbo engine works. Online; accessed October 1, 2016, http://s1.cdn.autoevolution.com/images/news/gallery/renault-details-new-formula-one-engine-photo-gallery_7.png.

[47] Picarelli, A. and Dempsey, M. (2014). Simulating the complete 2014 hybrid electric formula 1 cars. In *Hybrid and Electric Vehicles Conference (HEVC 2014), 5th IET*, pages 1–6. IET.

[48] Roeleveld, J. (2015). *On the Electrification of the American Muscle Car: An Analysis and Model Based Design*. Master's thesis, McMaster University.

[49] RONG, K. (2014). *Modeling of Turbocharged Spark Ignited Engine and Model Predictive Control of Hybrid Turbocharger*. Master's thesis, UNIVERSITY OF FLORIDA.

[50] Sadoun, R., Rizoug, N., Bartholomes, P., Barbedette, B., and Moigne, P. L. (2011a). Influence of the drive cycles on the sizing of hybrid storage system battery-supercapacitor supplying an electric vehicle. In *IECON 2011 - 37th Annual Conference on IEEE Industrial Electronics Society*, pages 4106–4112.

[51] Sadoun, R., Rizoug, N., Bartholomeüs, P., Barbedette, B., and Le Moigne, P. (2011b). Influence of the drive cycles on the sizing of hybrid storage system battery-supercapacitor supplying an electric vehicle. In *IECON 2011-37th Annual Conference on IEEE Industrial Electronics Society*, pages 4106–4112. IEEE.

[52] Statista (2016). Number of cars sold worldwide from 1990 to 2016 (in million units). Online; accessed October 12, 2016, `https://www.statista.com/statistics/200002/international-car-sales-since-1990/`.

[53] Tehrani, M. M., Bazargan, D., Hairi-Yazdi, M. R., and Esfahanian, M. (2011). Performance analysis of hybrid energy storage in different driving cycles. In *Power Electronics, Drive Systems and Technologies Conference (PEDSTC), 2011 2nd*, pages 330–335. IEEE.

[54] Villegas, J., Gao, B., Svancara, K., Thornton, W., and Parra, J. (2011). Real-time simulation and control of an electric supercharger for engine downsizing. In *2011 IEEE Vehicle Power and Propulsion Conference*, pages 1–6. IEEE.

[55] Warner, B. (2016a). Design and function of a turbocharger: Turbine. Online; accessed October 12, 2016, `http://www.turbos.borgwarner.com/en/products/turbochargerturbine.aspx`.

[56] Warner, B. (2016b). Matchbot. Online; accessed September 16, 2016, `http://www.turbos.bwauto.com/aftermarket/matchbot/index.html`.

[57] Wikimedia (2015). Usa cafe footprint curves with 2012 prius compliance fe.png. Online; accessed September 7, 2016 `https://commons.wikimedia.org/w/index.php?curid=42105527`.

[58] Wikipedia (2009). Ragone chart showing specific energy versus specific power for various energy-storing devices. Online; accessed September 7, 2016, `https://en.wikipedia.org/wiki/Ragone_chart#/media/File:Lithium_Ion_Capacitor_Chart.png`.

[59] Wikipedia (2016). Government incentives for plug-in electric vehicles. Online; accessed September 7, 2016 `https://en.wikipedia.org/wiki/Government_incentives_for_plug-in_electric_vehicles`.

[60] Yu, H., Lu, R., Wang, T., and Zhu, C. (2010). Battery/ultra-capacitor hybrid energy storage system used in hev. *Journal of Asian Electric Vehicles*, **8**(1), 1351–1356.

[61] Zhuge, K. and Kazerani, M. (2014). Development of a hybrid energy storage system (hess) for electric and hybrid electric vehicles. In *Transportation Electrification Conference and Expo (ITEC), 2014 IEEE*, pages 1–5. IEEE.

Appendix A

Battery Thermal Model

A.1 Battery Thermal Model Top Level

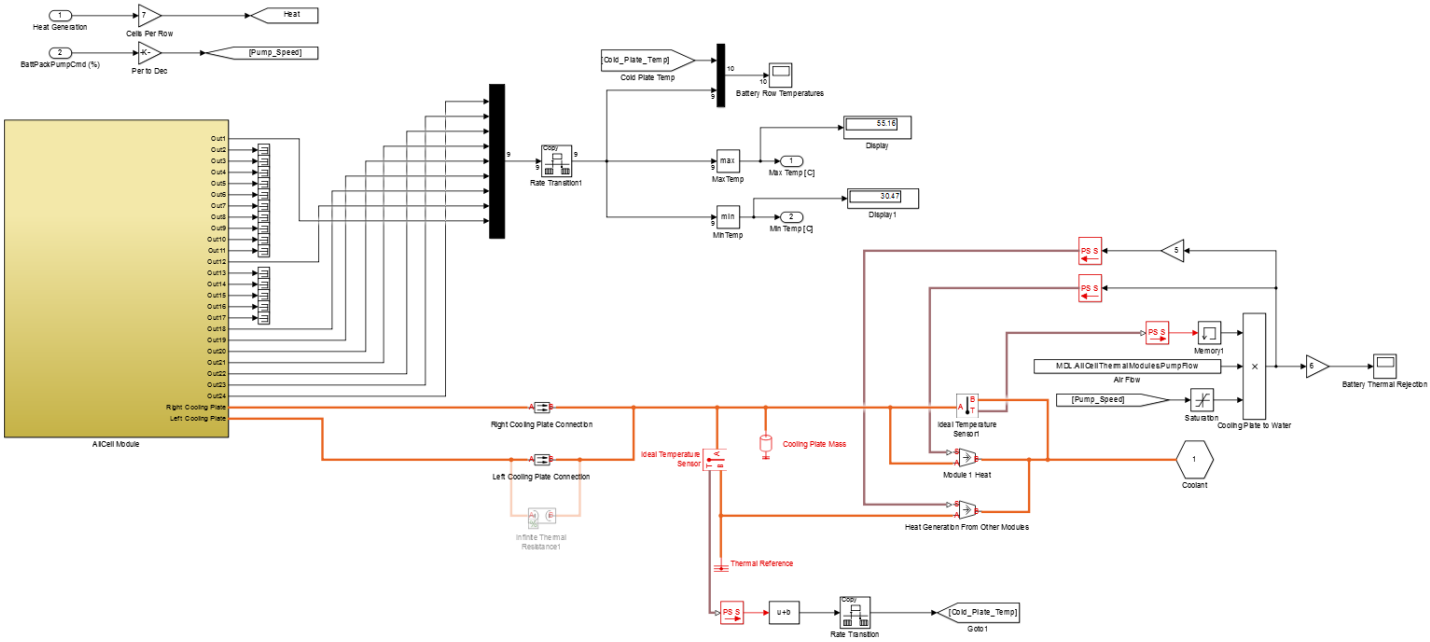

A.2 Battery Thermal Model Second Level

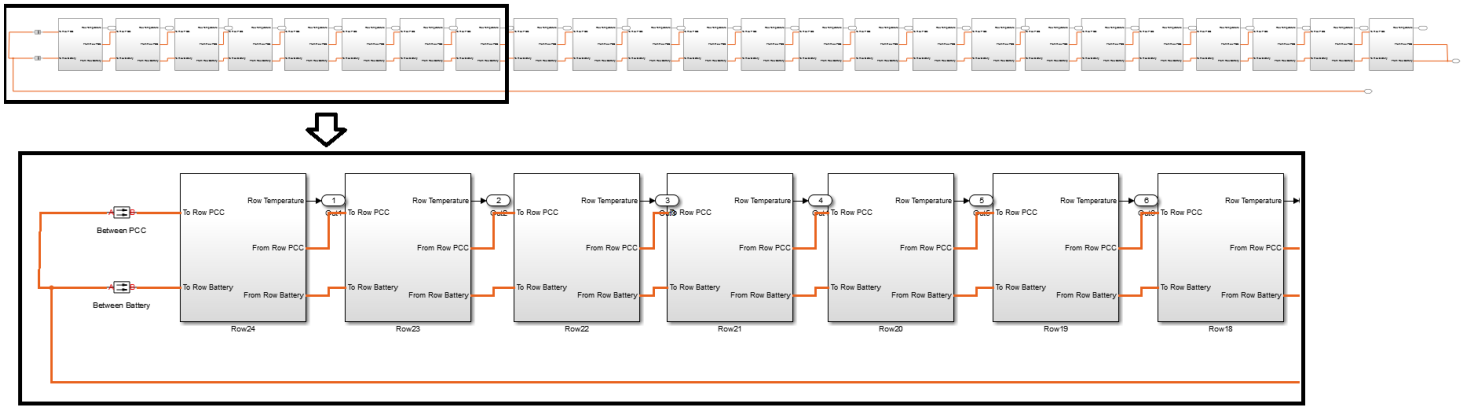

A.3 HESS Battery Thermal Row Temps During Performance Driving

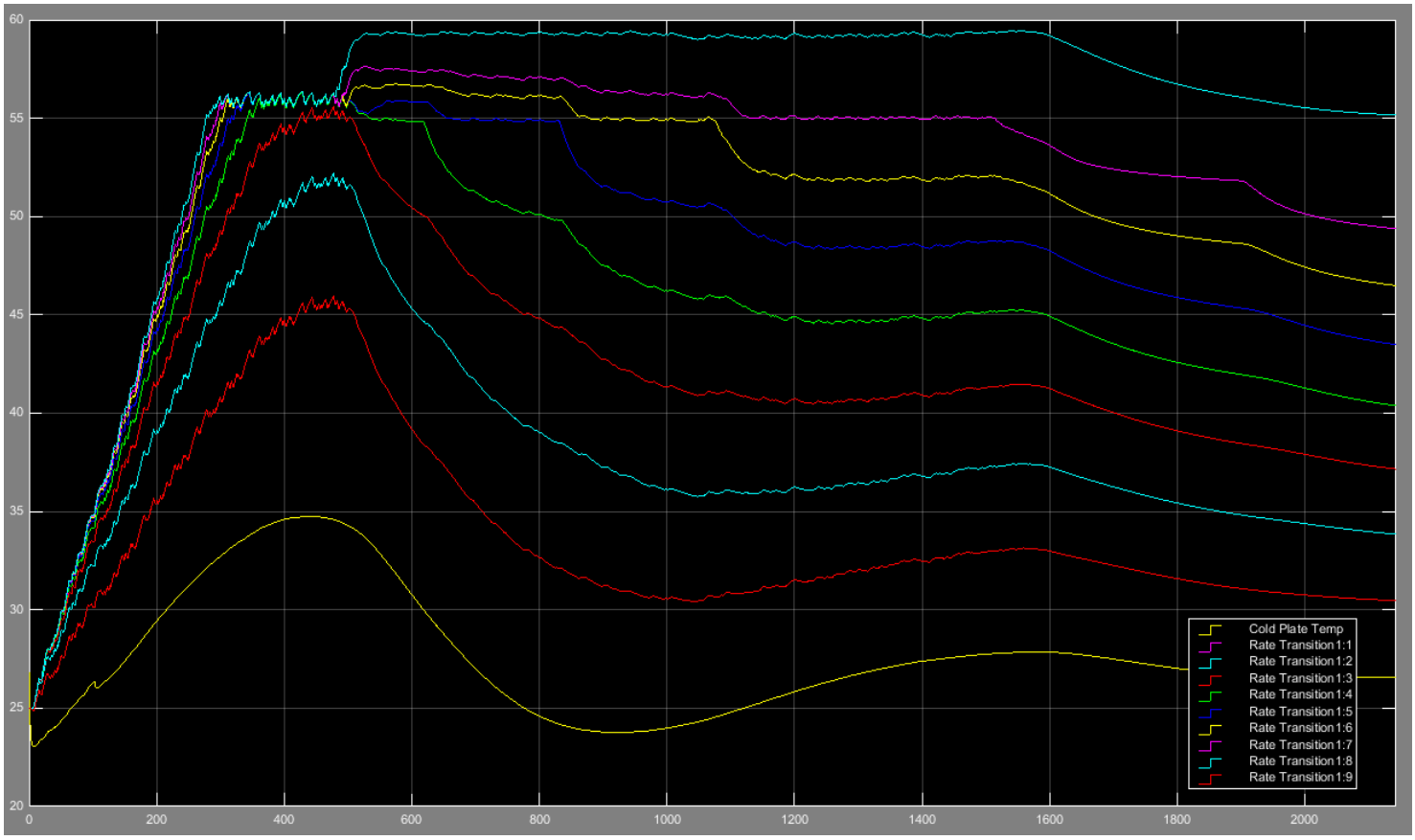

Appendix B

HESS Initialization

```
%% Script Information
%
% Filename: HESS_Init.m
% Description: HESS Model Intialization Script.
%
% Created By: Alexander Lebel
% Last Modified By: Tyler Stiene
% Mondification Date: See Git
%

%%
HESS_BusData;

% Ultracap Parameters Parameters
```

```
MDL.UltraCapModel.CapsSeries = 108;

MDL.UltraCapModel.VoltMax = 400;
MDL.UltraCapModel.VoltNom = 3.0*MDL.UltraCapModel.CapsSeries;
MDL.UltraCapModel.VoltMin = 2.2*MDL.UltraCapModel.CapsSeries;

MDL.UltraCapModel.Capacitance = ...
    3300/MDL.UltraCapModel.CapsSeries;

MDL.UltraCapModel.InitSOC = 1.00;

MDL.UltraCapModel.Q = ...
    (MDL.UltraCapModel.Capacitance*MDL.UltraCapModel.VoltMax) ...
    - (MDL.UltraCapModel.Capacitance*MDL.UltraCapModel.VoltMin);
MDL.UltraCapModel.InitQ = MDL.UltraCapModel.Q * ...
    MDL.UltraCapModel.InitSOC;

MDL.UltraCapModel.TotalEnergy = ...
    (1/2*(MDL.UltraCapModel.Capacitance*MDL.UltraCapModel.VoltMax^2)) ...
    - ...
    (1/2*(MDL.UltraCapModel.Capacitance*MDL.UltraCapModel.VoltMin^2));
MDL.UltraCapModel.TotalEnergy_Wh = ...
    MDL.UltraCapModel.TotalEnergy /3600;
MDL.UltraCapModel.InitEnergy = ...
    MDL.UltraCapModel.TotalEnergy * MDL.UltraCapModel.InitSOC;

MDL.UltraCapModel.PackResistance = 0.1440;
```

```
MDL.UltraCapModel.PackR_SQRT = ...
    sqrt(MDL.UltraCapModel.PackResistance);

%Voltage set points to determine the upper and lower bounds ...
    of the SOC
MDL.UltraCapModel.SOC_MaxVolt = 400; % Upper Operating Limit
MDL.UltraCapModel.SOC_MinVolt = MDL.UltraCapModel.VoltMin;

%Thermal
MDL.UltraCapThermalModel.InitTemp = 25; % Celcius

MDL.UltraCapThermalModel.Mass = 57.51; %KG
%MDL.UltraCapThermalModel.Mass = 6.39; %KG JSR TEST VALUES
MDL.UltraCapThermalModel.SpecificHeat = 1800; %J/kg/K
MDL.UltraCapThermalModel.Airflow = 219.5/60/60  * 1.205 * ...
    1005; %flow m^3/s * density kg/m^3 * specific heat J/KgK
%MDL.UltraCapThermalModel.Airflow = 15.725/60/60  * 1.205 * ...
    1005; %flow m^3/s * density kg/m^3 * specific heat J/KgK ...
    % JSR TEST VALUES
MDL.UltraCapThermalModel.TestCorrectionFactor = 0.1612;

MDL.UltraCapThermalModel.PumpFlow = (10/60)*4186; ...
    %10L/min/60 * Water Specific Heat

%%
% Battery Model Parameters
```

```
MDL.BatteryModel.RawData_02C = [7.704654895666181, ...
    4.1411063412287
73.1942215088282, 4.10256051214002
219.58266452648485, 4.0711588558797995
354.4141252006421, 4.046766044785938
485.39325842696627, 4.004803192229185
616.3723916532904, 3.9558145785483103
712.6805778491171, 3.920826739242391
913.0016051364364, 3.850862337935727
1051.6853932584268, 3.808910762684149
1198.0738362760833, 3.756431823051564
1394.5425361155696, 3.689974663654373
1617.9775280898873, 3.6305827359494174
1856.8218298555378, 3.585264885103056
2122.6324237560193, 3.522422102014503
2303.6918138041733, 3.459455268569023
2446.2279293739966, 3.4104835708459107
2554.0930979133227, 3.336870961315084
2650.4012841091494, 3.2597285552644344
2762.118780096308, 3.1369412565173427
2873.836276083467, 2.989563793835825
2931.621187800963, 2.8350816288939598
2973.9967897271267, 2.6559867454073176
2993.258426966292, 2.5119868356257586];

MDL.BatteryModel.RawData_20A = [3.8523274478330904, ...
    3.6949648711943794
42.37560192616377, 3.5861219602963677
```

```
261.9582664526485, 3.512672871690581
469.983948635634, 3.453258389375275
701.1235955056179, 3.383339097289312
955.3772070626003, 3.313453637118874
1205.7784911717495, 3.2576140605440926
1417.656500802568, 3.2087438585675567
1675.7624398073833, 3.149402678735889
1995.5056179775281, 3.0796130756594406
2234.349919743178, 3.016730822002774
2461.637239165329, 2.925728607891858
2681.2199036918137, 2.771483266358671
2789.0850722311397, 2.645177448396931
2862.279293739968, 2.50828224087572];

MDL.BatteryModel.SOCmax = 1; % Maximum of the SOC
MDL.BatteryModel.SOCint = 1.00; % SOC initial

MDL.BatteryModel.NomVolt = 3.6*84; % Pack nominal voltage (V)
MDL.BatteryModel.MinVolt = 2.0*84;
MDL.BatteryModel.MaxVolt = 4.2*84;

MDL.BatteryModel.MaxCap = 3*12;
MDL.BatteryModel.RatedCap = 3*12; % Rated capacity (Ah) @ 0.2
MDL.BatteryModel.NomDischageA = .2*3*12; % Rated capacity ...
    (Ah) @ 0.2
MDL.BatteryModel.CapNominalV = 2*12;
MDL.BatteryModel.ExpZone = [3.62*84 1.7*12];
```

```
MDL.BatteryModel.CellR0 = 0.027; %ohms
%MDL.BatteryModel.PackR = 0.189; %ohms
MDL.BatteryModel.PackR = ...
    ((12/(MDL.BatteryModel.CellR0*14*6))^-1); %ohms

MDL.BatteryModel.PackR_SQRT = sqrt(MDL.BatteryModel.PackR); ...
    %ohms

MDL.BatteryModel.NumberofCells = 6*14*12;

% Maximum Energy Capacity (kWh)
MDL.BatteryModel.TotalEnergy_Wh = ...
    MDL.BatteryModel.RatedCap*MDL.BatteryModel.NomVolt;

% Capacitor
%MDL.BatteryModel.CapEcap = 0.5*caps_capacitance*(vr^2 - ...
    vmin^2)*2.77777778e-7;

%Thermal
MDL.AllCellThermalModules.CellInitTemp = 273.15 + 25; % K
MDL.AllCellThermalModules.PCCInitTemp = 273.15 + 25; % K

MDL.AllCellThermalModules.BatteryMassPerRow = .047 * 7; % ...
    47g max
MDL.AllCellThermalModules.CellSpecificHeat = 980; % J/(kg*K)

MDL.AllCellThermalModules.PCCSectionVolume = 0.000076423; %m^3
MDL.AllCellThermalModules.PCCDDensity = 875;
```

```
MDL.AllCellThermalModules.PCCSectionWeight = ...
    MDL.AllCellThermalModules.PCCDDensity * ...
    MDL.AllCellThermalModules.PCCSectionVolume;

MDL.AllCellThermalModules.TotalMass = ...
    (MDL.AllCellThermalModules.BatteryMassPerRow * 24 *6) + ...
    (MDL.AllCellThermalModules.PCCDDensity * ...
    MDL.AllCellThermalModules.PCCSectionVolume * 24 * 6);

MDL.AllCellThermalModules.PCCSpecificHeatSolid = 1960; %J/kg/C
MDL.AllCellThermalModules.PCCSpecificHeatLiquid = 2200; %J/kg/C
MDL.AllCellThermalModules.PCCLatentHeatofMaterial = 155000; ...
    %J/kg
MDL.AllCellThermalModules.PCCMeltingTemp = 273.15 + 55; %K
MDL.AllCellThermalModules.PCCThermalConductivity = 25;

MDL.AllCellThermalModules.RowThickness = 10.05; %mm
MDL.AllCellThermalModules.RowArea = 250*63; %mm^2

MDL.AllCellThermalModules.RowContactRatio = ...
    1159795.43/2778802.32;%PCM/Cell

MDL.AllCellThermalModules.BetweenPCCThermalConductivity = 25;
MDL.AllCellThermalModules.BetweenBatteryThermalConductivity ...
    = 3;
MDL.AllCellThermalModules.BetweenPCCThermalArea = ...
    MDL.AllCellThermalModules.RowArea * ...
    MDL.AllCellThermalModules.RowContactRatio;
```

```
MDL.AllCellThermalModules.BetweenBatteryThermalArea = ...
   MDL.AllCellThermalModules.RowArea * (1 - ...
   MDL.AllCellThermalModules.RowContactRatio);

MDL.AllCellThermalModules.CelltoInnerPCCThickness = .5; %mm
MDL.AllCellThermalModules.CelltoInnerArea = 63 * 18.3; %mm^2

MDL.AllCellThermalModules.PumpFlow = (10/60)*4186; ...
   %10L/min/60 * Water Specific Heat

%% HESS Totals
MDL.HESS.TotalEnergy_Wh = MDL.UltraCapModel.TotalEnergy_Wh ...
   + MDL.BatteryModel.TotalEnergy_Wh;

%% DC/DC

MDL.DCDCModel.Eff = .96;
%MDL.DCDCModel.Switch_Res = (7/0.080)^-1;

MDL.DCDCModel.RawData = [-390.610796543529, 98.36386768447836;
-279.6028782021093, 98.48600508905852;
-214.1796357343905, 98.48600508905852;
-138.39355142541086, 98.38422391857506;
-90.9097878585431, 97.95674300254453;
-52.77689552827269, 97.16284987277353;
0, 70; % Manual
48.03903315189427, 96.85750636132315;
93.30828961634938, 97.95674300254453;
```

```
126.78874566024513, 98.24173027989822;
203.36337849233917, 98.36386768447836;
329.9122739768038, 98.34351145038168;
390.2033798065868, 98.24173027989822];

%% Fuse Tracking

MDL.HESSFuse.L70S175.F = '(1.881e+22)*u^(-8.018)'; %saved ...
    here as a backup
MDL.HESSFuse.L70S175.ZeroCrossing = 5.13e-7;
MDL.HESSFuse.L70S150.F = '(2.099e+20)*u^(-7.507)'; %saved ...
    here as a backup
MDL.HESSFuse.L70S150.ZeroCrossing = 1.033e-6;

MDL.HESSFuse.CB350A.F = '(2.205e+39)*u^(-12.86)'; %saved ...
    here as a backup
MDL.HESSFuse.CB350A.ZeroCrossing = 2.36e-9;
MDL.HESSFuse.CB205A.F =  '(1.751e+10)*u^(-3.282)'; %saved ...
    here as a backup
MDL.HESSFuse.CB250.ZeroCrossing = 4.23e-5;
```

Appendix C

Simscape Phase Change Material

```
component phase_change_mass
% Phase Changing Thermal Mass
% This block represents a thermal mass that changes state ...
    of matter
% depending on the amount of energy the thermal mass has ...
    stored. This block
% is characterized by a mass, a specific heat of each ...
    state, a latent heat
% of each state, a melting temperature and a starting ...
    temperature
%
% This block has two ports: A thermal port for heat flowing ...
    into the block
```

```
% (positive direction) and currently a physical signal port ...
    to monitor
% the total energy accumulated during the simulation (used ...
    for debugging)
%
% NOTE: In the variables tab, set the value of T to the ...
    same value that is put in
% for starting temperature in the parameters tab
%
% Created By: Tyler Stiene & Elisha (Nathanial) Jordan
% Last Modified By: See Git
% Mondification Date: See Git
%

outputs
O1 = { 0, 'J'}; % :bottom
end

nodes
M = foundation.thermal.thermal; % :top
end

parameters
mass = { 1, 'kg' };                % Mass
sp_heat_solid = { 2110, 'J/(kg*K)' };    % Specific heat ...
    solid phase
sp_heat_liquid = { 4181.3, 'J/(kg*K)' };  % Specific heat ...
    liquid phase
```

```
latent_heat = { 336000, 'J/kg' };            % Latent heat ...
    of material
melting_temperature = { 273.15, 'K'};   % Melting temp of ...
    material
starting_temperature = { 293, 'K'}   % Starting temperature ...
    of material

end

variables
Q = { 0, 'J/s' }; % Heat flow
end

variables(Conversion=absolute)
T = { 293, 'K' }; % Temperature
end

variables
Qcount = { 0, 'J' }; % Energy
end




function setup
% Parameter range checking
if mass ≤ 0
pm_error('simscape:GreaterThanZero','Mass')
end
```

```
if sp_heat_solid ≤ 0
pm_error('simscape:GreaterThanZero','Specific heat solid ...
    phase')
end
if sp_heat_liquid ≤ 0
pm_error('simscape:GreaterThanZero','Specific heat liquid ...
    phase')
end
if latent_heat ≤ 0
pm_error('simscape:GreaterThanZero','Latent heat of fusion')
end
if melting_temperature ≤ 0
pm_error('simscape:GreaterThanZero','Melting temperature')
end
if starting_temperature ≤ 0
pm_error('simscape:GreaterThanZero','Starting temperature')
end
end

branches
Q : M.Q -> *;
end

equations



if Qcount < mass * sp_heat_solid * (melting_temperature - ...
    starting_temperature)
```

```
T == M.T;
Q == mass * sp_heat_solid * T.der;
Qcount.der == Q;
O1 == Qcount;

elseif Qcount ≥ mass * sp_heat_solid * (melting_temperature ...
   - starting_temperature)  && Qcount ≤  (latent_heat * ...
   mass) + (mass * sp_heat_solid * (melting_temperature - ...
   starting_temperature))
T == M.T;
0 == T.der;
Qcount.der == Q;
O1 == Qcount;

else
T == M.T;
Q == mass * sp_heat_liquid * T.der;
Qcount.der == Q;
O1 == Qcount;



end

assert(T>0, 'Temperature must be greater than absolute zero')
end

end
```

Appendix D

Optimization Function

```
%% Script Information
%
% Filename: EC4CycleParallelFun.m
% Description: This function runs the EC4Cycle using a ...
   parallel pool. It
% can be used with the optimization tool box to optimize ...
   paramaters. It
% attempts to do as little repeat work as possible ie not ...
   recreating the
% pool, loading varaibles or model on every iteration.  It ...
   is recommended
% that your local parallel pool be configured to equal the ...
   number of core
```

```
% on the computer running the simulation. It is also ...
   recommend to manually
% close the pool and remove the CrntParam.mat when the ...
   model or additional
% variables have been modified.
%
% Created By: Tyler Stiene
% Last Modified By: See Git
% Mondification Date: See Git
%

function [ EnergyConsUF ] = EC4CycleParallelFun( input )

FunStartTime = tic;

if exist('CrntParam.mat', 'file') == 0
disp('Initializing Model Inputs ...')

SimModel = 'MEE3T_Simulation_Tool';

%% Vehicle Model
% Initialize the Plant Models

run Driver_Init;
run HESS_Init;
run Engine_Init;
run Motor_Init;
run Clutch_Init;
```

```
run TorqueConverter_Init_V2;
run Transmission_Init;
run FuelTank_Init;
run Powertrain_Init;
run Chassis_Init;
run Actuators_Init;
run Sensors_Init;
run SimData_Init;

%% Hybrid Supervisory Controller
% Initialize the Hybrid Supervisory Controller and the Soft ...
    ECUs

run HSCLogic_Init;

%% Drive Cycle
% Load drive cycles from excel file

MDL.DriveCycle.UDDS = ...
    {xlsread('DriveCycles.xlsx',2,'A4:B1373')};
MDL.DriveCycle.DC505 = ...
    {xlsread('DriveCycles.xlsx',3,'A4:B509')};
MDL.DriveCycle.HWFET = ...
    {xlsread('DriveCycles.xlsx',5,'A4:B769')};
MDL.DriveCycle.US06C = ...
    {xlsread('DriveCycles.xlsx',7,'A4:B236')};
MDL.DriveCycle.US06H = ...
    {xlsread('DriveCycles.xlsx',8,'A4:B374')};
```

```
MDL.DriveCycle.EC4Cycle = {MDL.DriveCycle.DC505 ...
    MDL.DriveCycle.HWFET MDL.DriveCycle.US06C ...
    MDL.DriveCycle.US06H};

MDL.ChargeMode.Mode = {'Charge Depleating', 'Charge ...
    Sustaining'};
MDL.ChargeMode.HESSSOC = [1.00, 0.30; 1.00, 1.00];

MDL.ModelConfig.StepSize    = 0.01;
MDL.ModelConfig.Decimation  = 10;

else
load('CrntParam.mat');
end

%% Set Varaible to be Optimized
% This section must should be altered to change the desired ...
    varaibles.

HSC.HESSSlope.CDCapUF           = 95;
HSC.HESSSlope.CDCapUS           = ...
    HSC.HESSSlope.CDCapUF-input(1);
HSC.HESSSlope.CDCapLS           = ...
    HSC.HESSSlope.CDCapUS-input(2);
HSC.HESSSlope.CDCapLF           = ...
    HSC.HESSSlope.CDCapLS-input(3);

HSC.HESSSlope.CSCapUF           = 90;
```

```
HSC.HESSSlope.CSCapUS           = ...
   HSC.HESSSlope.CSCapUF-input(4);
HSC.HESSSlope.CSCapLS           = ...
   HSC.HESSSlope.CSCapUS-input(5);
HSC.HESSSlope.CSCapLF           = ...
   HSC.HESSSlope.CSCapLS-input(6);

HSC.HESSSlope.CDCapSlope        = [0 HSC.HESSSlope.CDCapLF ...
   HSC.HESSSlope.CDCapLS HSC.HESSSlope.CDCapUS ...
   HSC.HESSSlope.CDCapUF 100];
HSC.HESSSlope.MapCDCapSlope     = [240 240 0 0 -240 -240];
HSC.HESSSlope.CSCapSlope        = [0 HSC.HESSSlope.CSCapLF ...
   HSC.HESSSlope.CSCapLS HSC.HESSSlope.CSCapUS ...
   HSC.HESSSlope.CSCapUF 100];
HSC.HESSSlope.MapCSCapSlope     = [240 240 0 0 -240 -240];

%save('CrntParam.mat');
save('CrntParam.mat','-regexp','^(?!(input)$).')

%Echo the current test
input

CD = HSC.HESSSlope.CDCapSlope
CS = HSC.HESSSlope.CSCapSlope

%%
% Loop over the number of iterations and perform the
% computation for different parameter values.
```

```
% Start Parpool if not present

if isempty(gcp('nocreate'))
parpool;
spmd
currDir = pwd;
addpath(currDir);
tmpDir = tempname;
mkdir(tmpDir);
cd(tmpDir);
load_system(SimModel);
set_param('MEE3T_Simulation_Tool/Simulation ...
   Parameters/Real-Time Pacer','commented','on');
set_param('MEE3T_Simulation_Tool/Simulation ...
   Parameters/Real-Time Pacer1','commented','on');
end
addAttachedFiles(gcp,'CrntParam.mat');
end

updateAttachedFiles(gcp);

NumDriveCycle = length(MDL.DriveCycle.EC4Cycle);
NumChargeMode = length(MDL.ChargeMode.HESSSOC);
ParallelSimOut(NumDriveCycle,NumChargeMode) = ...
   Simulink.SimulationOutput;
SimResults = struct;
```

```
SimStartTime = tic;

parfor JOB = 1:NumDriveCycle*NumChargeMode

[DriveCycleIndex, ChargeModeIndex]  = ind2sub([4,2], JOB);

assignin('base','DriveCycleIndex',DriveCycleIndex);  %Load ...
   input variables
evalin('base',['load',' ',sprintf('CrntParam.mat')]);  ...
   %Load input variables

if (NumDriveCycle ≤ 1)
evalin('base','u = ...
   [MDL.DriveCycle.EC4Cycle{DriveCycleIndex}];');
else
evalin('base','u = ...
   [MDL.DriveCycle.EC4Cycle{DriveCycleIndex}{1}];');
end

evalin('base','MDL.VehicleDynamics.Vi  = u(1,2)*0.44704;') ...
     % Set the initial velocity and convert to m/s
evalin('base','MDL.ModelConfig.Tf      = max(u(:,1));') ...
        % Sets the simulation end time


assignin('base','ChargeModeIndex',ChargeModeIndex);  %Load ...
   input variables
```

```
        evalin('base','MDL.BatteryModel.SOCint = ...
            MDL.ChargeMode.HESSSOC(1,ChargeModeIndex);')
        evalin('base','MDL.UltraCapModel.InitSOC = ...
            MDL.ChargeMode.HESSSOC(2,ChargeModeIndex);')

        DrvStartTime = tic;

        ParallelSimOut(JOB) = sim(SimModel, 'SimulationMode', ...
            'normal');

        DrvEndTime = toc(DrvStartTime);
        SimEndTime = toc(SimStartTime);

        fprintf('Completed Drive Cycle (%d of %d)\n\tSimulation ...
            Time: %.2f sec; Total Elapsed Time: %.2f sec\n', JOB, ...
            length(MDL.DriveCycle.EC4Cycle)*length(MDL.ChargeMode.Mode), ...
            DrvEndTime, SimEndTime);
        end

        for JOB = 1:NumDriveCycle*NumChargeMode
        SimOut = ParallelSimOut(JOB).get('SimOut');
        tout = ParallelSimOut(JOB).get('tout');

        [DriveCycleIndex, ChargeModeIndex]  = ind2sub([4,2], JOB);

        SimResults(DriveCycleIndex,ChargeModeIndex).SimTime          ...
            = tout;          % Simulation Time (s)
```

```
SimResults(DriveCycleIndex,ChargeModeIndex).DrvCycleVel     ...
    = SimOut(:,3);  % Drive Cycle Velocity (mph)
SimResults(DriveCycleIndex,ChargeModeIndex).AccelPdlPos     ...
    = SimOut(:,1);  % Accelerator Pedal Position (%)
SimResults(DriveCycleIndex,ChargeModeIndex).BrakePdlPos     ...
    = SimOut(:,2);  % Brake Pedal Position (%)
SimResults(DriveCycleIndex,ChargeModeIndex).P1MtrTrq        ...
    = SimOut(:,5);  % P1 Motor Torque (Nm)
SimResults(DriveCycleIndex,ChargeModeIndex).P1MtrSpd        ...
    = SimOut(:,10); % P1 Motor Speed (rad/s)
SimResults(DriveCycleIndex,ChargeModeIndex).P2MtrTrq        ...
    = SimOut(:,7);  % P2 Motor Torque (Nm)
SimResults(DriveCycleIndex,ChargeModeIndex).P2MtrSpd        ...
    = SimOut(:,14); % P2 Motor Speed (rad/s)
SimResults(DriveCycleIndex,ChargeModeIndex).EngTrq          ...
    = SimOut(:,9);  % Engine Torque (Nm)
SimResults(DriveCycleIndex,ChargeModeIndex).EngSpd          ...
    = SimOut(:,10); % Engine Speed (rad/s)
SimResults(DriveCycleIndex,ChargeModeIndex).EngFuel         ...
    = SimOut(:,15); % Remaining Engine Fuel (L)
SimResults(DriveCycleIndex,ChargeModeIndex).VehSpd          ...
    = SimOut(:,23); % Vehicle Velocity (m/s)
SimResults(DriveCycleIndex,ChargeModeIndex).VehAccel        ...
    = SimOut(:,24); % Vehicle Acceleration (m/s^2)
SimResults(DriveCycleIndex,ChargeModeIndex).VehPos          ...
    = SimOut(:,25); % Vehicle Position (m)
SimResults(DriveCycleIndex,ChargeModeIndex).TractForce      ...
    = SimOut(:,26); % Traction Force (N)
```

```
SimResults(DriveCycleIndex,ChargeModeIndex).GradeForce      ...
    = SimOut(:,27); % Grade Force (N)
SimResults(DriveCycleIndex,ChargeModeIndex).RollResForce    ...
    = SimOut(:,28); % Rolling Resistance Force (N)
SimResults(DriveCycleIndex,ChargeModeIndex).AeroForce       ...
    = SimOut(:,29); % Aerodynamic Force (N)
SimResults(DriveCycleIndex,ChargeModeIndex).RoadLoadForce   ...
    = SimOut(:,30); % Road Load Force (N)
SimResults(DriveCycleIndex,ChargeModeIndex).RearWhlSlip     ...
    = SimOut(:,31); % Rear Tire Slip %
SimResults(DriveCycleIndex,ChargeModeIndex).TotTrq          ...
    = SimOut(:,32); % Total Axle Torque (Nm)
SimResults(DriveCycleIndex,ChargeModeIndex).TractPwr        ...
    = SimOut(:,33); % Tractive Power (kW)
SimResults(DriveCycleIndex,ChargeModeIndex).TractEng        ...
    = SimOut(:,34); % Tractive Energy (J)
SimResults(DriveCycleIndex,ChargeModeIndex).FrontDrvSpd     ...
    = SimOut(:,35); % Front Input Speed (rad/s)
SimResults(DriveCycleIndex,ChargeModeIndex).RearDrvSpd      ...
    = SimOut(:,36); % Rear Input Speed (rad/s)
SimResults(DriveCycleIndex,ChargeModeIndex).HESSEnergy      ...
    = SimOut(:,16); % Energy into/out of the HESS (J)
SimResults(DriveCycleIndex,ChargeModeIndex).BattSOC         ...
    = SimOut(:,17); % Battery SOC (decimal)
SimResults(DriveCycleIndex,ChargeModeIndex).BattVolt        ...
    = SimOut(:,18); % Battery Open Circuit Voltage (V)
SimResults(DriveCycleIndex,ChargeModeIndex).BattCrnt        ...
    = SimOut(:,19); % Battery Current Output (A)
```

```
SimResults(DriveCycleIndex,ChargeModeIndex).CapSOC          ...
   = SimOut(:,20); % Ultracapacitor SOC (decimal)
SimResults(DriveCycleIndex,ChargeModeIndex).CapVolt         ...
   = SimOut(:,21); % Ultracapacitor Open Circuit Voltage (V)
SimResults(DriveCycleIndex,ChargeModeIndex).CapCrnt         ...
   = SimOut(:,22); % Ultracapacitor Current Output (A)
SimResults(DriveCycleIndex,ChargeModeIndex).MeanSimErr      ...
   = SimOut(:,42); % Mean Simulation Error (m/s)
SimResults(DriveCycleIndex,ChargeModeIndex).MaxSimErr       ...
   = SimOut(:,43); % Maximum Simulation Error (m/s)

end

fprintf('Post Processing Simulation Results ... ')

DrvCycleRes = PostProcessEC4Cycle(SimResults);

fprintf('Displaying Results\n');

fprintf('\n---- VTS-Related Information ...
   --------------------------\n');
fprintf('Charge Depleating Range:                    %.2f ...
   km\n', DrvCycleRes.RangeCD);
fprintf('Total Energy Consumption:                   %.2f ...
   kWh/km\n', DrvCycleRes.EnergyConsUF);
fprintf('Total Fuel Consumption:                     %.2f ...
   kWh/km\n', DrvCycleRes.FuelConsUF);
```

```
        fprintf('Well-to-Wheels Greenhouse Gas Emissions:   %.2f ...
            g/km\n', DrvCycleRes.GHGWTW);
        fprintf('Well-to-Wheels Petroleum Energy Use:       %.2f ...
            kWh/km\n', DrvCycleRes.PEUWTW);
        fprintf('THC Emissions:                             %.2f ...
            g/kWh\n', DrvCycleRes.UCETHC);
        fprintf('CO Emissions:                              %.2f ...
            g/kWh\n', DrvCycleRes.UCECO);
        fprintf('NOx Emissions:                             %.2f ...
            g/kWh\n', DrvCycleRes.UCENOx);
        fprintf('Criteria Emissions Score:                  ...
            %.2f\n', DrvCycleRes.CES);
        fprintf('-------------------------------------------------------\n\n');

        EnergyConsUF = DrvCycleRes.EnergyConsUF;

        fprintf('Function Time: %.2f\n\n', toc(FunStartTime));

        end
```

Appendix E

Simscape Compressor Code

```
component turbo_compressor
% Turbo Compressor - Tyler Stiene - McMaster University
% Simulating the compressor stage of Turbo using data from ...
   the compressors
% efficiency map.

outputs
G_out   = { 0, 'kg/s' }; % G:right
E_out   = { 1, '1' }; % Eff:right
C_W_out = { 0, 'J/s' }; %Work:right
PR      = { 0, '1' }; %Pr:right
end

nodes
```

```
R = foundation.mechanical.rotational.rotational; % Shaft:right
C = foundation.mechanical.rotational.rotational; % Ref:left
A = foundation.pneumatic.pneumatic; % In:left
B = foundation.pneumatic.pneumatic; % Out:right
end

parameters

x_PressureRatio = [1 2 3 4 5 6 7 8 9 10 11 12 13 14 15 16 ...
   17 18 19 20 21 22 23 24 25 26 27 28 29 30 31 32 33 34 35 ...
   36 37 38 39 40 41 42 43 44 45 46];  % T1 X: Presure Ratio
y_Speed = [1 2 3 4 5 6 7 8 9 10 11 12 13 14 15 16 17 18 19 ...
   20 21 22 23 24 25 26 27 28 29 30 31 32 33 34 35 36 37 38 ...
   39 40 41 42 43 44 45 46];  % T1 Y: Shaft Speed
z_CorrectedMassFlow = {zeros(46), 'kg/s'};  % T1 ...
   Z:Corrected Mass Flow

x_CorrectedMassFlow = [1 2 3 4 5 6 7 8 9 10 11 12 13 14 15 ...
   16 17 18 19 20 21 22 23 24 25 26 27 28 29 30 31 32 33 34 ...
   35 36 37 38 39 40 41 42 43 44 45 46];  % T2 X: Corrected ...
   Mass Flow
y_PressureRatio = [1 2 3 4 5 6 7 8 9 10 11 12 13 14 15 16 ...
   17 18 19 20 21 22 23 24 25 26 27 28 29 30 31 32 33 34 35 ...
   36 37 38 39 40 41 42 43 44 45 46];  % T2 Y: Presure Ratio
z_Eff = zeros(46);  % T2 Z: Eff
end

variables
```

```
% Pneumatic through variables
G   = { 0, 'kg/s' }; % Mass flow rate
Q_A = { 0, 'J/s' };  % Heat flow into port A
Q_B = { 0, 'J/s' };  % Heat flow into port B
% Mechanical through and across variables
t = { 0, 'N*m' };    % Torque
w = { 0, 'rad/s' };
%Internal Varaibles
E   = { 0, '1' };
C_W = { 0, 'J/s' };
end

branches
G   : A.G -> B.G;
Q_A : A.Q -> *;
Q_B : B.Q -> *;
t   : R.t -> C.t;
end

equations

w   == (R.w - C.w);

if w > { 100, 'rad/s' }
G == tablelookup(x_PressureRatio, y_Speed, ...
   z_CorrectedMassFlow, B.p/A.p, w*9.54929659643, ...
   interpolation=linear, extrapolation=nearest);
```

```
E == tablelookup(x_CorrectedMassFlow, y_PressureRatio, ...
   z_Eff, G, B.p/A.p, interpolation=linear, ...
   extrapolation=nearest);
C_W == t*w*E;
C_W == G * A.c_v * (B.T - A.T);
Q_A == G * A.c_p * A.T;
Q_B == -G * B.c_p * B.T;
else
G == tablelookup(x_PressureRatio, y_Speed, ...
   z_CorrectedMassFlow, B.p/A.p, w*9.54929659643, ...
   interpolation=linear, extrapolation=nearest);
E == tablelookup(x_CorrectedMassFlow, y_PressureRatio, ...
   z_Eff, G, B.p/A.p, interpolation=linear, ...
   extrapolation=nearest);
t == 0;
C_W == G * A.c_v * (B.T - A.T);
Q_A == G * A.c_p * A.T;
Q_B == -G * B.c_p * B.T;
end

G_out == G;
E_out == E;
C_W_out == C_W;
PR == B.p/A.p;
end

end
```

Appendix F

Simscape Engine Mass Flow Code

```
component turbo_engine
% Turbo Engine - Tyler Stiene - McMaster University
% Engine mass flow or air

inputs
G_in    = { 0, 'kg/s' }; % G:left
end

nodes
A = foundation.pneumatic.pneumatic; % In:left
B = foundation.pneumatic.pneumatic; % Out:right
end

variables
```

```
% Pneumatic through variables
G   = { 0, 'kg/s' }; % Mass flow rate
Q_A = { 0, 'J/s' };  % Heat flow into port A
Q_B = { 0, 'J/s' };  % Heat flow into port B
end

branches
G   : A.G -> B.G;
Q_A : A.Q -> *;
Q_B : B.Q -> *;
end

equations
G   == G_in;
Q_A == G * A.c_p * A.T;
Q_B == -G * B.c_p * B.T;
end

end
```

Appendix G

Simscape Turbine Code

```
component turbo_turbine
% Turbo Turbine - Tyler Stiene - McMaster University
% Simulating the turbine stage of Turbo using data from the ...
   turbine's
% efficiency map.

outputs
Phi_out = { 1, 'kg/s' }; % Phi:right
G_out   = { 0, 'kg/s' }; % G:right
E_out   = { 1, '1' }; % Eff:right
T_W_out = { 0, 'J/s' }; %Power:right
Exit_Temp = { 0, 'K' }; %Tout:right
end
```

```
nodes
R = foundation.mechanical.rotational.rotational; % Shaft:left
C = foundation.mechanical.rotational.rotational; % Ref:right
A = foundation.pneumatic.pneumatic; % In:left
B = foundation.pneumatic.pneumatic; % Out:right
end

parameters
%     x_PressureRatio = [1 2 3 4 5];  % Table 1,2: Presure ...
   Ratio
%     y_Phi = {[.01 .23 .3 .3 .3], 'kg/s'};   %Table 1 Y: Phi
%
%     y_Eff = [.5 .6 .6 .6 .6];  % Table 2 Y: Efficiency

Phi_x_PR = [1 2 3 4 5 6 7 8 9 10 11]; % T1: Pressure Ratio
Phi_y = {[1 2 3 4 5 6 7 8 9 10 11], 'kg/s'}; % T1: Phi

Eff_x_PR = [1 2 3 4 5 6 7 8 9 10 11]; % T2: Pressure Ratio
Eff_y = [1 2 3 4 5 6 7 8 9 10 11]; % T2: Phi

gam = 1.15; % gam
end

variables
% Pneumatic through variables
G   = { 0, 'kg/s' }; % Mass flow rate
Q_A = { 0, 'J/s' };  % Heat flow into port A
Q_B = { 0, 'J/s' };  % Heat flow into port B
```

```
% Mechanical through and across variables
t = { 0, 'N*m' };     % Torque
%Internal Varaibles
Phi = { 0, 'kg/s' };
E   = { 0, '1' };
T_W = { 0, 'J/s' };
end

branches
G   : A.G -> B.G;
Q_A : A.Q -> *;
Q_B : B.Q -> *;
t   : R.t -> C.t;
end

equations
Phi == tablelookup(Phi_x_PR, Phi_y, A.p/B.p, ...
   interpolation=linear, extrapolation=nearest);
G * A.T^(1/2) / A.p * 100  == Phi * {1,'K'}^(1/2) / {1,'Pa'};
E   == tablelookup(Eff_x_PR, Eff_y, A.p/B.p, ...
   interpolation=linear, extrapolation=nearest);
T_W == -t*abs(R.w - C.w);
%T_W == Q_A * ( 1 - (B.p/A.p)^((gam-1)/gam)) * E;
T_W == G * A.c_p * ( A.T - B.T ) * E;
Q_A == G * A.c_p * A.T;
Q_B == -G * B.c_p * B.T;

Phi_out == Phi;
```

```
        G_out   == G;
        E_out   == E;
        T_W_out == T_W;
        B.p/A.p == (Exit_Temp/A.T)^(gam-1/gam);
        end

        end
```

Appendix H

Simscape Exhaust Code

```
component variable_temp_pressure

nodes
A = foundation.pneumatic.pneumatic; % In:left
end

inputs
T = { 0, 'K' }; % T:left
P = { 0, 'Pa' }; % P:left

end

variables(Access=protected)
G = { 0 , 'kg/s' }; % Mass flow rate
```

```
Q = { 0 , 'J/s' }; % Heat flow rate
end

branches
G  : A.G -> *;
Q : A.Q -> *;
end

equations
% Set absolute pressure and temperature to pneumatic domain ...
   values
A.p == P;
A.T == T;
end
```

Appendix I

eTurbo Dynamometer Test

I.1 Compressor and Turbine Internal Variables During Dyno Test

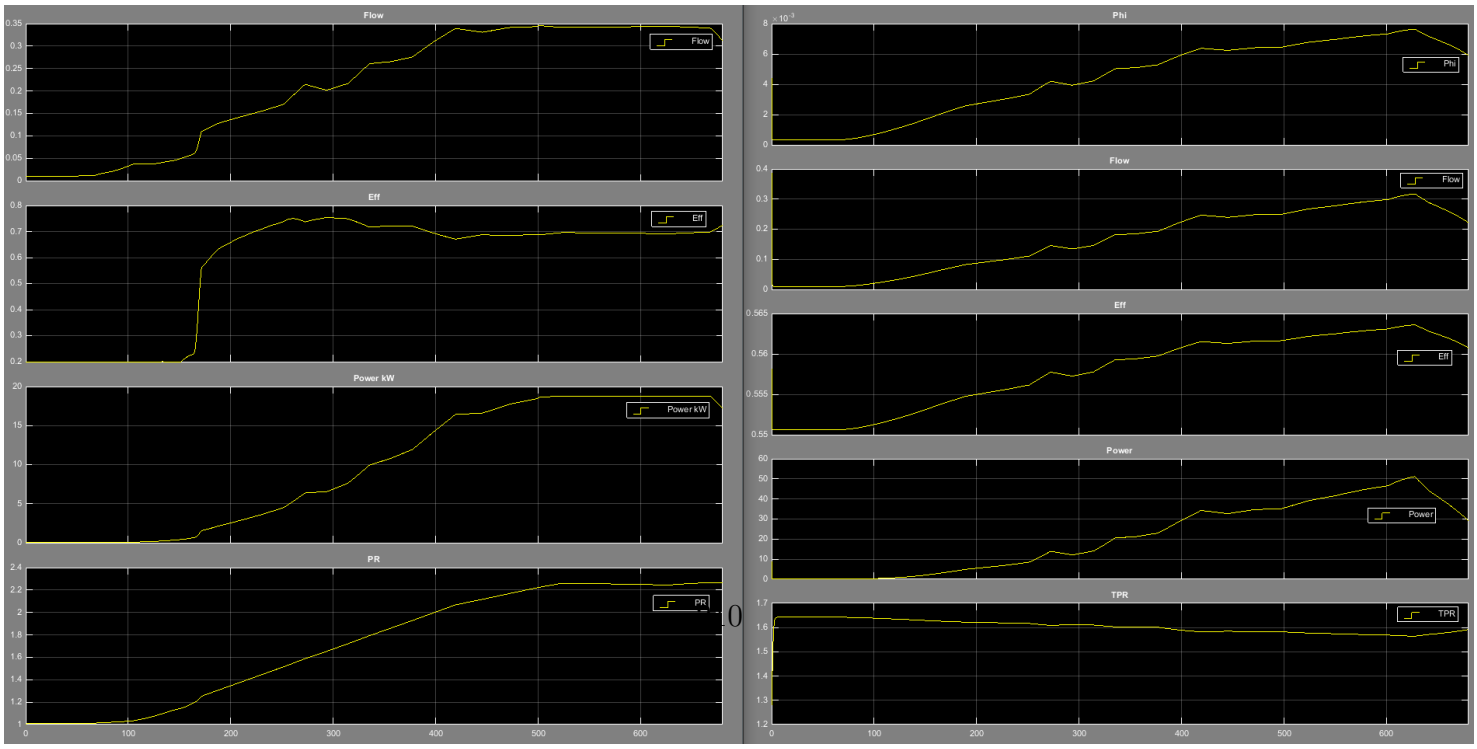

I.2 eTurbo Temperatures and Pressures During Dyno Test